Non-perturbative Methods in Quantum Field Theory

by

Cengiz Pehlevan

B.Sc., Electrical Engineering, Bogazici Universitesi; Istanbul, Turkey, 2004

B.Sc., Physics, Bogazici Universitesi; Istanbul, Turkey, 2004

Sc.M., Physics, Brown University; Providence, RI, 2006

A dissertation submitted in partial fulfillment of the
requirements for the degree of Doctor of Philosophy
in Department of Physics at Brown University

PROVIDENCE, RHODE ISLAND

May 2011

This dissertation by Cengiz Pehlevan is accepted in its present form
by Department of Physics as satisfying the
dissertation requirement for the degree of Doctor of Philosophy.

Date_____ _____

Gerald S. Guralnik, Ph.D., Advisor

Recommended to the Graduate Council

Date_____ _____

Ian Dell'Antonio, Ph.D., Reader

Date_____ _____

Marcus Spradlin, Ph.D., Reader

Approved by the Graduate Council

Date_____ _____

Peter Weber, Dean of the Graduate School

Vitae

Cengiz Pehlevan was born in Tosya, Turkey. He received his Bachelor of Science degrees from İstanbul's Boğaziçi Üniversitesi in 2004.

Acknowledgements

I would like to express my gratitude to my advisor, Dr. Gerald Guralnik, for his invaluable support and guidance. His wisdom taught me a lot about physics and life in general. I consider an honor to be his student. I thank Dr. Zachary Guralnik for sharing his ideas, being a creative collaborator, his advice and help. I want to thank my committee members, Dr. Marcus Spradlin and Dr. Ian Dell'Antonio, for their extensive help in my job search. Finally, I would like to thank Dr. J. Michael Kosterlitz for discussions.

Special thanks go to Daniel Ferrante for our informative discussions, for being a great friend, for lunches and dinners and for taking care of my Linux.

Finally, I would like to thank my family for the support they provided me through my entire life. I thank Dina for everything she has done for me, the list would be longer than this thesis.

During my last year of study, I was supported by a generous fellowship from the Julian Schwinger Foundation for Physics Research.

Abstract of " Non-perturbative Methods in Quantum Field Theory " by Cengiz Pehlevan, Ph.D., Brown University, August 2010

In this thesis we first study various aspects of stationary distributions of certain deterministic and stochastic dynamical systems. We look at the 30 year old proposal to use complex Langevin equations to sample complex path integral weights of quantum field theories. We solve for possible stationary distributions of complex Langevin equations and relate these to the solution space of Schwinger-Dyson equations. We introduce an effective potential for the whole complex Langevin evolution, which allows us to identify the particular stationary distribution sampled.

Next we look at deterministic dynamical systems and ask a very general question: Can one engineer dynamical systems with a given stationary distribution? We explicitly engineer such systems and using this knowledge we introduce novel Monte Carlo based methods to calculate various quantities associated with these dynamical systems. Through Monte Carlo simulations and series resummations, we study the analytic structure of the associated autocorrelation functions, which gives the exponential decay constant of the power spectrum.

Finally we study a first order phase transition in large N_c, $\mathcal{N} = 2$ SYM theory using the methods of AdS/CFT correspondence. We discuss AdS/CFT description of the latent heat in the phase transition. We further investigate an out-of-equilibrium evolution of the theory at high temperatures. Through AdS/CFT correspondence, this problem is mapped to an evolution of a D7-brane in a time-dependent gravitational background.

Contents

List of Tables

List of Figures

Chapter One

Introduction

In this thesis, we describe three distinct research projects. Two of them are directly related to theoretical high energy physics. The other one can be classified under the theme of dynamical systems, however a remote connection to theoretical high energy physics also exists. Here we give a brief introduction to the projects described, however extended introductions appear in the beginning of each chapter. We start by introducing the theoretical high energy physics related projects.

Increasing our understanding of the behavior of quantum field theories is essential for describing experimental data from current experiments. This clearly requires new calculational tools that extend the domain of conventional methods, namely perturbation theory and lattice gauge theory. We describe below two research directions that have the potential to evolve into productive methods, especially for the study of nonequilibrium behavior of quantum field theories.

Perturbation theory works well for theories, where the coupling constants are small. For strongly coupled phenomena, Monte Carlo simulation of path integrals is the main tool to extract numbers out of quantum field theories. However, the range of high energy problems that can be solved using Monte Carlo methods is very limited because of the "sign problem". Monte Carlo methods work on probabilistic interpretation of the path integral weight, however many interesting physical phenomena do not satisy this constraint. In these cases, path integral weights are complex and hence are not probability distributions. Examples include quantum field theories in Lorentzian signature, gauge theories with finite chemical potential, out-of-equilibrium quantum field theories etc. Complex Langevin equations were proposed as a solution to this problem [92, 66]. In this approach, a d dimensional QFT is described by a $d+1$ dimensional stochastic equation, whose long time averages describe the Green's functions of the QFT. Complex Langevin equations were known to have multiple stationary distributions that satisfy stationary limit equations but

it was not known how to identify to which one of these that the complex Langevin equation will converge to, see e.g. [100]. In this thesis, we analyze and solve this probelm in two steps. In Chapter 2, we show that previous ambiguities are related to the multiple solutions of a QFT defined by Schwinger-Dyson equations [45]. We then constructe an effective potential for the complex Langevin equation dynamics using the path integral representation of Langevin systems, which is formulated in $d+1$ dimensions for a d dimensional theory and has a real path integral weight. We then identify the sampled stationary distribution by matching its asymptotics with the asymptotics of the effective potential [46]. This is done in Chapter 3.

A particular problem where methods beyond perturbation theory and Monte Carlo methods are needed is the analysis of experiments from RHIC (Relativistic Heavy Ion Collider). At the RHIC, gold nuclei are collided at high energies to form a state of hot, dense matter, the quark-gluon plasma (QGP). Of particular interest is the chiral phase transition in QGP. Chiral symmetry is broken at high temperatures and restored at low temperatures. As the plasma is cooling, (for a moment let us abuse thermodynamic terminology) the QGP passes through the chiral phase transition. In reality this is a non-equilibrium process, that is well beyond the domain of conventional calculational methods in quantum field theory. Perturbation theory is not applicable due to the QGP being strongly coupled and Euclidean lattice gauge theory is not suited for studying non-equilibrium phenomena. At present, the most promising approach is AdS/CFT duality, which conjectures a correspondence between Type IIB string theory on $\mathrm{AdS}_5 \times S_5$ space and a supersymmetric $\mathcal{N} = 4$ Yang-Mills gauge theory (which is a conformal field theory) on the four dimensional boundary of AdS_5 [74, 114, 41]. Generalizations of the correspondence in which conformal symmetry and supersymmetry are broken are potentially useful for describing realistic QFTs, in particular LHC and RHIC data. In this setting, non-perturbative

properties of strong coupling theories in four dimensions are described by calculable classical gravity problems in five dimensions. The Euclidean AdS description of first order phase transitions that are like chiral phase transitions in QCD has been described in [9] and subsequent papers, see [27] for a dated review. The generic feature of the relevant string theory backgrounds is the presence of a static, Euclidean black hole in an asymptotically AdS space, in which the probe D-branes end either at or away from the horizon, depending on whether the temperature is above or below the critical temperature. The degrees of freedom of the embedded D-branes are dual to the operators involving fundamental fields (quarks). The change in the topology of the embedding corresponds to a jump in the expectation value of the chiral condensate at the phase transition.

In this thesis, we study this transition from several points of view. We first look for a description of the latent heat in this transition in terms of the stress-energy tensor of the D-brane. We calculate the stress-energy tensor of the D-brane and compare it to the thermodynamic internal energy and, as also noted in [61], find that these quantities do not match. There is another contribution to the energy that is related to the backreaction of the D-brane to the background geometry . We identify the latent heat to be a contribution totally of this latter type. While doing this, we clarify some issues that were not addressed in the literature such as the holographic renormalization of the stress-energy tensor. Then we study the AdS/CFT description of an expanding plasma with flavors. We propose a gravitational background that is consistent with the phenomenology of the evolution of the cooling QGP, and compare it to existing backgrounds in the literature which are late time expansions [57]. Existing work on the nonequilibrium behavior of QGP either only considers gluon plasmas, see i.e. [22], with no quark degrees of freedom or focuses on adiabatic approximations to late time asymptotics bypassing the chiral phase transition [40].

To allow for the dynamics, the Euclidean description should be extended a Lorentzian background. In this setting, space-time no longer ends at the horizon. We find that in the high temperature phase, the D-branes fall through the horizon, but end before reaching the black hole singularity. The D-branes do not end smoothly, but have a conical singularity which is interpreted as an annihilation diagram. As the plasma cools, the component of the D-branes within the horizon annihilates into gravitons, thus giving the appearance of 'pulling out' of the black hole. Next, we propose to perform a numerical simulation of the non-equilibrium dynamics of the passage of a quark-gluon plasma through a first order chiral phase transition, by modelling the process as a D-brane evolving in a time dependent Lorentzian gravitational background. This transition is of critical importance in cosmology and in current experiments involving heavy ion collisions and has phenomenological implications through the formation of disoriented chiral condensates [82]. The numerical analysis of the resulting equations of motion present enormous difficulties. We deal with these difficulties to the extent that enables us to do a first time simulation of a D-brane dynamically going through the topological phase transition. These developments are described in Chapter 5.

The third project described in this thesis is about invariant distributions of dynamical systems. A vast number of physically important phenomena exhibit chaos. One of the defining features of chaotic systems is that it is, in practice, impossible to predict their behavior over a long time. The types of questions for which there is some hope of finding an answer, with regard to the long time behavior of chaotic systems, are statistical in nature. The standard approach of computing statistical properties involves direct numerical simulation of the system over a sufficiently long period, with the assumption that the statistics converge rapidly to the correct answer, compared with the rate at which numerical errors are compounded by

the properties of chaos. In [47, 44] an inverse approach formulated in terms of the statistics is introduced. It was shown that it is possible to reverse engineer chaotic systems, beginning with an invariant distribution and a two-form, for which statistical properties such as polynomial correlation functions are captured by this invariant distribution. In fact, infinite classes of chaotic systems can be constructed for which statistical quantities are exactly known. These chaotic systems have different physical properties, depending on the analytic structure of the invariant distribution and the two-form, suggesting a novel classification of chaotic systems. In [47], several examples of chaotic systems for which direct numerical simulation and the inverse approach agree precisely are given. In this thesis, Monte-Carlo algorithms are applied with remarkable success to the computation of auto-correlation functions and power spectral densities of a chaotic system. To the best of my knowledge, this is the first time an auto-correlation function of a chaotic dynamical system has ever been computed by means other than direct numerical solution of the defining equations.

Let us pause for a moment to describe another connection between our deterministic dynamical systems and complex Langevin equation projects. Both projects are about constructing dynamical systems, whose long time averages correspond to desired distributions. The latter one includes random noise terms while the former does not. In the case of complex Langevin equations, this distribution is the path integral measure of a quantum field theory. In the case of deterministic dynamical systems, this distribution will be given by an experiment. In both cases, we will be interested in an equation that governs the stationary distribution. Both cases can be considered as subclasses of a generic system of Langevin equations,

$$\frac{dx_i}{dt} = F_i(x) + a_{ij}\eta_j, \tag{1.1}$$

where η_j are independent Gaussian random noises. Evolution of the associated

probability distribution of a system of Langevin equations is given by the famous Fokker-Planck equation. The deterministic dynamical systems project deals with the above system with a_{ij} set to zero. In this case there are complications related to ergodicity of measures formed by long time averages. In the complex Langevin case, the a_{ij} have to satisfy some certain constraints as shown in the appendix.

The second and third chapters of this thesis are based on publications co-authored with Gerald Guralnik, [45] and [46] respectively. The fourth chapter is based on an article co-authored with Gerald Guralnik and Zachary Guralnik, [44], expanded significantly with unpublished results. The material in the fifth chapter evolved from unpublished suggestions by R. Brower, F. Cooper, G. Guralnik and Z. Guralnik and was done in collaboration with Gerald Guralnik and Zachary Guralnik and has not appeared elsewhere.

Chapter Two

Stationary Distributions of Complex Langevin Equations

Besides the conventional Feynman path integral formalism, a quantum field theory can also be defined by a differential equation based method: the Schwinger action principle. Given by the variational formula,

$$\delta \langle t_1 |\, t_2 \rangle = i \langle t_1 |\, \delta S \,| t_2 \rangle \,,$$

where S in the action of a quantum field theory in a Minkowski space, the action principle leads to a set of functional differential equations that define the quantum field theory. Of these functional differential equations, the ones that involve variations with respect to the source fields are known as Schwinger-Dyson equations. The crucial point is that Schwinger-Dyson equations are differential equations and they have more than one solution. Only one of them corresponds to the Feynman path integral, if it exists at all. Other solutions, which we will call "exotic", can be written as complexified path integrals. These exotic solutions are important, among other things, in yielding a description of phase transitions in quantum field theories [33, 43]. We will summarize some of these results later in this section. In the rest of this section, we will use the phrase "solutions of a quantum field theory" to refer to the solutions of the associated Schwinger-Dyson equations.[1]

To see if the exotic solutions are useful for explaining physical phenomena, one needs analytical and numerical methods to study them. Perturbation theory is good for Feynman path integral, but not for a general solution of Schwinger-Dyson equations. As for numerical methods, standard Monte Carlo methods do not work in this case either, where the path integral weight is not positive-definite. This is the famous "sign problem". The root of the problem lies in the fact that Monte Carlo

[1] Other functional differential equations also follow from the action principle, those involving variations with respect to the couplings. It has been shown in [43] that in the continuum limit, solutions of the Schwinger-Dyson equations do satisfy these latter type of functional differential equations. Therefore, it is sufficient to study only the Schwinger-Dyson equations.

methods work on the probabilistic interpretation of the exponential path integral weight. In the case of complexified path integrals, the exponent becomes complex and the probabilistic interpretation fails. This chapter is a first attempt to use complex Langevin equations to calculate exotic solutions of a quantum field theory.

Complex Langevin equations were proposed by Parisi [92] and Klauder [66] to simulate systems with complex valued path integral weights. For d dimensional systems with real weights, a Langevin equation in $d+1$ dimensions may be used to study the partition function of the system. When properly set up, the Langevin process converges to a unique stationary distribution, which is the partition function of the associated system, in the limit of the additional dimension going to infinity. This fact was used by Parisi and Wu in the stochastic quantization of quantum fields [93]. For systems with complex actions, one can still write down a (complex) Langevin equation, as suggested by Parisi and Klauder, but this approach comes with many problems. First of all, it is not certain that the complex Langevin simulation will ever converge to a stationary distribution and if it does, there may be many such stationary distributions, see e.g. [37, 35, 36, 100, 72]. Salcedo noted that these stationary distributions may be constructed by path integrals over contours that connect zeros of the path integral weight e^{-S} [100]. Other authors noted that these stationary distributions satisfy Schwinger-Dyson equations, e.g. [14, 5, 55, 116]. On a completely different track of research, G. Guralnik with S. Garcia and Z. Guralnik studied the solution space of Schwinger-Dyson equations and noted that different solutions to Schwinger-Dyson equations may be written as path integrals over contours that connect zeros of the path integral weight e^{-S} [33, 43], exactly as Salcedo suggested for stationary distributions of the complex Langevin equation. Our aim in this chapter is to point out and clarify the connection between these two lines of research and attempt at using complex Langevin equations as a numerical

method of studying different solutions of a quantum field theory.

We start by a rather detailed explanation of the mechanism of complex Langevin equations and the problems associated with them in section 2.1. Section 2.2 contains the main result of this chapter. There, in a zero dimensional setting, we show that the stationary distributions of a complex Langevin equation are the solutions of the Schwinger-Dyson equations for the associated quantum field theory. Furthermore, these solutions may be constructed by changing the integration contour of path integrals from real paths to contours that connect the zeros of the path integral weight e^{-S} on the complex plane. In section 2.3, we do the trivial generalization of the problem to a lattice and discuss related issues. We conclude by further summarizing the results of [33] and [43] and point out the connection between solution space of a quantum field theory and stationary distributions of complex Langevin equations. Based on this observation, we propose complex Langevin equations as a numerical method of studying solution space of a quantum field theory.

2.1 The Complex Langevin Equation

In this section, we introduce Langevin equations. We discuss zero dimensional quantum field theories with a scalar field for simplicity. Generalization to vector fields and higher dimensions is straightforward, see e.g. [86]. For systems with action $S(\phi)$, we are interested in calculating expectation values like

$$\langle \mathcal{O} \rangle = \frac{\int d\phi \, \mathcal{O}(\phi) e^{-S(\phi)}}{\int d\phi \, e^{-S(\phi)}}, \tag{2.1}$$

using Langevin equations. We will assume $S(z)$ to be an analytic function of the complex variable z.

Note that our formulation is a Euclidean space formulation, i.e. the path integral weight will be complex only when the action is complex. However in Minkowski space formulations of quantum field theories, the path integral weight will still be complex even though the action is real, since the weight is defined by $e^{iS_M(\phi)}$. When we speak about complex actions in Euclidean space, our results will be applicable to Minkowski space actions after necessary modifications. One has to note that $S(\phi) = -iS_M(\phi)$ and introduce appropriate factors of i's in the generating function definition and terms of Schwinger-Dyson equation.

2.1.1 Real Actions

When the action is real (for the moment ϕ is a real field), one can create a stochastic process using a Langevin equation with a unique stationary distribution $\frac{e^{-S(\phi)}}{\int d\phi\, e^{-S(\phi)}}$:

$$d\phi(\tau) = -\frac{\partial S}{\partial \phi(\tau)} d\tau + dw(\tau), \tag{2.2}$$

where τ is a fictitious time and $w(\tau)$ is the Wiener process normalized to satisfy:

$$\langle dw(\tau) \rangle = 0, \qquad \langle dw(\tau) dw(\tau) \rangle = 2d\tau, \qquad \langle dw(\tau_1) dw(\tau_2) \rangle = 0 \quad (\tau_1 \neq \tau_2). \tag{2.3}$$

Then one can run this Langevin process to calculate the intended expectation values as in equation (2.1). We first show that this Langevin process really converges to the intended stationary distribution.

Associated with the Langevin process is a probability density $P(\phi, \tau)$

$$\langle F(\phi(\tau))\rangle = \int d\phi\, F(\phi) P(\phi, \tau), \tag{2.4}$$

which can be shown (e.g. [34]) to satisfy the Fokker-Plack equation

$$\frac{\partial P(\phi, \tau)}{\partial \tau} = \frac{\partial}{\partial \phi}\left(\frac{\partial}{\partial \phi} + \frac{\partial S}{\partial \phi}\right) P(\phi, \tau). \tag{2.5}$$

Note that the Fokker-Planck equation enables the normalization condition

$$\int d\phi\, P(\phi, \tau) = 1 \tag{2.6}$$

to be independent of time since

$$\frac{d}{d\tau}\int d\phi\, P(\phi, \tau) = \int d\phi\, \frac{\partial}{\partial \phi}\left[\left(\frac{\partial}{\partial \phi} + \frac{\partial S}{\partial \phi}\right) P(\phi, \tau)\right] = 0, \tag{2.7}$$

with an appropriate boundary condition on $P(\phi, \tau)$.

Now we look at the asymptotic behavior of $P(\phi, \tau)$ as fictitous time goes to infinity. Introducing the quantity

$$Q(\phi, \tau) \equiv P(\phi, \tau) e^{S(\phi)/2}, \tag{2.8}$$

we can rewrite equation (2.5) as

$$\begin{aligned}
\frac{\partial Q(\phi, \tau)}{d\tau} &= -\left(-\frac{\partial}{\partial \phi} + \frac{1}{2}\frac{\partial S}{\partial \phi}\right)\left(\frac{\partial}{\partial \phi} + \frac{1}{2}\frac{\partial S}{\partial \phi}\right) Q(\phi, \tau) \\
&= -\left[-\frac{\partial^2}{\partial \phi^2} - \frac{1}{2}\frac{\partial^2 S}{\partial \phi^2} + \frac{1}{4}\left(\frac{\partial S}{\partial \phi}\right)^2\right] Q(\phi, \tau) \\
&= -H_{FP}\, Q(\phi, \tau).
\end{aligned} \tag{2.9}$$

where the Hermitian operator H_{FP} is called the Fokker-Planck Hamiltonian. Then

$$Q_0(\phi) = e^{-S(\phi)/2} \tag{2.10}$$

is an eigenstate of the Hamiltonian H_{FP} with eigenvalue 0. Furthermore, (assuming $Q_0 \in L^2$) it is the ground state since it is nowhere vanishing. Then the time independent eigenvalue equation

$$H_{FP}Q_n(\phi) = E_nQ_n(\phi), \tag{2.11}$$

has solutions with the property $E_n > 0$, for $n > 0$. Using these eigenvalues and eigenfunctions, one can write any solution to equation (2.9) as

$$Q(\phi,\tau) = P(\phi,\tau)e^{S(\phi)/2} = \sum_{n=0}^{\infty} a_n\, Q_n(\phi)e^{-E_n\tau}. \tag{2.12}$$

Since we are looking for solutions $P(\phi,\tau)$ that are probability distributions, we apply the normalization condition (2.6), which sets $a_0 = 1/\int d\phi\, e^{-S(\phi)}$. This result is obtained by using the orthonormality of the eigenfunctions Q_n. Other coefficients are set by the initial probability distribution associated with the random variable $\phi(\tau)$ at $\tau = 0$. Then the limit

$$\lim_{\tau\to\infty} Q(\phi,\tau) = a_0\, Q_0(\phi), \tag{2.13}$$

implies that one recovers the desired stationary probability distribution for the Langevin process as the fictitous time goes to infinity:

$$\lim_{\tau\to\infty} P(\phi,\tau) = \frac{e^{-S(\phi)}}{\int d\phi\, e^{-S(\phi)}}. \tag{2.14}$$

Note that this result is independent of the initial conditions. Going back to the

expectation value problem (2.1),

$$\lim_{\tau\to\infty} \langle \mathcal{O}(\phi(\tau))\rangle = \langle \mathcal{O}(\phi)\rangle \,, \tag{2.15}$$

with $\langle \mathcal{O}(\phi)\rangle$ given by (2.1) and ergodicity assures the averaging over the path prescription

$$\langle \mathcal{O}(\phi)\rangle = \lim_{T\to\infty} \frac{1}{T}\int_0^T \mathcal{O}(\phi(\tau))d\tau. \tag{2.16}$$

These observations have been used by Parisi and Wu in the past to formulate the stochastic quantization of quantum fields [93]. See e.g. [25, 86, 87] for a detailed discussion.

2.1.2 Complex Actions

Now we turn to the case where the action is complex. We want to know if we can still use the Langevin equation to calculate desired expectation values. We start by rewriting equation (2.2) (now S being complex) in terms of two real variables $\phi_R(\tau)$ and $\phi_I(\tau)$ as

$$\begin{aligned} d\phi_R(\tau) &= -Re\left[\frac{\partial S}{\partial \phi(\tau)}\right] d\tau + dw(\tau), \\ d\phi_I(\tau) &= -Im\left[\frac{\partial S}{\partial \phi(\tau)}\right], \end{aligned} \tag{2.17}$$

where $\phi(\tau) = \phi_R(\tau) + i\phi_I(\tau)$. $w(\tau)$ is again the Wiener process that is normalized to satisfy the mean and variance conditions of equation (2.3). Note that the equation for $d\phi_I$ has a zero diffusion coefficient (see [85] for an example where it is not zero), but still is a stochastic equation through its dependence on ϕ_R. Complex Langevin

equations may be modified to include a term, the kernel, that may be useful to stabilize the system, e.g [108, 90]. For our purposes, we focus on equation (2.17). Note that we have two different random variables $\phi_R(\tau)$ and $\phi_I(\tau)$, therefore the real probability distribution associated with equation (2.17) will be of the form

$$\langle F(\phi(\tau))\rangle = \int d\phi_R d\phi_I \, F(\phi_R + i\phi_I) P(\phi_R, \phi_I, \tau) \tag{2.18}$$

where we assume F to be analytic.

There are two important questions related to this process. The first question is whether the probability distribution $P(\phi_R, \phi_I, \tau)$ converges to a stationary distribution at all,

$$\lim_{\tau\to\infty} P(\phi_R, \phi_I, \tau) \stackrel{?}{=} \hat{P}(\phi_R, \phi_I). \tag{2.19}$$

If it does, does it converge to the desired result:

$$\int d\phi_R d\phi_I \, F(\phi_R + i\phi_I)\hat{P}(\phi_R, \phi_I) \stackrel{?}{=} \frac{\int d\phi_R \, F(\phi_R) e^{-S(\phi_R)}}{\int d\phi_R \, e^{-S(\phi_R)}}. \tag{2.20}$$

None of these questions have been completely answered so far. Some rigorous conditions to verify aposteriori the correct convergence of the process are given in [37, 35, 36].

To understand the difficulties related to the convergence problem, we derive the Fokker-Planck equation. First we note that applying the rules of Ito calculus (see for example [34]) to the complex Langevin equation (2.17) will give the identity

$$\begin{aligned} \frac{d}{d\tau}\langle F(\phi(\tau))\rangle &= \left\langle \frac{\partial^2 F}{\partial \phi_R^2} - \frac{\partial F}{\partial \phi_R} Re\left[\frac{\partial S}{\partial \phi}\right] - \frac{\partial F}{\partial \phi_I} Im\left[\frac{\partial S}{\partial \phi}\right]\right\rangle \\ &= \left\langle \frac{\partial^2 F}{\partial \phi^2} - \frac{\partial F}{\partial \phi}\left[\frac{\partial S}{\partial \phi}\right]\right\rangle, \end{aligned} \tag{2.21}$$

where the last line follows from the analyticity of $F(\phi)$. Then using equation (2.18) one can show that $P(\phi_R, \phi_I, \tau)$ (assuming appropriate differentiability and boundary conditions) satisfies the following Fokker-Planck equation:

$$\begin{aligned}\frac{\partial P(\phi_R,\phi_I,\tau)}{\partial \tau} &= O_{FP} P(\phi_R,\phi_I,\tau) \\ &= \left(\frac{\partial^2}{\partial \phi_R^2} + \frac{\partial}{\partial \phi_R} Re\left[\frac{\partial S}{\partial \phi}\right] + \frac{\partial}{\partial \phi_I} Im\left[\frac{\partial S}{\partial \phi}\right]\right) P(\phi_R,\phi_I,\tau). \end{aligned} \tag{2.22}$$

A general statement on the existence of a unique zero eigenvalue (stationary) solution $\hat{P}(\phi_R, \phi_I)$ for the operator O_{FP} cannot be made. Furthermore, zero eigenvalue solutions may exist in the sense of distributions [36].

One can assume a complex valued function $\tilde{P}(\phi_R, \tau)$ on the real axis such that

$$\int_{\Re} d\phi_R \, F(\phi_R)\tilde{P}(\phi_R,\tau) = \int d\phi_R d\phi_I \, F(\phi_R + i\phi_I) \, P(\phi_R,\phi_I,\tau), \tag{2.23}$$

based on the implicit assumption that this equation actually has a solution [92]. The reverse question, existence of a positive $P(\phi_R, \phi_I, \tau)$ given a complex $\tilde{P}(\phi_R, \tau)$ is disscussed in [101, 113, 102]. Using this definition, analyticity of $F(\phi)$ and integration by parts in equation (2.21) one can show that $\tilde{P}(\phi_R, \tau)$ satisfies the pseudo Fokker-Planck equation

$$\frac{\partial \tilde{P}(\phi_R,\tau)}{\partial \tau} = \tilde{O}_{FP}\tilde{P}(\phi_R,\tau) = \frac{\partial}{\partial \phi_R}\left(\frac{\partial}{\partial \phi_R} + \frac{\partial S}{\partial \phi_R}\right)\tilde{P}(\phi_R,\tau), \tag{2.24}$$

which has the same form as that of equation (2.5).

A formal solution to equation (2.23) was introduced in [84]. First note that

$$F(\phi_R + i\phi_I) = e^{i\phi_I \frac{\partial}{\partial \phi_R}} F(\phi_R), \tag{2.25}$$

due to the analyticity of $F(\phi)$. Inserting this statement into equation (2.23) and performing the partial integration assuming necessary boundary and differentiability conditions,

$$\tilde{P}(\phi_R, \tau) = \int d\phi_I \, e^{-i\phi_I \frac{\partial}{\partial \phi_R}} P(\phi_R, \phi_I, \tau). \tag{2.26}$$

Because the action $S(\phi_R)$ is complex, one cannot make general statements about the spectrum of $\tilde{O}_{FP}$ (see [67] for the spectral theorem for a limited class of such operators). Furthermore, the relation between the pseudo Fokker-Planck equation and the complex Langevin equation were derived based on certain assumptions. This should be understood in the sense of distributions, meaning only a formal expression of the identity (2.21). Note that $e^{-S(\phi_R)}$ is still a stationary solution (i.e. $\tilde{O}_{FP}\, e^{-S(\phi_R)} = 0$), but in general the stationary solutions exist as distributions and the uniqueness of stationary solution is not certain [100].

2.2 Stationary Distributions of the Complex Langevin Equation and the Boundary Conditions of the Schwinger-Dyson Equation

Despite the difficulties in proving rigorous results, complex Langevin simulations have been used to study many different problems. Interesting cases are those for which the simulation converges to a stationary distribution which is not equivalent to the original complex distribution, e.g. [92, 73, 100, 49, 72, 30]. This must be related to the existence of other stationary distributions. Here we discuss a conjecture related to the stationary distributions by Salcedo [100] and the well know result that stationary distributions satisfy Schwinger-Dyson identities, e.g. [14, 5, 55, 116].

We show that they follow from one another, based on other work on the boundary conditions of Schwinger-Dyson equations [33, 43]. We will point out the results of these references during our discussion.

We start by assuming that the complex Langevin process has a stationary state. For the stationary distribution, the LHS of equation (2.21) must be zero. Then setting $F(\phi) = \phi^n$, $n = 1, 2, 3, \ldots$, reproduces the Schwinger-Dyson identities for the Green's functions of the quantum field theory defined by the action S, i.e.

$$\begin{aligned} n = 1 \quad &\longrightarrow \quad \left\langle \frac{\partial S}{\partial \phi} \right\rangle = 0, \\ n = 2 \quad &\longrightarrow \quad \left\langle \phi \frac{\partial S}{\partial \phi} \right\rangle = 1, \\ &\ldots, \\ n = k \quad &\longrightarrow \quad \left\langle \phi^{k-1} \frac{\partial S}{\partial \phi} \right\rangle = (k-1) \left\langle \phi^{k-2} \right\rangle . \end{aligned} \tag{2.27}$$

Now define the generating function $Z(j)$ for the stationary distribution

$$Z(j) = \sum_{n=0}^{\infty} \frac{\langle \phi^n \rangle \, j^n}{n!} = \left\langle e^{j\phi} \right\rangle . \tag{2.28}$$

We will assume that the radius of convergence for this series is nonzero. Then there exists a neighbourhood of j around $j = 0$ such that the Schwinger-Dyson differential equation holds. i.e.

$$\left. \frac{\partial S}{\partial \phi} \right|_{\phi = \frac{d}{dj}} Z(j) = jZ(j). \tag{2.29}$$

To see that (2.29) produces the same identites as (2.27), substitute the definition of the generating function $Z(j)$, equation (2.28), in the Schwinger-Dyson equation, differentiate with respect to j an appropriate number of times and set $j = 0$ at the end. One gets the identities (2.27) order by order at the end of this procedure.

Solutions of the Schwinger-Dyson equation are the stationary distributions of the complex Langevin equation. We solve equation (2.29) following [33]. First define

$$Z_\Gamma(j) = \int_\Gamma d\phi\, G(\phi) e^{j\phi}, \tag{2.30}$$

where Γ is a contour over the complex plane. Inserting this into equation (2.29) one gets:

$$0 = -\, G(\phi) e^{j\phi}\big|_{\partial\Gamma} + \int_\Gamma d\phi \left[\frac{\partial S}{\partial \phi} G(\phi) + \frac{dG(\phi)}{d\phi}\right] e^{j\phi}. \tag{2.31}$$

This equation can be solved for

$$G(\phi) = e^{-S(\phi)}, \tag{2.32}$$

and Γ is contour that connects the zeros of $e^{-S(\phi)+j\phi}$ on the complex ϕ plane.

Now consider polynomial actions,

$$S(\phi) = \sum_{i=1}^{m} \frac{1}{l} g_l \phi^l, \quad m > 1. \tag{2.33}$$

The contours will be defined by m wedges, where m is the order of $S(\phi)$, such that $Re(g_m \phi^m) \to +\infty$ as $|\phi| \to \infty$. Contours obtained by deforming Γ without crossing singularities of $e^{-S(\phi)}$ and keeping boundary points fixed result in the same generating function. Note that set of all $Z_\Gamma(j)$ will not be independent. The Schwinger-Dyson equation will be of order $(m-1)$, and will have $(m-1)$ independent solutions. For example, if $S = i\phi^3$, then $e^{-S(\phi)}$ will have three zeros in the complex plane, Figure 2.1,which will define three different generating functions. However the Schwinger-Dyson equation will be a second order linear differential equation, which has two independent solutions. Therefore any two of the three possible paths will define an independent solution set.

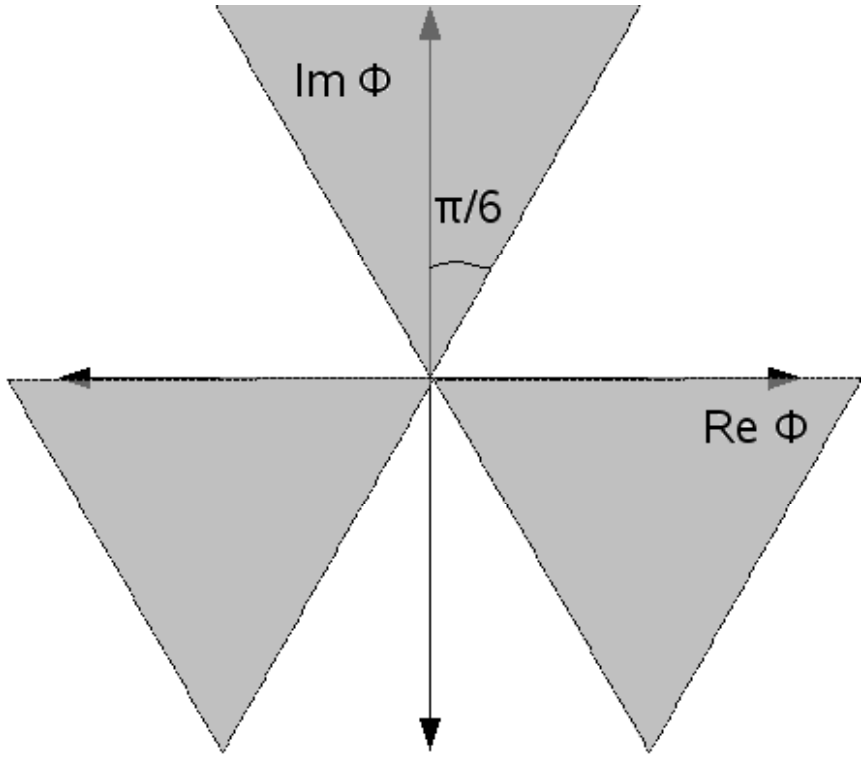

Figure 2.1: The region defined by $\sin(3\theta) < 0$.
θ is the argument of ϕ. Shaded region corresponds to $\sin(3\theta) < 0$. Any path starting and ending at infinity within these wedges corresponds to a particular solution of zero dimensional $i\phi^3$ theory.

Since the Schwinger-Dyson equation is linear, any linear combination of the (independent) solutions will also be a solution,

$$Z(j) = \sum_{\Gamma_I} a_{\Gamma_I} Z_{\Gamma_I}(j), \tag{2.34}$$

where Γ_I define an independent subset of paths Γ. Now defining the distribution $\tilde{P}_\Gamma(\phi_R)$ on the real plane as

$$\int_{\Re} d\phi_R \, \phi^n(\phi_R) \tilde{P}_\Gamma(\phi_R) = \frac{1}{Z_\Gamma(0)} \left. \frac{d^n Z_\Gamma(j)}{dj^n} \right|_{j=0}, \tag{2.35}$$

which can always be done by a real parametrization of the complex contour Γ, one sees that the equilibrium distribution can be written as a linear combination

$$\tilde{P}_{eq}(\phi_R) = \sum_{\Gamma_I} a_{\Gamma_I} \tilde{P}_{\Gamma_I}(\phi_R), \tag{2.36}$$

which is exactly the conjecture that was made by Salcedo [100], where he derived the same result for a general complex distribution by considering the stationary solutions of the pseudo Fokker-Planck equation (2.24) to be realized as distributions rather than functions. Actually, we managed to refine his conjecture (which considers a sum over all Γ instead of Γ_I on the RHS of equation (2.36)) by showing that not all of $\tilde{P}_\Gamma(\phi_R)$ are independent through the use of Schwinger-Dyson equations. A final note is that the coefficients a_Γ may depend on initial conditions. We will illustrate these points with numerical examples in the next section. [100] has other examples discussed along the lines mentioned here.

2.2.1 Zero Dimensional Examples

We consider two examples here,

$$S_1(\phi) = i\frac{\phi^3}{3}, \quad S_2(\phi) = -\frac{\phi^4}{4}. \tag{2.37}$$

In both cases, we will derive an independent set of generating functionals and identify the particular solution of the Schwinger-Dyson equation to which the simulation converges by observing the sampling points in the complex plane. We will see that the change of initial conditions may change the resulting stationary distribution. Zero dimensional field theories have been heavily studied with complex Langevin equations before, e.g.[16, 92, 73, 90, 55, 49, 30, 100]. What makes our presentation different from the previous studies is the relation to complex path integral solutions of Schwinger-Dyson equations.

In our simulations, we used the Euler method which is a first-order algorithm, see e.g. [34]. The complex Langevin equation (2.17) with this discretization is given by

$$\begin{aligned}
\phi_R(\tau_{j+1}) &= \phi_R(\tau_j) - Re\left[\frac{\partial S}{\partial \phi(\tau_j)}\right]\Delta\tau + \sqrt{2\Delta\tau}\eta_j, \\
\phi_I(\tau_{j+1}) &= \phi_I(\tau_j) - Im\left[\frac{\partial S}{\partial \phi(\tau_j)}\right]\Delta\tau, \\
\tau_{j+1} &= \tau_j + \Delta\tau, \qquad j \in \mathbb{Z},
\end{aligned} \tag{2.38}$$

where $\Delta\tau$ is the time step, and η_j is a Gaussian random variable with zero mean and unit variance satisfying

$$\langle \eta_j \rangle = 0, \quad \langle \eta_j \eta_k \rangle = \delta_{jk}. \tag{2.39}$$

Table 2.1: Comparison of Langevin simulation results of action $S_1(\phi)$ with the correlators of the generating functions $Z_1^{(1)}(j)$ and $Z_2^{(1)}(j)$.

The simulation ran from $\tau_i = 0$ to $\tau_f = 1000$ with $\Delta\tau = 0.001$ with different initial conditions. We start calculating expectation values after $\tau = 5$. Error bars stand for the standard deviation over 50 runs. 5 diverging paths discarded for the second initial condition. Average is over 45 converging paths. See [6] for a justification of this procedure. The last two rows show the corresponding exact values for the generating functions calculated by numerical integration.

	$\langle\phi\rangle$	$\langle\phi^2\rangle$	$\langle\phi^3\rangle$
$\phi(0) = 0$	$-0.0034 - i0.7289$	$i0.0053$	$0.0025 - i0.9998$
	$\pm 0.0190 \pm i0.0076$	$\pm 0.0003 \pm i0.0364$	$\pm 0.0292 \pm i0.0347$
$\phi(0) = 5i$	$-0.0016 - i0.7315$	$i0.0026$	$0.0012 - i1.0080$
	$\pm 0.0176 \pm i0.0079$	$\pm 0.0003 \pm i0.0325$	$\pm 0.0260 \pm i0.0330$
$\phi(0) = 1 - i$	$-0.0049 - i0.7289$	$i0.0085$	$0.0053 - i0.9994$
	$\pm 0.0246 \pm i0.0071$	$\pm 0.0003 \pm i0.0457$	$\pm 0.0343 \pm i0.0307$
$Z_1^{(1)}$	$-i0.7290$	0	$-i$
$Z_2^{(1)}$	$-0.6313 + i0.3645$	0	$-i$

All our simulations run from $\tau_i = 0$ to $\tau_f = 1000$ with $\Delta\tau = 0.001$. We start calculating expectation values after $\tau = 5$. Error bars stand for the standard deviation of 50 runs.

For $S_1(\phi)$, an independent set of solutions to the Schwinger-Dyson equation (3.12) can be written by connecting the three zeros shown in Figure 2.1, i.e. $i\infty$, $e^{-i\frac{\pi}{6}}\infty$ and $e^{-i\frac{5\pi}{6}}\infty$. We choose the following generating functions $Z_1^{(1)}(j)$ and $Z_2^{(1)}(j)$:

$$
\begin{aligned}
Z_{1,2}^{(1)}(j) &= \frac{\int_{\Gamma_{1,2}} d\phi \, \exp\left\{-i\frac{\phi^3}{3} + j\phi\right\}}{\int_{\Gamma_{1,2}} d\phi \, \exp\left\{-i\frac{\phi^3}{3}\right\}}, \\
\Gamma_1 &= [e^{-i\frac{5\pi}{6}}\infty, 0] + [0, e^{-i\frac{\pi}{6}}\infty], \\
\Gamma_2 &= [e^{-i\frac{5\pi}{6}}\infty, 0] + [0, i\infty].
\end{aligned} \tag{2.40}
$$

We expect the result of the complex Langevin simulation to converge to a linear combination of the distributions defined by these generating functions.

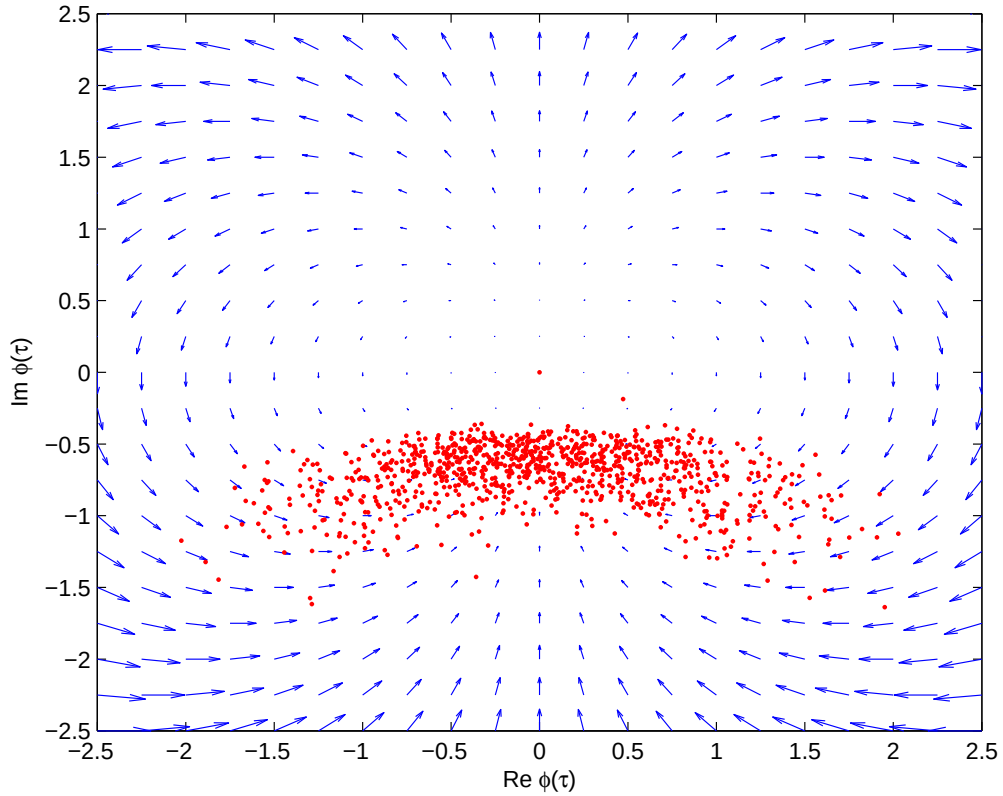

Figure 2.2: A sample path for the complex Langevin simulation of the action $S_1(\phi)$. Parameters are the same as in Table 2.1. 1000 sample points are shown with equal time intervals. Initial condition is $\phi(0) = 0$. We also plot the velocity field for the deterministic complex Langevin equation.

Table 2.1 shows the results of simulations for this theory. We compare with the exact results for the Green's functions of $Z_1^{(1)}(j)$ and $Z_2^{(1)}(j)$. Figure 2.2 shows a sample path for the simulation of this action. We repeated the simulations with different initial conditions, some of which are given in Table 2.1. For the converging simulations, the sample paths localized around the same region as of Figure 2.2 and the obtained numerical values were similar to those of Table 2.1. For some initial conditions with large $|\partial S/\partial\phi|$ values (e.g. $\phi(0) = 5i$), we observed nonconverging paths, which could be made to converge (and localized in the same region of Figure 2.2) by decreasing the step size. This behavior can be understood by inspecting the deterministic part of the complex Langevin equation (i.e. without a noise term in equation (2.17)).[2] The solution to to the deterministic part will be:

$$\phi_d(\tau) = \frac{\phi_d(0)}{1 + i\phi_d(0)\tau}, \tag{2.41}$$

where $\phi_d(0)$ is the initial condition. We see that $\phi = 0$ is a global attractor for all points except the positive imaginary axis. Any path starting from the positive imaginary axis will go to infinity staying on the imaginary axis (i.e. $i\infty$) in finite time. When the noise term is included, which points along the real axis, these diverging paths will come out the positive imaginary axis and eventually approach the sampling region shown in Figure 2.2. However, numerically these paths may cause a problem. When the step size is not small enough, the simulation may go to infinity around these points in finite time. This is called the "runaway solution" problem, see [6] for other examples and more details. Despite this numerical problem, which can be cured by smaller step sizes, the simulations suggest that for the action $S_1(\phi)$ the complex Langevin algorithm always converges. Inspecting Table 2.1 we see that the

[2]Recently in [15] and [1] it was emphasized that the fixed point structure of the deterministic complex Langevin equation has important role in the convergence behavior of the complex Langevin dynamics. In Figures 2.2 and 2.3 we plot the velocity fields of the deterministic complex Langevin equation. We thank the anonymous reviewer of [45] for bringing these papers to our attention.

Table 2.2: Comparison of Langevin simulation results of action $S_2(\phi)$ with correlators of the generating functions $Z_a^{(2)}(j)$, $Z_b^{(2)}(j)$ and $Z_c^{(2)}(j)$.

The simulation ran form $\tau_i = 0$ to $\tau_f = 1000$ with $\Delta\tau = 0.001$ with different initial conditions. We start calculating expectation values after $\tau = 5$. Error bars stand for the standard deviation over 50 runs. The last two rows show the corresponding exact values for the generating functions calculated by numerical integration.

	$\langle\phi\rangle$	$\langle\phi^2\rangle$	$\langle\phi^3\rangle$	$\langle\phi^4\rangle$
$\phi(0) = 0$	no convergence	no convergence	no convergence	no convergence
$\phi(0) = i$	$-0.0014 + i0.9781$	$-0.6765 - i0.0029$	0.0038	$-1.0014 - i0.0035$
	$\pm 0.0126 \pm i0.0057$	$\pm 0.0078 \pm i0.0295$	$\pm 0.0452 \pm i0.0003$	$\pm 0.0462 \pm i0.0242$
$\phi(0) = -i$	$-0.0008 - i0.9794$	$-0.6781 + i0.0081$	0.0024	$-1.0054 - i0.0041$
	$\pm 0.0138 \pm i0.0071$	$\pm 0.0098 \pm i0.0318$	$\pm 0.0480 \pm i0.0003$	$\pm 0.0312 \pm i0.0491$
$Z_a^{(2)}$	$i0.9777$	-0.6760	0	-1
$Z_b^{(2)}$	$-i0.9777$	-0.6760	0	-1
$Z_c^{(2)}$	-0.9777	0.6760	0	-1

distribution defined by $Z_1^{(1)}(j)$ has correlators within the error range of numerical data. The sample path of Figure 2.2 shows that the simulation does sample around the path of $Z_1^{(1)}(j)$. It definitely does not sample around the positive imaginary axis. Based on these observations, we conjecture that the complex Langevin simulation for $S_1(\phi) = i\frac{\phi^3}{3}$ theory always converge to the distribution defined by the generating function $Z_1^{(1)}(j)$.

Now we turn to $S_2(\phi) = -\phi^4/4$. Note that this action is real, however $e^{-S(\phi)}$ does not define a probability distribution on the real line, as the integral is divergent. The complex evolution of the associated Langevin equation is introduced by a choice of complex initial conditions. This procedure, choosing complex initial conditions, will turn every real Langevin process to a complex Langevin process. The statements we made about complex Langevin equations are valid for these cases also.

An independent set of generating functions for this theory can be written by connecting the four zeros of $S_2(\phi)$ on the complex plane, i.e. $e^{i\frac{\pi}{4}}\infty$, $e^{-i\frac{\pi}{4}}\infty$, $e^{i\frac{3\pi}{4}}\infty$ and

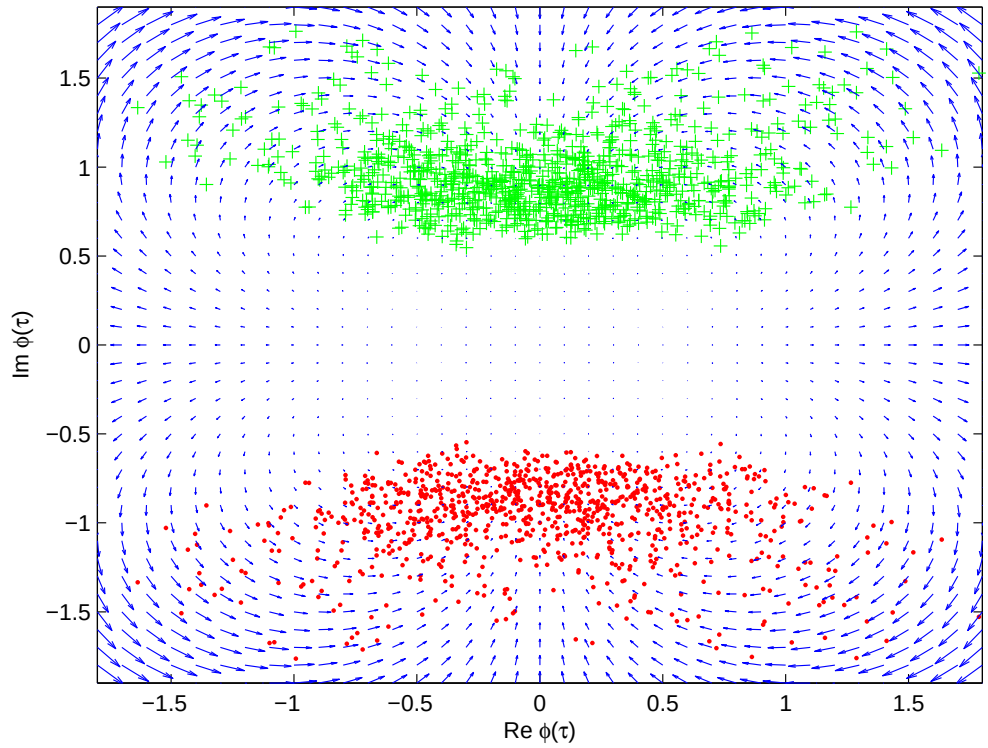

Figure 2.3: Two sample paths for the complex Langevin simulation of the action $S_2(\phi)$.
Parameters are the same as in Table 2.2. 1000 sample points are shown with equal time intervals. Initial condition is $\phi(0) = i$ for the path marked by "+"s and $\phi(0) = -i$ for the path marked by "·"s. We also plot the velocity field for the deterministic complex Langevin equation.

$e^{-i\frac{3\pi}{4}}\infty$. We choose the following generating functions $Z_1^{(2)}(j)$, $Z_2^{(2)}(j)$ and $Z_3^{(2)}(j)$:

$$
\begin{aligned}
Z^{(2)}_{a,b,c}(j) &= \frac{\int_{\Gamma_{a,b,c}} d\phi \, \exp\left\{\frac{\phi^4}{4} + j\phi\right\}}{\int_{\Gamma_{a,b,c}} d\phi \, \exp\left\{\frac{\phi^4}{4}\right\}}, \\
\Gamma_a &= [e^{i\frac{3\pi}{4}}\infty, 0] + [0, e^{i\frac{\pi}{4}}\infty], \\
\Gamma_b &= [e^{-i\frac{3\pi}{4}}\infty, 0] + [0, e^{-i\frac{\pi}{4}}\infty], \\
\Gamma_c &= [e^{-i\frac{3\pi}{4}}\infty, 0] + [0, e^{i\frac{3\pi}{4}}\infty].
\end{aligned} \tag{2.42}
$$

We expect to see the complex Langevin simulation converge to a linear combination of the distributions defined by these generating functions.

Table 2.2 shows the simulation results with different initial conditions compared with the correlators of the generating functions. In contrast to the previous case, we see that the results of the simulation is initial value dependent. Initial points on the real axis do not converge at all. Initial values above and below the real axis converge, but the sample points localize in different regions of the complex ϕ plane giving different results, see Figure 2.3. We can understand this behavior again by inspecting the deterministic part of the complex Langevin equation. This time the solution will be:

$$
\phi_d(\tau) = \frac{\phi_d(0)}{\sqrt{1 - 2[\phi_d(0)]^2\tau}} \tag{2.43}
$$

1 where $\phi_d(0)$ is the initial condition and the square root function gives the principal root. We see that $\phi = 0$ is a global attractor for every point on the complex plane except the real line. The origin will repell any path starting on the real line; these paths will diverge in finite time. When the real noise term is added, simulations with real initial points will stay on the real line and due to the repulsion they will diverge. Initial points on the upper/lower half of the complex plane will be attracted by the origin and the simulations will sample in the upper/lower half plane as seen

in Figure 2.3. As a result, upper half plane initial points will converge to a different solution of the Schwinger-Dyson equation than those of the lower half plane initial points. Table 2.2 shows two simulations starting with $\phi(0) = i$ and $\phi(0) = -i$. We see that the correlators of $Z_a^{(2)}$ are in the error range of the former initial condition, while the correlators of $Z_b^{(2)}$ are in the range of the latter simulation. Based on these observations, we conjecture that for $S_2(\phi)$, the complex Langevin equation will diverge if the initial condition is real, converge to the distribution defined by $Z_a^{(2)}(j)$ if the initial condition is on the upper half of the complex plane or converge to the distribution defined by $Z_b^{(2)}(j)$ otherwise.

One might suspect that either or both of the two stationary states we discussed are quasi-stationary states and consequently expect to see the system converge to a unique stable stationary state after a long enough simulation time. Assuming convergence to a stationary state, we will argue that this is not the case, initial points above and below the real line will behave differently in the whole range of simulation. Since the path of the complex field ϕ is continuous (but not differentiable), a complex Langevin process starting from above the real line will never end up below the real line. The reverse statement holds also. The reason is that any path going from one half plane to the other must pass through the real line, and once the path is on the real line, it stays on the real line. Both the noise term and the drift term points along the real line. Furthermore, the path on the real line will show nonconvergent behavior as discussed above. So either, all paths diverge at the end, or, assuming convergence, initial point above and below the real line end up sampling in different regions of the complex plane, converging to different stationary distributions. This initial value dependence is crucial in complex Langevin equations.

Actions $S_1(\phi)$ and $S_2(\phi)$ were studied in the context of $\mathcal{PT}$-symmetric quantum field theories in [16], where only one of the path integral solutions to the Schwinger-

Dyson equation is considered, e.g. [11]. In fact, the authors of [16], Bernard and Savage, provided a formal proof that the complex Langevin equation for $S_1(\phi)$ should always converge to the distribution defined by $Z_1^{(1)}(j)$, regardless of the initial condition, which we have also observed in our simulations. The formal proof is based on the methods of [84] and involves defining $\tilde{P}(\phi_c, \tau)$ of equation (2.23) as a projection of $P(\phi_R, \phi_I, \tau)$ to the complex integration contour Γ_1 (after necessary partial integrations), as opposed to the real line as of equation (2.26). Then the associated Fokker-Planck Hamiltonian will have a real and positive spectrum with one zero eigenvalue. Bernard and Savage argued that with slight modifications the same reasoning applies for $S_2(\phi)$ with the integration contour of Γ_b. They also noted that in simulations of $S_2(\phi)$ one has to choose the initial point $\phi(0)$ to be in the lower half of the complex ϕ plane or else the numerical simulations will be unstable. In our studies, we observed instabilities for initial points on the real line, which we interpreted to be nonconvergent behavior. Initial points in the lower and upper halves of the complex ϕ plane were observed to converge to different probability distributions (solutions of the Schwinger-Dyson equation). Our results suggest that the proof given by Bernard and Savage should be modified to include the effects of different initial conditions and all possible solutions of the Schwinger-Dyson equation. We believe that more attention must be paid on the boundary conditions of $P(\phi_R, \phi_I, \tau)$ when doing the projection.

Another point to note is that in both cases, we could not recover the whole solution set of the Schwinger-Dyson equations from the complex Langevin equation. In general, ϕ^N theories will have $N-1$ independent solutions to the Schwinger-Dyson equations. In the cases that we studied, we could recover only $N-2$ of them. We may need to consider other stochastic processes to recover the whole solution set.

2.3 Lattice Study

It is trivial to generalize this discussion to a lattice. In particular, consider a general Euclidean scalar field theory with a polynomial potential term,

$$\mathcal{L} = \partial^2\phi(x) + \sum_{l=1}^{n} \frac{g_l}{l}\phi^l(x). \tag{2.44}$$

For simplicity we consider a lattice in one dimension, which we call time and denote by t. The generating functional of the theory is now a function of m variables, where m is the number of lattice points. We denote the generating functional by $Z(j) = Z(j_1, \ldots, j_m)$. j_i is the source at i^{th} lattice point. We will use $j = 0$ to mean $j_1 = \ldots = j_m = 0$. By definition, correlation functions are given by

$$\left\langle \phi_1^{k_1} \ldots \phi_m^{k_m} \right\rangle = \frac{\partial^{k_1}}{\partial j_1^{k_1}} \ldots \frac{\partial^{k_m}}{\partial j_m^{k_m}} Z(j)\bigg|_{j=0}. \tag{2.45}$$

Next, we introduce the difference operators on the lattice,

$$\Delta_+ = \phi_{i+1} - \phi_{i-1}, \qquad \Delta_- = \phi_i - \phi_{i-1}, \tag{2.46}$$

where ϕ_i stands for the field value at i^{th} lattice point. The Schwinger-Dyson equation for the scalar field theory (2.44) can be written by a coupled set of partial differential equations. Using a centered discretization for time derivatives, the system is composed of a partial differential equation for every lattice point, given by

$$\left(\Delta_+\Delta_-\frac{\partial}{\partial j_i} + \sum_{l=1}^{n} g_l \frac{\partial^{l-1}}{\partial j_i^{l-1}}\right) Z(j) = j_i Z(j), \tag{2.47}$$

where the lattice spacing is set to one.

This discretization requires one to set boundary conditions on $Z(j)$ at initial and final lattice points. There are many possible choices, we choose periodic boundary conditions. We assume that the whole space is filled with a lattice of period m.

In the absence of the kinetic term, each lattice point acts independently. Therefore, study of the complex Langevin equation for zero dimensional case immediately tells us what will happen on the lattice. When the kinetic term is included, couplings between lattice points take action and problem is more complicated.

A general solution to the lattice Schwinger-Dyson equation can be written as

$$Z(j) = \frac{1}{\mathcal{N}} \int_{\Gamma_1} d\phi_1 \ldots \int_{\Gamma_m} d\phi_m \exp\left\{ -\sum_{i=1}^{m} \left(\frac{1}{2}\phi_i \Delta_+ \Delta_- \phi_i + \sum_{l=1}^{n} \frac{g_l}{l} \phi_i^l \right) + \sum_{i=0}^{m+1} j_i \phi_i \right\}, \quad (2.48)$$

where Γ_i denote contours that connect the zeros of the integrand on complex ϕ_i plane. We again normalize so that $Z(0) = 1$. For each lattice point there are n independent solutions, which leads to $m \times n$ independent solutions to the whole lattice Schwinger-Dyson equation. Because of linearity any combination of these solutions is also a solution. We note that there is no ambiguity in the solution written in this form, one can do the integrations in any order.

We turn to the complex Langevin equation for this problem. We again introduce a fictitious time coordinate τ. The complex Langevin system is now written in terms of stochastic variables $\phi_j(\tau) = \phi_{Rj}(\tau) + i\phi_{Ij}(\tau)$. For each lattice point $j = 1, \ldots, m$, there is a stochastic equation:

$$d\phi_j(\tau) = -\Delta_+ \Delta_- \phi_j(\tau) - \sum_{l=1}^{n} g_l \phi_j(\tau)^l + dw_j(\tau), \quad (2.49)$$

Table 2.3: A complex Langevin simulation is done for the one dimensional $-\phi^4/4$ theory.

128 lattice points are taken with spacing set to 1. An Euler method is used for fictitous time evolution. Simulations ran from $\tau_i = 0$ to $\tau_f = 10000$, with $\Delta\tau = 0.001$. The table below lists the first four equal time correlation functions obtained for two different initial conditions. We observed translation symmetry on the equal time correlation functions, therefore we list average values over lattice points, e.g. $\langle\phi\rangle = \frac{1}{128}\sum_{i=1}^{128}\langle\phi_i\rangle$. Standard deviations are calculated over lattice points. We also considered other initial conditions, which resulted in either nonconvergence or convergence to one of the two cases shown below. A detailed study of initial condition dependence is beyond the scope of this chapter.

	$\langle\phi\rangle$	$\langle\phi^2\rangle$	$\langle\phi^3\rangle$	$\langle\phi^4\rangle$
$\phi(0,t) = -i$	$-i0.8891$	$-0.5537 + i0.0001$	0.0001	$-0.6307 - i0.0001$
	$\pm 0.0032 \pm i0.0012$	$\pm 0.0013 \pm i0.0065$	$\pm 0.0083 \pm i0.0018$	$\pm 0.0069 \pm i0.0063$
$\phi(0,t) = i$	$i0.8891$	$-0.5537 - i0.0001$	0.0001	$-0.6306 + i0.0001$
	$\pm 0.0037 \pm i0.0013$	$\pm 0.0013 \pm i0.0075$	$\pm 0.0095 \pm i0.0021$	$\pm 0.0071 \pm i0.0071$

where $dw_j(\tau)$ are m independent Wiener processes normalized as before. We set $\phi_0(\tau) = \phi_0$ and $\phi_{m+1}(\tau) = \phi_{m+1}$. A repetition of the analysis of the previous section is sufficient to conclude that the stationary distributions of this set of stochastic equations will satisfy lattice Schwinger-Dyson equations (2.47).

Let's consider again the $-\phi^4/4$ theory, this time in one dimension. The Lagrangian is given by

$$\mathcal{L} = \frac{1}{2}\left(\frac{d\phi}{dt}\right)^2 - \frac{g}{4}\phi^4. \tag{2.50}$$

We again note that this theory is bottomless, a normal (real line contour) path integral solution to the Schwinger-Dyson equations does not exist. However, complex contour contour solutions do exist. Table 2.3 shows the results of numerical simulations for this theory on a one dimensional lattice. As in zero dimensional case, we see that the complex Langevin equation has at least two different stationary distributions. Choice of initial conditions can alter the stationary distributions. We note that this theory was also studied in [16] and there initial conditions were restricted to lower half of the complex plane. This led to the observation of only one of the stationary distributions.

More studies on the lattice must be done to understand the convergence behavior of complex Langevin equations. Some specific questions are listed in the next section.

2.4 Discussion of Results

In our numerical examples above, we saw that complex Langevin equations allowed us to calculate different solutions of a given quantum field theory, including the cases where a Feynman path integral is not defined. In the case of zero dimensional and one dimensional ϕ^4 theories, the obtained solutions showed symmetry breaking phenomena. Existence of nonunique stationary distributions of complex Langevin equations was known for a long time in the literature. Salcedo [100] suggested that stationary distributions of the complex Langevin equation may be interpreted as different phases of the action, with the same equations of motion but different boundary conditions. Some authors used Langevin and complex Langevin equation to give physical meaning to bottomless actions, e.g. [39, 90, 111, 112, 55][3]. Our discussion shows that these suggestions are inevitably tied with the solution space of Schwinger-Dyson equations [33, 43] and therefore to the Schwinger action principle.

Schwinger-Dyson equations are differential equations and admit more than one solution. Therefore it is necessary to set boundary conditions to specify the particular solution one is looking for. If one is solving for a quantum field theory using Schwinger-Dyson equations, it seems reasonable to choose the boundary condition so that the solution is the standard path integral over real fields. However, in many cases this solution actually will not be the physical one, e.g. symmetry breaking

[3]Some of these references use nonconstant kernels in the complex Langevin equation which enlarges the set of stationary distributions [100] and changes the Schwinger-Dyson equation, e.g. [55]

phases. Also, in theories with actions unbounded below, the integrals over real fields are not even convergent. In these cases, it is reasonable to look at other solutions of the Schwinger-Dyson equations and study them as possible generating functionals of the associated quantum field theory. Of course, different solutions require specification of different boundary conditions. One way of specifying different solutions is to consider path integrals over complex paths (as opposed to real paths) that connect zeros of the partition function on the complex plane, as was demonstrated in equation (2.31). Some of these also happen to be the stationary distributions of the associated complex Langevin equation constructed by Salcedo [100] as shown in this chapter. The problem with this approach is the large number of different boundary conditions/solutions and if all these different solutions define a phase or vacuum of the associated quantum field theory. A possible reduction of the solution set comes from taking the thermodynamic limit of the lattice. These issues are discussed in detail in[33, 43].

Access to the whole solution space of quantum field theories requires new numerical methods. One suggestion is the Source-Galerkin method, see e.g. [95] and references therein. This method proposes an expansion of the generating functional in polynomials of the source term and optimizes this expansion by a Galerkin procedure using the Schwinger-Dyson equation. It is successful in many problems, but also proved to be very difficult in many other cases. Another approach is given by mollification of the path integral weight [28]. The connection between complex Langevin and Schwinger-Dyson equations suggests the use of complex Langevin simulations as a numerical method to study the solution space of quantum field theories.

Some questions and speculations in this quest are:

- Is it possible to know a priori if the complex Langevin equation will converge?

- What is the exact relation between the initial condition and the stationary distributions of the complex Langevin equation?

- Is it possible to recover the whole solution set of the Schwinger-Dyson equation using the complex Langevin equation? If not, can we use other stochastic systems to recover the whole set? Also, what is special about the recovered solutions?

- How are these results modified in the continuum? There are an infinite number of solutions to Schwinger-Dyson equations on the lattice. Continuum limit may cause a collapse in the solution set [33, 43]. Can one see this collapse using complex Langevin equations?

We address some of these problems in the next chapter.

Chapter Three

Effective Potential for Complex Langevin Equations

Sampling complex integral weights of the form e^{-S} is important for many applications in high energy physics. Complex Langevin equations have been proposed for this purpose [92, 66]. Many theoretical questions are still to be answered for complex Langevin equations. Most importantly, it is not known a priori if a complex Langevin simulation will converge to a stationary distribution. Even if it does, there are multiple stationary distributions that satisfy stationary limit equations (Fokker-Planck equation [100] or Schwinger-Dyson equation [45]) and it is not known how to identify to which one of these that the complex Langevin equation converges. In the previous chapter, we discussed these issues and provided references to literature.

Identification of the particular stationary distribution sampled by the complex Langevin equation needs input from the dynamics of the complex Langevin simulation. Analysis depending only on the quantities in the stationary limit has not been successful in differentiating between stationary distributions. To account for this fact, we consider a path integral description of the complex Langevin process. To our knowledge this has not been done before. Then we introduce an effective potential that governs the complex Langevin dynamics. Even though this effective potential does not have all the properties of the conventional quantum field theory effective potential, we show that it governs the probability that the spacetime and Langevin time average of the fields takes on specific values. In the infinite Langevin time limit, it is shown that the spacetime and Langevin time average of the field must be equal to the minimum of the effective potential. As in quantum field theory, a loop expansion for this effective action can be defined. The parameter that defines loops is a factor that multiplies the noise in the complex Langevin equation. The same parameter is shown to count derivatives in the Schwinger-Dyson equation derived from the action S. This point is important, because it is known that the stationary distributions of the complex Langevin equation are complexified path in-

tegral solutions of the Schwinger-Dyson equation, i.e. see [45]. The main idea of this chapter is to use the minimum of the effective action to identify the stationary distribution to which the complex Langevin equation converges by matching the loop expansion with the derivative expansion. This provides an approach to addressing the multiple stationary distributions problem.

In two recent studies [1, 15], the classical fixed point structure of complex Langevin equations were shown to be important for the convergence behavior. Our results will also parallel this result since to leading order the minima of the effective potential will be given by classical fixed points. The next order will be used to remove the degeneracy and this will lead us to the identification of the stationary distribution that is sampled by the complex Langevin simulation.

There is a large gap between the results of this chapter and realistic problems of quantum field theory. One should look at this chapter as a general statement about complex Langevin processes, rather than an attempt at solving for example QCD. We hope that the novel approach we present in this chapter will help in coming up with a scheme to control the complex Langevin process resulting in a good numerical scheme to solve realistic problems.

We start by reviewing relevant results in Section 3.1. We then introduce the effective potential in a lattice setting, discuss its properties and calculate it to one loop order (Section 3.2). Before we conclude, we give a simple application of these ideas (Section 3.3).

One point we omit in this chapter is the discussion of the continuum limit. The question of renormalizability is a nontrivial problem and deserves a separate study of its own.

3.1 Stationary Distributions of Complex Langevin Equations

In this section we review the relevant results of [45] and the previous chapter in a field theoretic setting. Even though, our ultimate goal in this chapter is to do calculations in a lattice setting, the arguments in this section are given in the continuum for ease of notation. The lattice versions of these results are either in [45] or [14].

Given a complex action S of a scalar field $\phi(x)$ in a Euclidean space,

$$S[\phi] = \int d^d x \left[\frac{1}{2}\phi(x)\left(-\Box + m^2\right)\phi(x) + \sum_l \frac{g_l}{l}\phi^l(x) \right], \tag{3.1}$$

we want to study the stochastic dynamics given by

$$\frac{\partial \phi(x,\tau)}{\partial \tau} = -\frac{\delta S[\phi]}{\delta \phi(x,\tau)} + \eta^R(x,\tau) + i\eta^I(x,\tau), \tag{3.2}$$

where η^R and η^I are independent Gaussian noises with correlators given by

$$\begin{aligned} \left\langle \eta^R(x,\tau) \right\rangle &= 0, \\ \left\langle \eta^R(x,\tau)\,\eta^R(x',\tau') \right\rangle &= 2\Omega\alpha\delta^d(x-x')\,\delta(\tau-\tau'), \end{aligned} \tag{3.3}$$

and

$$\begin{aligned} \left\langle \eta^I(x,\tau) \right\rangle &= 0, \\ \left\langle \eta^I(x,\tau)\,\eta^I(x',\tau') \right\rangle &= 2\Omega\,(\alpha-1)\,\delta^d(x-x')\,\delta(\tau-\tau'). \end{aligned} \tag{3.4}$$

α and Ω are real constants and $\alpha \geq 1$. $\Omega = 1$ corresponds to the complex Langevin equation. We will not set Ω to any particular value for the moment. Ω will define

orders in the approximations we do below. Equation (3.2) can be written as a stochastic system of two real fields, $\phi(x,\tau) = \phi^R(x,\tau) + i\phi^I(x,\tau)$. In fact, this is what we will do in the rest of this chapter.

Note that most of the time in the literature α is set to 1. There is only a real noise in the complex Langevin equation. As shown in [45], this may lead to initial condition dependence of the stationary distribution sampled by the complex Langevin equation. This happens because for some actions the complex Langevin dynamics may be confined to sampling in lower or upper half planes depending on the initial condition, not having access to all of the complex plane. In this chapter, we want to avoid such initial condition dependence and assume that the stationary distribution sampled by the complex Langevin equation is unique. Furthermore, setting α to some value larger then 1 will be important for deriving a path integral representation of the generating functional for the complex Langevin process in the next section.

Given some initial conditions for the field, Langevin equation (3.2) has a time dependent probability distribution, see e.g [117],

$$P\left(\tau,\phi^R(x),\phi^I(x)\right) = \left\langle \delta\left(\phi^R(x,\tau)-\phi^R(x)\right)\,\delta\left(\phi^I(x,\tau)-\phi^I(x)\right)\right\rangle_{\eta^R,\eta^I}, \tag{3.5}$$

which can be shown to satisfy a Fokker-Planck equation,

$$\begin{aligned}\frac{\partial P\left(\tau,\phi^R,\phi^I\right)}{\partial\tau} = \int d^dx \Bigg[&\frac{\delta}{\delta\phi^R(x)}\left(\Omega\alpha\frac{\delta P}{\delta\phi^R(x)} + \mathrm{Re}\frac{\delta S[\phi]}{\delta\phi(x)}P\right)\\ &+ \frac{\delta}{\delta\phi^I(x)}\left(\Omega\left(\alpha-1\right)\frac{\delta P}{\delta\phi^I(x)} + \mathrm{Im}\frac{\delta S[\phi]}{\delta\phi(x)}P\right)\Bigg].\end{aligned} \tag{3.6}$$

The existence and uniqueness of stationary distributions for this Fokker-Planck equation is still an unanswered question.

We continue by defining a generating functional for equal time correlation functions

$$Z[J(x),\tau] \equiv \left\langle e^{\int d^d x \left(\phi^{R,\eta}(x,\tau)+i\phi^{I,\eta}(x,\tau)\right)J(x)} \right\rangle_{\eta^R,\eta^I}, \tag{3.7}$$

where $J(x)$ is a real source field. Here the brackets denote an average over the noise. Field variables are considered as functionals of the noise through equation (3.2), hence we include a superscript η. The effect of noise appears in the stochastic average through the probability distribution P (see e.g. [117]),

$$Z[J,\tau] = \int [d\phi^R][d\phi^I]\, P(\tau,\phi^R,\phi^I)\, e^{\int d^d x \left(\phi^R(x,\tau)+i\phi^I(x,\tau)\right)J(x)}. \tag{3.8}$$

This is now an integral over all field configurations weighted by P. This point will be treated in more detail in the next section. Using the Fokker-Planck equation (3.6), one can show that the following equation holds

$$\frac{\partial Z[J,\tau)}{\partial \tau} = \int d^d x \left\{ J(x) \left[\Omega J(x) - \frac{\delta S[\phi]}{\delta \phi(x)} \left(\frac{\delta}{\delta J} \right) \right] \right\} Z[J,\tau). \tag{3.9}$$

If there is a stationary distribution, the left hand side is zero. When $\Omega = 1$, functional derivatives of the right hand side with respect to J produce Schwinger-Dyson identities for the action $S[\phi]$, since the integrand must vanish due to the arbitrariness of J. Ω plays the role of $\hbar$ in quantum field theory. It is easy to see this by defining a making a change of variables $J(x) \to J(x)/\Omega$.[1] Then, the stationary distribution condition becomes

$$\int d^d x \left\{ \frac{J(x)}{\Omega} \left[J(x) - \frac{\delta S[\phi]}{\delta \phi(x)} \left(\Omega \frac{\delta}{\delta J} \right) \right] \right\} Z[J,\tau) = 0. \tag{3.10}$$

Ω counts the number of functional derivatives, as $\hbar$ would. As is well known, see

[1] In terms of this new variable, the correlation functions are given by functional derivatives of $Z[J,\tau)$ with respect to $\Omega \frac{\delta}{\delta J}$.

[12], a derivative expansion of Schwinger-Dyson equations is equivalent to a loop expansion of the associated path integral around a local minimum.

If one considers zero dimensional theories, an explicit construction of the stationary equal time correlation functional can be given. Generalization to a lattice is straightforward, see [45]. Now, the action S is a function of ϕ. Equation (3.9) becomes

$$\frac{\partial Z(j,\tau)}{\partial \tau} = \Omega j^2 Z(j,\tau) - j\frac{\partial S}{\partial \phi}\left(\frac{\partial}{\partial j}\right) Z(j,\tau). \tag{3.11}$$

In particular, the generating function for the stationary distribution satisfies

$$\frac{\partial S}{\partial \phi}\left(\frac{d}{dj}\right) Z_{st}(j) = \Omega j Z_{st}(j). \tag{3.12}$$

We can solve this equation following [33]. Our ansatz is

$$Z_\Gamma(j) = \int_\Gamma d\phi\, G(\phi) e^{j\phi}, \tag{3.13}$$

where Γ is a contour over the complex plane. Inserting this into equation (3.12) one gets:

$$0 = -\Omega G(\phi) e^{j\phi}\big|_{\partial\Gamma} + \int_\Gamma d\phi \left[\frac{\partial S}{\partial \phi} G(\phi) + \Omega \frac{dG(\phi)}{d\phi}\right] e^{j\phi}. \tag{3.14}$$

This equation can be solved for

$$G(\phi) = e^{-\frac{S(\phi)}{\Omega}}, \tag{3.15}$$

and Γ is contour that connects the zeros of $e^{-S(\phi)+j\phi}$ on the complex ϕ plane. As advertised, Ω plays the role of $\hbar$. Since equation (3.12) is linear, any linear combination

of the (independent) solutions will also be a solution,

$$Z_{st}(j) = \sum_{\Gamma_I} a_{\Gamma_I} Z_{\Gamma_I}(j), \tag{3.16}$$

where Γ_I define an independent subset of paths Γ.[2] The only constraint on the coefficients at this point is the normalization condition for correct distribution interpretation, namely that $Z_{st}(0) = 1$. We restricted the form of the generating function, but did not identify it completely. Examples are given in [45] and in the previous chapter.

In this chapter, we use an effective action approach to identify the stationary distribution. The Ω expansion gives a small noise expansion for the complex Langevin equation and a loop expansion of the stationary distribution generating function. Matching of both series order by order will tell us the exact form of the stationary distribution.

3.2 Effective Action for Complex Langevin Equation

In this section, we will define the effective action for complex Langevin equation and do an Ω expansion to gather information about the stationary distribution. We choose to use a lattice regularization. We work with an Ito type discretization for equation (3.2).

First we define our notation. We introduce a Euclidean spacetime lattice with

[2]Essentially the same result is derived by another method in [100].

isotropic lattice spacing a. Lattice points are denoted by a d dimensional vector $n = (n_1, \ldots, n_d)$, where $n_i = 0, \ldots, (N-1)$. The coordinate of a lattice point is given by $x_i = n_i a$. Our convention is to denote Euclidean time with x_d. Periodic boundary conditions are assumed for the space-time lattice. We discretize Langevin time τ with $\Delta\tau$ intervals. Langevin simulation is assumed to start at $\tau = \tau_i$ and run for N_τ time steps untill $\tau_f = \tau_i + N_\tau \Delta\tau$. In terms of dimensionless lattice variables $\hat{\phi}_n(\kappa) = a^{(d-2)/2}\phi(na, \kappa\Delta\tau)$, $\hat{\epsilon} = \Delta\tau/a^2$, $\hat{m} = am$, $\hat{g}_l = a^{d(1-l/2)+l} g_l$, $\hat{\eta}^{R,I} = \sqrt{a^d \Delta\tau}\eta^{R,I}$, where the noise correlators are now

$$\begin{aligned} \left\langle \hat{\eta}_n^R(\kappa)\, \hat{\eta}_{n'}^R(\kappa') \right\rangle &= 2\Omega\alpha\delta_{nn'}\delta_{\kappa\kappa'}, \\ \left\langle \hat{\eta}_n^I(\kappa)\, \hat{\eta}_{n'}^I(\kappa') \right\rangle &= 2\Omega\,(\alpha-1)\,\delta_{nn'}\delta_{\kappa\kappa'}, \end{aligned} \tag{3.17}$$

the discretized equation (3.2) in Ito calculus reads

$$\hat{\phi}_n(\kappa+1) = \hat{\phi}_n(\kappa) - \hat{\epsilon}\left(-\hat{\Box} + \hat{m}^2\right)\hat{\phi}_n(\kappa) - \hat{\epsilon}\sum_l \hat{g}_l \hat{\phi}_n^{l-1}(\kappa) + \sqrt{\hat{\epsilon}}\left(\hat{\eta}_n^R(\kappa) + i\hat{\eta}_n^I(\kappa)\right). \tag{3.18}$$

In the rest of this chapter we assume $\alpha > 1$. To avoid confusions, we note that $\hat{\phi}_n(\kappa)$ is the lattice variable at the spacetime point na and Langevin time $\tau_i + \kappa\Delta\tau$.Here, the dimensionless lattice Laplacian is defined by

$$\hat{\Box}\hat{\phi}_n(\kappa) = \sum_m \sum_{k=1}^{d} \left(\delta_{m,n+\hat{e}_k} + \delta_{m,n-\hat{e}_k} - 2\delta_{m,n}\right)\hat{\phi}_m(\kappa), \tag{3.19}$$

where $\hat{e}_\mu$ is a unit vector pointing along the k-direction. We assume an initial condition is set at $\tau = \tau_i$ by specifying the field on the spacetime lattice.

3.2.1 Generating Functional for Dynamic Correlation Functions

First step in our anaylsis is to define a generating functional for dynamic correlation functions,

$$Z_d[\hat{J}^R, \hat{J}^I] \equiv \left\langle \exp\left[\sum_{\kappa=1}^{N_\tau}\sum_n \hat{J}_n^R(\kappa)\hat{\phi}_n^{R,\eta}(\kappa) + \hat{J}_n^I(\kappa)\hat{\phi}_n^{I,\eta}(\kappa)\right]\right\rangle_{\hat{\eta}^R,\hat{\eta}^I}. \tag{3.20}$$

ϕ^η is a functional of the noise fields through the Langevin equation (3.18). The sum in κ parameter starts from 1, since we assume an initial condition $\phi_n(0)$ is given. Unless explicitly stated, κ sums and products run from 0 to $N_\tau - 1$. We use subscript d to differentiate Z_d from the generating functional of equal time correlation functions defined by equation (3.7). Z_d is more general than Z since it generates correlation functions of the field variable at different times as well as equal times. We will define an effective action using this generating functional. Before doing that, we derive a path integral representation for Z_d. Although we will not follow their work directly, see [62] for a discussion of path integral representations of generating functionals based on Ito discretization and [38] for continuum formulation. By definition, Z_d is an average over the probability density functions of the Gaussian random variables,

$$\begin{aligned} Z_d[\hat{J}^R, \hat{J}^I] = \mathcal{C}\int \prod_{n,\kappa} d\hat{\eta}_n^R(\kappa) d\hat{\eta}_n^I(\kappa)\, \exp\left[-\sum_{n,\kappa}\left(\frac{\hat{\eta}_n^R(\kappa)^2}{4\Omega\alpha} + \frac{\hat{\eta}_n^I(\kappa)^2}{4\Omega(\alpha-1)}\right)\right] \\ \times \exp\left[\sum_n\sum_{\kappa=1}^{N_\tau}\left(\hat{J}_n^R(\kappa)\phi_n^{R,\eta}(\kappa) + \hat{J}_n^I(\kappa)\phi_n^{I,\eta}(\kappa)\right)\right]. \end{aligned} \tag{3.21}$$

$\mathcal{C}$ is a proper normalization constant for each equation it appears in. The next step is to rewrite this expression as an integral over field configurations. Using equation (3.18), we can change integration variables from the Gaussian random variables $\hat{\eta}_n^R(\kappa)$ and $\hat{\eta}_n^I(\kappa)$ to $\hat{\phi}_n^R(\kappa+1)$ and $\hat{\phi}_n^I(\kappa+1)$. Note that due to our discretization,

the Jacobian of this transformation is a constant. Defining

$$\begin{aligned}
\hat{\Delta}\hat{\phi}_n(\kappa) &= \sum_{\gamma}(\delta_{\gamma,\kappa+1} - \delta_{\gamma,\kappa})\hat{\phi}_n(\gamma), \\
\hat{\mathcal{D}}\hat{\phi}_n(\kappa) &= \left(\hat{\Delta} - \hat{\epsilon}\hat{\Box}\right)\hat{\phi}_n(\kappa), \\
\hat{F}_n^R(\kappa) &= \hat{F}^R\left(\hat{\phi}_n^R(\kappa), \hat{\phi}_n^I(\kappa)\right) = \mathrm{Re}\left[\hat{m}^2\hat{\phi}_n(\kappa) + \sum_l \hat{g}_l\hat{\phi}_n^{l-1}(\kappa)\right], \\
\hat{F}_n^I(\kappa) &= \hat{F}^I\left(\hat{\phi}_n^R(\kappa), \hat{\phi}_n^I(\kappa)\right) = \mathrm{Im}\left[\hat{m}^2\hat{\phi}_n(\kappa) + \sum_l \hat{g}_l\hat{\phi}_n^{l-1}(\kappa)\right],
\end{aligned} \tag{3.22}$$

the generating functional Z_d becomes

$$\begin{aligned}
Z_d[\hat{J}^R, \hat{J}^I] = \mathcal{C}\int[d\hat{\phi}]\,\exp\left[\sum_n\sum_{\kappa=1}^{N_\tau}\left(\hat{J}_n^R(\kappa)\hat{\phi}_n^R(\kappa) + \hat{J}_n^I(\kappa)\hat{\phi}_n^I(\kappa)\right)\right] \\
\times\exp\left\{-\frac{1}{\Omega}\sum_{n,\kappa}\left[\frac{\left[\hat{\mathcal{D}}\hat{\phi}_n^R(\kappa) + \hat{\epsilon}\hat{F}_n^R(\kappa)\right]^2}{4\alpha\hat{\epsilon}} + \frac{\left[\hat{\mathcal{D}}\hat{\phi}_n^I(\kappa) + \hat{\epsilon}\hat{F}_n^I(\kappa)\right]^2}{4(\alpha-1)\hat{\epsilon}}\right]\right\},
\end{aligned} \tag{3.23}$$

where the measure is

$$[d\hat{\phi}] = \prod_n\prod_{\kappa=1}^{N_\tau} d\hat{\phi}_n^R(\kappa)d\hat{\phi}_n^I(\kappa) \tag{3.24}$$

There is no integration over $\hat{\phi}_n(0)$, since we assume it to be set by initial conditions. The exponent in the second line, with the normalization factor $\mathcal{C}$, is the probability density of a particular realization of the Langevin process given some initial $\hat{\phi}_n(0)$. We will denote it by $T\left(\hat{\phi}(N_\tau)|\hat{\phi}(0)\right)$. The previously defined probability distribution (3.5) and $T\left(\hat{\phi}(N_\tau)|\hat{\phi}(0)\right)$ are very closely related, see e.g. [86]. For T, $1/\Omega$ is an overall factor for the exponent, which will allow us to define a loop expansion for this generating functional.

For later convenience, we define the quantity in the exponent of the second line of equation (3.23) as

$$I[\hat{\phi}^R, \hat{\phi}^I] = \sum_{n,\kappa} \left[\frac{\left[\hat{\mathcal{D}}\hat{\phi}_n^R(\kappa) + \hat{\epsilon}\hat{F}_n^R(\kappa)\right]^2}{4\alpha\hat{\epsilon}} + \frac{\left[\hat{\mathcal{D}}\hat{\phi}_n^I(\kappa) + \hat{\epsilon}\hat{F}_n^I(\kappa)\right]^2}{4(\alpha-1)\hat{\epsilon}} \right]. \tag{3.25}$$

Forgetting the complex Langevin equation roots for one moment, one can think of equation (3.23) as a the generating functional of a field theory on a $d+1$ dimensional lattice with an action given by equation (3.25). This is not a usual field theory, because it does not have translational invariance due to $\kappa = 0$ terms appearing in equation (3.25). One end of the lattice ($\kappa = 0$) is fixed, whereas the other end ($\kappa = N_\tau$) is free. This picture will be useful later when we discuss the effective potential.

Before continuing, we note that having $\alpha > 1$ was a great convenience for this calculation. Otherwise, we would start with averages over only the real noise variables and this would lead to a difficulty when changing variables in the path integral from noise to field variables. The number of field variables $\hat{\phi}_n^{R,I}(\kappa)$ would be half of $\hat{\eta}^R(\kappa)$. Therefore, one would need to choose half of the field variables as independent ones and express the remaining in terms of the independent ones. Having $\alpha > 1$ saved us from these difficulties.

3.2.2 Effective Action, Effective Potential and Their Interpretation

Now we do the standart quantum field theoretic procedure to define an effective action for this generating functional,

$$W[\hat{J}^R, \hat{J}^I] = \ln Z_d[\hat{J}^R, \hat{J}^I],$$
$$\Gamma[\hat{\phi}^R, \hat{\phi}^I] = -W[\hat{J}^{R,\hat{\phi}}, \hat{J}^{I,\hat{\phi}}] + \left[\sum_n \sum_{\kappa=1}^{N_\tau} \left(\hat{J}_n^{R,\hat{\phi}}(\kappa)\hat{\phi}_n^R(\kappa) + \hat{J}_n^{I,\hat{\phi}}(\kappa)\hat{\phi}_n^I(\kappa)\right)\right], \quad (3.26)$$

where

$$\hat{\phi}_n^{R,J}(\kappa) = \frac{\partial W[\hat{J}^R, \hat{J}^I]}{\partial \hat{J}_n^R(\kappa)}, \qquad \hat{\phi}_n^{I,J}(\kappa) = \frac{\partial W[\hat{J}^R, \hat{J}^I]}{\partial \hat{J}_n^R(\kappa)},$$
$$\hat{\phi}_n^{R,J}(\kappa) = \hat{\phi}_n^R(\kappa) \qquad \text{if} \qquad \hat{J}_n^R(\kappa) = \hat{J}_n^{R,\hat{\phi}}(\kappa),$$
$$\hat{\phi}_n^{I,J}(\kappa) = \hat{\phi}_n^I(\kappa) \qquad \text{if} \qquad \hat{J}_n^I(\kappa) = \hat{J}_n^{I,\hat{\phi}}(\kappa). \quad (3.27)$$

By definition, it follows that

$$\frac{\partial \Gamma[\hat{\phi}^R, \hat{\phi}^I]}{\partial \hat{\phi}_n^R(\kappa)} = \hat{J}_n^{R,\hat{\phi}}(\kappa), \qquad \frac{\partial \Gamma[\hat{\phi}^R, \hat{\phi}^I]}{\partial \hat{\phi}_n^I(\kappa)} = \hat{J}_n^{I,\hat{\phi}}(\kappa). \quad (3.28)$$

For field configurations that are homogenous and static in Langevin time, the effective action reduces to "effective potential",

$$\mathcal{V}(\hat{\phi}^R, \hat{\phi}^I) = \frac{\Gamma[\hat{\phi}^R, \hat{\phi}^I]}{N^d N_\tau}. \quad (3.29)$$

In the next section, we will calculate the effective potential to one loop order (first order in Ω).

We note that the effective action defined above does not have all the properties

one remembers from quantum field theory. In particular, it does not have the energy interpretation [23] because the complex Langevin equation (3.2) as a system of two real Langevin equations is not derivable from an action.[3] See [53] for a detailed discussion. However, one useful property is still valid. The effective potential governs the probability that the spacetime and Langevin time average of the field takes specific values. To show this, we follow closely the argument of [53].

We ask the probability of spacetime and Langevin time average of the field variables taking a specific value,

$$\begin{aligned}
&\text{Prob}\left(\frac{1}{N^d N_\tau}\sum_n\sum_{\kappa=1}^{N_\tau}\hat{\phi}_n(\kappa)=\bar{\phi}\right)\\
&=\int[d\hat{\phi}]\,T\left(\hat{\phi}(N_\tau)|\hat{\phi}(0)\right)\delta\left(\sum_n\sum_{\kappa=1}^{N_\tau}\hat{\phi}_n^R(\kappa)-N^dN_\tau\bar{\phi}^R\right)\delta\left(\sum_n\sum_{\kappa=1}^{N_\tau}\hat{\phi}_n^I(\kappa)-N^dN_\tau\bar{\phi}^I\right)\\
&=\int[d\hat{\phi}]\,T\left(\hat{\phi}(N_\tau)|\hat{\phi}(0)\right)\int d\lambda^R d\lambda^I\exp\left[i2\pi\lambda^R\left(\sum_n\sum_{\kappa=1}^{N_\tau}\hat{\phi}_n^R(\kappa)-N^dN_\tau\bar{\phi}^R\right)\right]\\
&\qquad\qquad\times\exp\left[i2\pi\lambda^I\left(\sum_n\sum_{\kappa=1}^{N_\tau}\hat{\phi}_n^I(\kappa)-N^dN_\tau\bar{\phi}^I\right)\right]\\
&=\int d\lambda^R d\lambda^I\,Z_d[\hat{J}^R=i2\pi\lambda^R,\hat{J}^R=i2\pi\lambda^I]\exp\left[-i2\pi N^dN_\tau\left(\lambda^R\bar{\phi}^R+\lambda^I\bar{\phi}^I\right)\right].
\end{aligned}\tag{3.30}$$

At this point we will make an approximation, though we will argue that our approximation becomes exact in the infinite Langevin time limit. We are looking for a simplification of the effective action evaluated in the presence of a constant source field. For this purpose, we consider a derivative expansion of the effective action. The first term will be the effective potential, as defined above. Other terms will have factors of (lattice) derivatives of the field variable $\hat{\phi}_n(\kappa)$. Note that we are now regarding the field variable as the expactation value of a "quantum" operator of the

[3] A Langevin system that is derived from an action will have component equations $\dot{q}_i=-\frac{\partial S}{\partial q_i}+\eta_i$.

lattice field theory given by (3.23). Consider complex Langevin initial conditions that have no space-time dependence. Then, for a constant source field, one expects the derivatives along the space-time directions to vanish due to periodic boundary conditions and translation invariance. On the Langevin time direction translation invariance breaks, because of the existence of an initial condition. Even though this is the case, we will argue that in the long Langevin time limit, one can ignore higher order terms and safely approximate the effective action by the effective potential. Consider for a moment a complex Langevin simulation starting with space-time independent initial conditions. Assuming convergence to a stationary distribution, in the long Langevin time limit the field expectation values will "forget" the initials conditions and approach a stationary value. This means that the Langevin time derivatives of the field expectation values will be small, in fact will vanish in the long time limit. By definition, one would be able to calculate this effect using the generating functional given by (3.23) by setting the source fields to zero. We are interested in constant source fields that are not vanishing. Now let's go back to the Euclidean lattice field theory picture defined by (3.23). For zero source fields, in the very large κ region the lattice looks pretty much translationally invariant as argued above. Adding a constant source field will not break this invariance. Therefore, vanishing of the Langevin time derivatives must still hold. We argue that if this is the case, the effective potential will dominate over all higher order terms in the derivative expansion. To motivate this last comment a little more rigorously, consider a constant γ (like the effective potential) and a function $\beta(\kappa)$ (like the higher order terms in the derivative expansion) that dies as $\kappa \to \infty$. Now consider the quantity

$$\left| \lim_{N_\tau \to \infty} \frac{\sum_{\kappa=1}^{N_\tau} \beta(\kappa)}{\sum_{\kappa=1}^{N_\tau} \gamma} \right|. \tag{3.31}$$

We will show that this limit is zero, which will prove that our comment is valid, that

the effective potential dominates over higher terms in the derivative expansion. To prove that it is zero, we will show that it is smaller than any positive ξ. We will need to recall the definition of a convergent sequence. A sequence Q_κ converges to the limit Q if, for any $\epsilon > 0$, there exists a P such that $|Q_\kappa - Q| < \epsilon$ for $\kappa > P$. Now we apply this definition to sequence $\beta(\kappa)$, such that $\epsilon = |\gamma|\,\xi$. Now there exists a P_ξ such that $|\beta(\kappa)| < |\gamma|\,\xi$ for $\kappa > P_\xi$. Then

$$\begin{aligned}\left|\lim_{N_\tau\to\infty}\frac{\sum_{\kappa=1}^{N_\tau}\beta(\kappa)}{\sum_{\kappa=1}^{N_\tau}\gamma}\right| &= \left|\lim_{N_\tau\to\infty}\left(\frac{1}{N_\tau}\sum_{\kappa=1}^{P_\xi}\frac{\beta(\kappa)}{\gamma}+\frac{1}{N_\tau}\sum_{\kappa=P_\xi+1}^{N_\tau}\frac{\beta(\kappa)}{\gamma}\right)\right| = \left|\lim_{N_\tau\to\infty}\frac{1}{N_\tau}\sum_{\kappa=P_\xi+1}^{N_\tau}\frac{\beta(\kappa)}{\gamma}\right| \\ &\leq \lim_{N_\tau\to\infty}\frac{1}{N_\tau}\sum_{\kappa=P_\xi+1}^{N_\tau}\left|\frac{\beta(\kappa)}{\gamma}\right| < \lim_{N_\tau\to\infty}\frac{1}{N_\tau}\sum_{\kappa=P_\xi+1}^{N_\tau}\left|\frac{\gamma\xi}{\gamma}\right| = \xi \\ \Longrightarrow \left|\lim_{N_\tau\to\infty}\frac{\sum_{\kappa=1}^{N_\tau}\beta(\kappa)}{\sum_{\kappa=1}^{N_\tau}\gamma}\right| &< \xi \qquad \text{for any } \xi > 0. \end{aligned} \tag{3.32}$$

Therefore, we can safely assume that a constant source field implies constant $\hat{\phi}_n^J(\kappa)$. As discussed above, this constant $\hat{\phi}_n^J$ is the expectation value of the field variable in the long Langevin time limit in the presence of a constant source field. Then

$$Z_d[\hat{J}^R = i2\pi\lambda^R, \hat{J}^R = i2\pi\lambda^I] = \exp\left\{N^d N_\tau\left(i2\pi\lambda^R\hat{\phi}^{R,\lambda} + i2\pi\lambda^I\hat{\phi}^{I,\lambda} - \mathcal{V}[\hat{\phi}^{R,\lambda}, \hat{\phi}^{I,\lambda}]\right)\right\}. \tag{3.33}$$

Here the superscpript λ is used to denote that fields are functions of the constant source field. We will look at infinite Langevin time limit. Then using the method of stationary phase

$$\text{Prob}\left(\frac{1}{N^d N_\tau}\sum_n\sum_{\kappa=1}^{N_\tau}\hat{\phi}_n(\kappa) = \bar{\phi}\right) \propto \exp\left[-N^d N_\tau \mathcal{V}(\bar{\phi^R}, \bar{\phi^I}) + \mathcal{O}(1)\right]. \tag{3.34}$$

Thus, the effective potential governs the probability distribution of the spacetime and Langevin time average of the field. As the simulation time N_τ goes to infinity,

the space-time and Langevin time average of the fields must equal to the minimum of the effective potential[4]. Our argument for effective potential dominance assumed space-time indenpendent initial conditions. However, the stationary distribution that the complex Langevin equation converges should be independent of the initial condition. Therefore this result can be generalized to any initial conditions. Note that if our argument on the dominance of the effective potential is valid, this is an exact result in the infinite N_τ limit.

This interpretation of the effective potential will enable us to determine the stationary distribution to which the complex Langevin equation converges.

3.2.3 Effective Potential in One Loop

In this section, we will calculate effective potential to first order in Ω in the infinite Langevin time limit. As we showed in the previous section, in this limit the space-time and Langevin time average of the field must equal to the minimum of the effective potential.

Calculation of the effective potential for a complex Langevin simulation that runs for a finite time is not easy. The calculation requires, as we will see, the evaluation of a $2N_\tau N^d$-by-$2N_\tau N^d$ matrix determinant and to the authors, there does not seem to be a way of simplifying this calculation. Instead we will do our calculation in the infinite Langevin time limit, but we will take this limit in a different way than what we have been considering until now. Until now, we let the complex Langevin simulation to start at $\kappa = 0$ with a fixed initial condition and run until a finite time N_τ. Then we took the limit $N_\tau \to \infty$. Instead, we now start our simulation at time

[4]We assume no degeneracy among the minima.

$\kappa = -N_\tau$ with a fixed initial condition and run it until N_τ. Then we let N_τ go to infinity. In the large N_τ limit, due to ergodicity and Langevin time independence of the complex Langevin equation, the Langevin time averages of these two processes will converge to the same stationary distribution. Another way to see the equivalence is by shifting the latter process by N_τ steps in Langevin time and thus reaching a process of the former type. Note that this changing of limiting process does not effect the Schwinger-Dyson equation related arguments. Since stationary distributions sampled by the complex Langevin equation for both processes are the same, we can calculate the effective potential for the latter process, and its minimum will match the minimum of the former one. Matching of minima is sufficient for our purposes, but it is very likely true that the effective actions themselves match also. From now on, we work in the limit $N_\tau \to \infty$ where the limit is taken in the latter way.

We start by expanding the integrand of the generating functional for dynamical correlation functions around constant field configurations $\bar{\phi}^R$ and $\bar{\phi}^I$. First, we choose the constant source fields as

$$\bar{J}^{R,I} = \frac{1}{\Omega} \left. \frac{\partial I[\hat{\phi}^R, \hat{\phi}^I]}{\partial \hat{\phi}_n^{R,I}(\kappa)} \right|_{\bar{\phi}} . \tag{3.35}$$

Using these values of the source fields, we get

$$\begin{aligned} \exp W[\bar{J}^R, \bar{J}^I] = \exp &\left[\sum_n \sum_\kappa \left(\bar{J}^R \bar{\phi}^R + \bar{J}^I \bar{\phi}^I \right) \right] \\ &\times \exp \left[-\frac{\hat{\epsilon}}{4\Omega} \sum_n \sum \kappa \left[\frac{\left[\hat{F}^R(\bar{\phi}^R, \bar{\phi}^I) \right]^2}{\alpha} + \frac{\left[\hat{F}^I(\bar{\phi}^R, \bar{\phi}^I) \right]^2}{\alpha - 1} \right] \right] \\ &\times \mathcal{C} \int [d\hat{\phi}] \exp \left[-\frac{1}{2\Omega} \sum_{n,m} \sum_{\kappa,\gamma} \sum_{A,B=R,I} \hat{\phi}_n^A(\kappa) M_{n\kappa A, m\gamma B} \hat{\phi}_m^B(\gamma) + \mathcal{O}(\hat{\phi}^3) \right] \end{aligned} \tag{3.36}$$

Here the κ sums go from $-\infty$ to ∞. The matrix M is given by

$$
\begin{aligned}
M_{n\kappa R,m\gamma R} &= \frac{1}{2\hat{\epsilon}\alpha}\sum_{p\sigma}\hat{\mathcal{D}}_{p\sigma,n\kappa}\hat{\mathcal{D}}_{p\sigma,m\gamma}+\frac{1}{2\alpha}\left(\hat{\mathcal{D}}_{n\kappa,m\gamma}+\hat{\mathcal{D}}_{m\gamma,n\kappa}\right)\frac{\partial\hat{F}^R}{\partial\hat{\phi}^R}\bigg|_{\bar{\phi}^R,\bar{\phi}^I}\\
&+\frac{\delta_{nm}\delta_{\gamma\kappa}\hat{\epsilon}}{2}\left[\frac{1}{\alpha}\left(\frac{\partial\hat{F}^R}{\partial\hat{\phi}^R}\right)^2+\frac{1}{\alpha}\hat{F}^R\frac{\partial^2\hat{F}^R}{\partial\hat{\phi}^{R\,2}}+\frac{1}{\alpha-1}\left(\frac{\partial\hat{F}^I}{\partial\hat{\phi}^R}\right)^2+\frac{1}{\alpha-1}\hat{F}^I\frac{\partial^2\hat{F}^I}{\partial\phi^{R\,2}}\right]\bigg|_{\bar{\phi}^R,\bar{\phi}^I},\\
M_{n\kappa I,m\gamma I} &= \frac{1}{2\hat{\epsilon}(\alpha-1)}\sum_{p\sigma}\hat{\mathcal{D}}_{p\sigma,n\kappa}\hat{\mathcal{D}}_{p\sigma,m\gamma}+\frac{1}{2(\alpha-1)}\left(\hat{\mathcal{D}}_{n\kappa,m\gamma}+\hat{\mathcal{D}}_{m\gamma,n\kappa}\right)\frac{\partial\hat{F}^I}{\partial\hat{\phi}^I}\bigg|_{\bar{\phi}^R,\bar{\phi}^I}\\
&+\frac{\delta_{nm}\delta_{\gamma\kappa}\hat{\epsilon}}{2}\left[\frac{1}{(\alpha-1)}\left(\frac{\partial\hat{F}^I}{\partial\hat{\phi}^I}\right)^2+\frac{1}{\alpha-1}\hat{F}^I\frac{\partial^2\hat{F}^I}{\partial\hat{\phi}^{I\,2}}+\frac{1}{\alpha}\left(\frac{\partial\hat{F}^R}{\partial\hat{\phi}^I}\right)^2+\frac{1}{\alpha}\hat{F}^R\frac{\partial^2\hat{F}^R}{\partial\phi^{I\,2}}\right]\bigg|_{\bar{\phi}^R,\bar{\phi}^I},\\
M_{n\kappa I,m\gamma R} &= M_{m\gamma R,n\kappa I}=\frac{1}{2}\left(\frac{\hat{\mathcal{D}}_{n\kappa,m\gamma}}{\alpha}-\frac{\hat{\mathcal{D}}_{m\gamma,n\kappa}}{\alpha-1}\right)\frac{\partial\hat{F}^R}{\partial\hat{\phi}^I}\bigg|_{\bar{\phi}^R\bar{\phi}^I}\\
&+\frac{\delta_{nm}\delta_{\kappa\gamma}\hat{\epsilon}}{2}\left[\frac{1}{\alpha}\hat{F}^R\frac{\partial^2\hat{F}^R}{\partial\hat{\phi}^R\partial\hat{\phi}^I}+\frac{1}{\alpha-1}\hat{F}^I\frac{\partial^2\hat{F}^I}{\partial\hat{\phi}^R\partial\hat{\phi}^I}+\frac{1}{\alpha(1-\alpha)}\frac{\partial\hat{F}^R}{\partial\hat{\phi}^R}\frac{\partial\hat{F}^R}{\partial\hat{\phi}^I}\right]\bigg|_{\bar{\phi}^R,\bar{\phi}^I},
\end{aligned}
\tag{3.37}
$$

where

$$
\hat{\mathcal{D}}_{n\kappa,m\gamma}=\delta_{nm}\left(\delta_{\kappa+1,\gamma}-\delta_{\kappa\gamma}\right)-\hat{\epsilon}\delta_{\kappa\gamma}\sum_k\left(\delta_{n+\hat{e}_k,m}+\delta_{n-\hat{e}_k,m}-2\delta_{nm}\right). \tag{3.38}
$$

When deriving these equations, we made use of the Cauchy-Riemann equations. They are evaluated at the constant field configurations $\bar{\phi}^R$ and $\bar{\phi}^I$. Now, using the definition of the effective potential, it is easy to see that

$$
\mathcal{V}(\bar{\phi^R},\bar{\phi^I})=\frac{1}{\Omega}\frac{\hat{\epsilon}\left[\hat{F}^R\left(\bar{\phi}^R,\bar{\phi}^I\right)\right]^2}{4\alpha}+\frac{1}{\Omega}\frac{\hat{\epsilon}\left[\hat{F}^I\left(\bar{\phi}^R,\bar{\phi}^I\right)\right]^2}{4(\alpha-1)}+\frac{\ln\det M}{2\sum_n\sum_\kappa}+\mathcal{O}(\Omega). \tag{3.39}
$$

Before continuing our calculation, we stop to discuss this result. As expected, the leading order term sets the minima of the effective potential at the classical fixed

points, which are saddle points of the action S. This is just saying that if there were no noise (and the simulation did not diverge), the fields will evolve to a fixed point and stay there for ever. Averages over space-time and Langevin time in the infinite Langevin time limit will be set by the classical fixed points. At the classical level, all saddle points of S are degenerate, meaning they are all minima of the effective potential. Adding noise will remove the degeneracy through higher terms in the Ω expansion. We will calculate the determinant term below and show in a specific example how it removes the degeneracy.

On a different line of argument, we showed above that if the complex Langevin equation converges to a stationary distribution, this distribution will be a solution of the Schwinger-Dyson equation for the theory with complex action S. Moreover, we showed that Ω counts the number of derivatives (loops) for this theory. Now we merge this result with the discussion of the previous paragraph as follows:

Assuming ergodicity, averages over the stationary distribution is equivalent to averages over Langevin time in the infinite Langevin time limit. Since we set periodic boundary conditions on the space-time lattice, the resulting stationary distribution will have translation invariance in space-time. In particular, the Langevin time averages for the field variable $\hat{\phi}$ will be constant in space-time. Therefore, we can say that Langevin time average of the field variable $\hat{\phi}$ is equal to the Langevin time and space-time average of $\hat{\phi}$. Based on our results above, we know that the latter is equal to the minimum of the effective action for the complex Langevin equation which is given in equation (3.39) *to* 0^{th} *order in* Ω. *Since* Ω *simultaneously counts loop order for the stationary distribution, which is a solution to the Schwinger-Dyson equations, we conclude that the complex Langevin equation converges to a stationary distribution that is quantized around a saddle point of the complex action S. This saddle point is given by the minimum of the effective action of the complex Langevin equation.*

The last statement needs more explanation. First of all, by quantization of a complex action S we mean not the Feynman path integral quantization but a Schwinger action principle quantization. From Schwinger action principle, one derives Schwinger-Dyson equations, which have multiple solutions [43, 33].[5] A solution of Schwinger-Dyson equations defines a generating functional for a quantization of S. This is consistent with equation (3.16), where we showed that in zero-dimensions solutions of Schwinger-Dyson equations can be represented by linear combinations of complexified path integrals. This result trivially generalizes to a lattice [43, 45].[6] Complex Langevin simulations have only one stationary distribution, the question is to find which quantization of S this distribution gives. Our argument shows that the stationary distribution will contain contributions only from one of the saddle points of S.[7] One way of making this statement precise is through the results of [43]. There it was shown that for zero-dimensional theories, loop expansions of Schwinger-Dyson equations can be Borel resummed to give path integrals of type (3.13) with the path Γ being equivalent to a steepest descent path passing through a dominant saddle point of S. It is these generating functionals for zero-dimensions, and their generalizations to higher dimensions that we argue to be the stationary distributions of the complex Langevin equations. Examples of this will be given in the next section.

Now we go back to the determinant calculation. Calculation of the determinant of matrix M is most easily done in the Fourier basis. The discrete time Fourier

[5]Other differential equations also follow from Schwinger action principle, but it was shown in [43] that a study of Schwinger-Dyson equations is sufficient since in the continuum limit solutions of Schwinger-Dyson equations satisfy the remaining differential equations.

[6]To our knowledge generalizations of generating functionals with complex integration paths are not yet constructed on the continuum. Complex Langevin equations can be of help in defining these continuum generating functionals.

[7]Here we assumed that the 0^{th} order term of the equation (3.39) breaks the degeneracy among the minima completely. If not, one may need to go to higher orders. If the degeneracy is not broken at all, it may be that the stationary distribution contains contributions from all degenerate minima. The generating functional for this distribution may be defined by a linear combination of the generating functionals that contain only contributions from one of the degenerate minima. See [43].

transform and the inverse transform are given by

$$\tilde{\phi}_l^{R,I}(\omega) = \frac{1}{(2\pi)^{(d+1)/2}} \sum_n \sum_\kappa \hat{\phi}_n^{R,I}(\kappa)\, e^{-i\omega\kappa - in\cdot l},$$
$$\hat{\phi}_n^{R,I}(\kappa) = \frac{1}{(2\pi)^{(d+1)/2}} \int_{-\pi}^{\pi} dw \int_{-\pi}^{\pi} dl_1 \ldots \int_{-\pi}^{\pi} dl_d\, \tilde{\phi}_l^{R,I}(\omega)\, e^{i\omega\kappa + in\cdot l}. \tag{3.40}$$

The nonzero elements of the matrix M in this new basis are:[8]

$$\begin{aligned}
M_{l\omega R,l'\omega' R} =& \delta(l-l')\,\delta(w-w') \left\{ \frac{1}{2\hat{\epsilon}\alpha} \left(\tilde{\mathcal{D}}_{l\omega} + \hat{\epsilon}\frac{\partial \hat{F}^R}{\partial \hat{\phi}^R}\right)\left(\tilde{\mathcal{D}}^*_{l\omega} + \hat{\epsilon}\frac{\partial \hat{F}^R}{\partial \hat{\phi}^R}\right)\Big|_{\bar{\phi}^R,\bar{\phi}^I} \right. \\
&\left. + \frac{\hat{\epsilon}}{2}\left[\frac{1}{\alpha}\hat{F}^R\frac{\partial^2 \hat{F}^R}{\partial \hat{\phi}^{R\,2}} + \frac{1}{\alpha-1}\left(\frac{\partial \hat{F}^I}{\partial \hat{\phi}^R}\right)^2 + \frac{1}{\alpha-1}\hat{F}^I\frac{\partial^2 \hat{F}^I}{\partial \phi^{R\,2}}\right]\Big|_{\bar{\phi}^R,\bar{\phi}^I} \right\}, \\
M_{l\omega I,l'\omega' I} =& \delta(l-l')\,\delta(w-w') \left\{ \frac{1}{2\hat{\epsilon}(\alpha-1)} \left(\tilde{\mathcal{D}}_{l\omega} + \hat{\epsilon}\frac{\partial \hat{F}^I}{\partial \hat{\phi}^I}\right)\left(\tilde{\mathcal{D}}^*_{l\omega} + \hat{\epsilon}\frac{\partial \hat{F}^I}{\partial \hat{\phi}^I}\right)\Big|_{\bar{\phi}^R,\bar{\phi}^I} \right. \\
&\left. + \frac{\hat{\epsilon}}{2}\left[\frac{1}{\alpha-1}\hat{F}^I\frac{\partial^2 \hat{F}^I}{\partial \hat{\phi}^{I\,2}} + \frac{1}{\alpha}\left(\frac{\partial \hat{F}^R}{\partial \hat{\phi}^I}\right)^2 + \frac{1}{\alpha}\hat{F}^R\frac{\partial^2 \hat{F}^R}{\partial \phi^{I\,2}}\right]\Big|_{\bar{\phi}^R,\bar{\phi}^I} \right\}, \\
M_{l\omega I,l'\omega' R} = M^*_{l'\omega' R,l\omega I} =& \delta(l-l')\,\delta(w-w') \left\{ \frac{1}{2}\frac{\partial \hat{F}^R}{\partial \hat{\phi}^I}\left(\frac{\tilde{\mathcal{D}}_{l\omega}}{\alpha} - \frac{\tilde{\mathcal{D}}^*_{l\omega}}{\alpha-1}\right)\Big|_{\bar{\phi}^R\bar{\phi}^I} \right. \\
&\left. + \frac{\hat{\epsilon}}{2}\left[\frac{1}{\alpha}\hat{F}^R\frac{\partial^2 \hat{F}^R}{\partial \hat{\phi}^R\partial \hat{\phi}^I} + \frac{1}{\alpha-1}\hat{F}^I\frac{\partial^2 \hat{F}^I}{\partial \hat{\phi}^R\partial \hat{\phi}^I} + \frac{1}{\alpha(1-\alpha)}\frac{\partial \hat{F}^R}{\partial \hat{\phi}^R}\frac{\partial \hat{F}^R}{\partial \hat{\phi}^I}\right]\Big|_{\bar{\phi}^R,\bar{\phi}^I} \right\}.
\end{aligned} \tag{3.42}$$

Here,

$$\tilde{\mathcal{D}}_{l\omega} = e^{iw} - 1 + 4\hat{\epsilon}\sum_{k=1}^{d} \sin^2\frac{l_k}{2}. \tag{3.43}$$

[8] recall the Fourier series representation of the δ function:

$$\delta(\omega) = \frac{1}{2\pi}\sum_\kappa e^{-i\kappa\omega}. \tag{3.41}$$

It is now easy to calculate the logarithm of the determinant of this block-diagonal matrix where each block is a 2-by-2 matrix.

$$\frac{\det M}{2\sum_n \sum_\kappa} = \frac{1}{2}\int_{-\pi}^{\pi}\frac{dw}{2\pi}\int_{-\pi}^{\pi}\frac{dl_1}{2\pi}\cdots\int_{-\pi}^{\pi}\frac{dl_d}{2\pi}\,\ln\left(M_{l\omega R,l\omega R}M_{l\omega I,l\omega I}-\left|M_{l\omega R,l\omega I}\right|^2\right). \tag{3.44}$$

Using these results, the final expression for effective action in one loop is

$$\begin{aligned}\lim_{N_\tau\to\infty}\mathcal{V}(\bar{\phi^R},\bar{\phi^I}) &= \frac{1}{\Omega}\frac{\hat{\epsilon}\left[\hat{F}^R\left(\bar{\phi}^R,\bar{\phi}^I\right)\right]^2}{4\alpha}+\frac{1}{\Omega}\frac{\hat{\epsilon}\left[\hat{F}^I\left(\bar{\phi}^R,\bar{\phi}^I\right)\right]^2}{4(\alpha-1)}\\ &+\frac{1}{2}\int_{-\pi}^{\pi}\frac{dw}{2\pi}\int_{-\pi}^{\pi}\frac{dl_1}{2\pi}\cdots\int_{-\pi}^{\pi}\frac{dl_d}{2\pi}\,\ln\left(M_{l\omega R,l\omega R}M_{l\omega I,l\omega I}-\left|M_{l\omega R,l\omega I}\right|^2\right)+\mathcal{O}(\Omega).\end{aligned} \tag{3.45}$$

In the next section, we will put equation (3.45) into use for specific examples.

3.3 An Example: Zero-Dimensional Cubic Theory

In this section, we will study zero-dimensional ϕ^3 theory as an example. The action is given by,

$$S=-i\phi-\frac{i}{3}\phi^3, \tag{3.46}$$

while the Schwinger-Dyson equation is

$$-i\frac{d^2Z}{dj^2}-iZ(j)=j\,Z\,(j)\,. \tag{3.47}$$

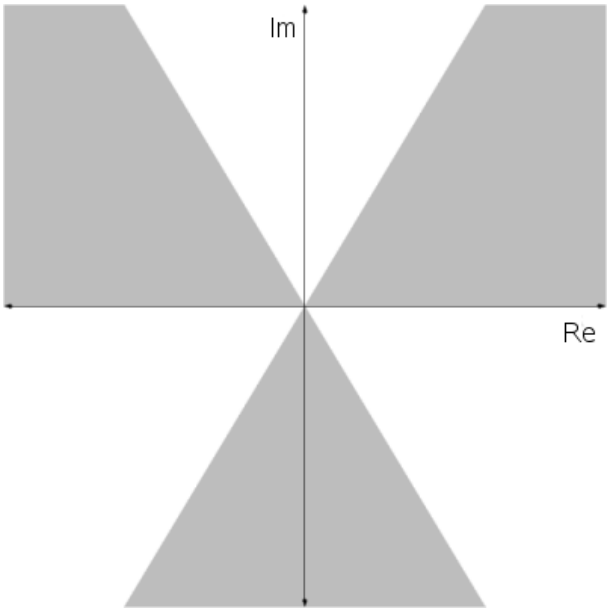

Figure 3.1: The region defined by $\sin(3\theta) > 0$, where θ is the argument of ϕ is shaded.
Each wedge is $\pi/3$ radians wide. Any path starting and ending at the infinity within this area corresponds to a particular solution of ultralocal ϕ^3 theory.

We can construct the path integral solutions to this equation as:

$$Z(j) = \frac{\int_\Gamma d\phi \, \exp\left\{i\phi + \frac{i}{3}\phi^3 + j\phi\right\}}{\int_\Gamma d\phi \, \exp\left\{i\phi + \frac{i}{3}\phi^3\right\}}, \tag{3.48}$$

where Γ is a path that starts and ends in one of the wedges shown in Figure 3.1. Since the Schwinger-Dyson equation is second order, only two of these solutions are independent. One needs two boundary/initial conditions to fix a solution. One condition is given by the normalization $Z(0) = 1$. Setting another condition will fix the solution completely.

Now we turn to the complex Langevin dynamics defined by the action (3.46).

The discretized complex Langevin equation is

$$\begin{aligned}\phi^R(\kappa+1) &= \phi^R(\kappa) - 2\Delta\tau\phi^R(\kappa)\phi^I(\kappa) + \sqrt{\Delta\tau}\,\hat{\eta}^R(\kappa)\\ \phi^I(\kappa+1) &= \phi^I(\kappa) - \Delta\tau\left(-1-\phi^R(\kappa)^2+\phi^I(\kappa)^2\right) + \sqrt{\Delta\tau}\,\hat{\eta}^I(\kappa),\end{aligned} \tag{3.49}$$

Noise correlators are

$$\begin{aligned}\left\langle\hat{\eta}^R(\kappa)\,\hat{\eta}^R(\kappa')\right\rangle &= 2\Omega\alpha\delta_{\kappa\kappa'}\\ \left\langle\hat{\eta}^I(\kappa)\,\hat{\eta}^I(\kappa')\right\rangle &= 2\Omega(\alpha-1)\delta_{\kappa\kappa'}.\end{aligned} \tag{3.50}$$

Classical fixed points of the complex Langevin equation is given by $\phi = i$ and $\phi = -i$. As mentioned before, both fixed points are minima for the effective potential in the leading order. The next order for $\phi = i$ is given by

$$\frac{1}{2}\ln\frac{1}{4\left(\Delta\tau\right)^2\alpha(\alpha-1)} + \int_{-\pi}^{\pi}\frac{dw}{2\pi}\,\ln\left[4\left(\Delta\tau\right)^2 + 4(1-2\Delta\tau)\sin^2\frac{\omega}{2}\right], \tag{3.51}$$

and for $\phi = -i$ it is

$$\frac{1}{2}\ln\frac{1}{4\left(\Delta\tau\right)^2\alpha(\alpha-1)} + \int_{-\pi}^{\pi}\frac{dw}{2\pi}\,\ln\left[4\left(\Delta\tau\right)^2 + 4(1+2\Delta\tau)\sin^2\frac{\omega}{2}\right]. \tag{3.52}$$

The integral in the above expression are convergent and $\phi = i$ classical fixed point leads to a smaller term. Based on our discussion in the previous sections, we conclude that the complex langevin equation will converge a stationary distribution that is quantized around $\phi = i$. To be more precise, we mean that the correlators of this theory are given by

$$\left\langle\phi^k\right\rangle = \frac{\int_\Gamma d\phi\,\phi^k\exp\left\{i\phi+\frac{i}{3}\phi^3\right\}}{\int_\Gamma d\phi\,\exp\left\{i\phi+\frac{i}{3}\phi^3\right\}}, \tag{3.53}$$

where Γ is the steepest descent path that passes from $\phi = i$. This steepest descent

path is easy to identify is one changes variables to $\phi = -i\psi$. Then

$$\langle \phi^k \rangle = \frac{(-i)^k \int_{\Gamma'} d\psi \, \psi^k \exp\left\{\psi - \frac{1}{3}\psi^3\right\}}{\int_{\Gamma'} d\psi \, \exp\left\{\psi - \frac{1}{3}\psi^3\right\}}, \tag{3.54}$$

and now the saddle point that we want to quantize around is at $\psi = -1$. In this form, Γ' is recognized as the steepest descent path that defines an Airy function evaulated at 1, i.e. Ai(1). We refer the reader to [81] and [13] for details of this analysis. In particular,

$$\langle \phi \rangle = -i \frac{\mathrm{Ai}'(1)}{\mathrm{Ai}(1)} = 1.176i, \tag{3.55}$$

which was calculated by MATLAB's built in Airy functions to 3 decimal places. In this equation, $'$ refers to a derivative with respect to the argument. Now, going back to equation (3.47), one concludes that

$$\langle \phi^2 \rangle = -1, \qquad \langle \phi^3 \rangle = i - \langle \phi \rangle = -0.176i, \qquad \ldots. \tag{3.56}$$

$\langle \phi \rangle$ fixes all the other correlators through algebraic relations. This is expected since setting $\langle \phi \rangle$ to some number means imposing a second condition, aside from normalization, on the solutions of the Schwinger-Dyson equation (3.47). This fixes the solution completely.

We expect a long time complex Langevin simulation to give us these correlators. We did 100 complex Langevin simulations that ran from $\tau = 0$ to $\tau = 10000$. The step size was $\Delta\tau = 1 \times 10^{-3}$ and α was chosen to be 1.001. Each simulation started

from a random initial condition. The first three correlators calculated were

$$\langle\phi\rangle_{CL} = 0.001(5) + 1.176(1)i, \qquad \langle\phi^2\rangle_{CL} = -0.9999(5) + 0.003(13)i,$$
$$\langle\phi^3\rangle_{CL} = -0.006(21) - 0.176(7)i. \tag{3.57}$$

Here the Langevin time averages are averaged over 100 simulations and the error bars stand for the standard deviation over 100 simulations. These numbers are in good agreement with theoretical results, as expected.

We note that one could expect the $\phi = i$ classical fixed point to dominate over $\phi = -i$ classical fixed point by noticing that the former is a stable fixed point for the classical process, whereas the latter is not. Adding noise eventually makes the simulation sample around the stable fixed point, leading to a quantization around the stable fixed point. This parallels the results of [1, 15]. Figure 3.2 shows a set of sample points from the complex Langevin equation with classical flow on the background. The simulation is seen to sample around the stable fixed point $\phi = i$.

3.4 Discussion of Results

In this chapter, we attempted a new approach to the question of identifying the stationary distribution sampled by a complex Langevin equation. We worked in a lattice setting. The continuum limit and renormalizability issues are not trivial and deserves another study of its own.

Our idea is based on a two step process. First, by solving a Schwinger-Dyson equation [45] one finds a possible set of stationary distributions. These are complexified path integrals [33, 43]. To identify the particular stationary distribution sampled

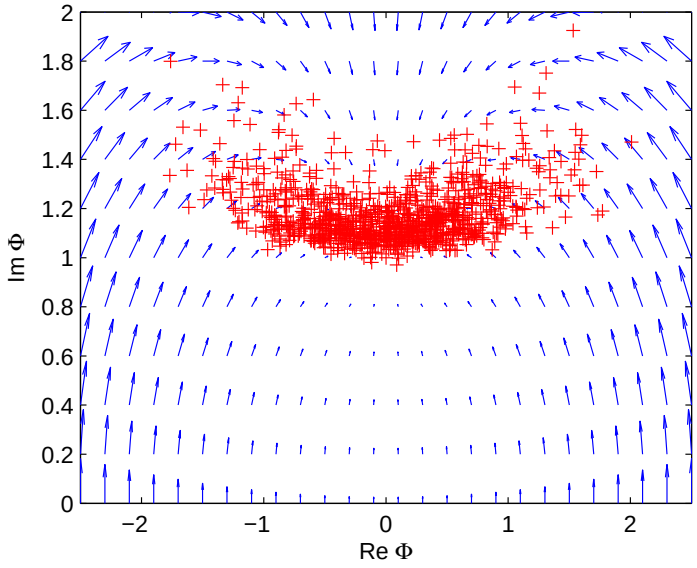

Figure 3.2: 1000 sample points (marked by +'s) from a complex Langevin simulation of action (3.46) with classical flow plotted in the background.

by the complex Langevin equation, one needs to use information from the dynamics of the complex Langevin process. All the information about the dynamics of a complex Langevin process is in its generating functional. Our second step, whose details are given in this chapter, is to use this generating functional and define an effective potential based on it. We argued that this effective potential governs the probability distribution of space-time and Langevin time averages of the simulated field variable. In particular, in the infinite Langevin time limit, the field average must equal to the minimum of the effective potential. We calculated this effective potential, expanding it in a parameter that multiplies the noise in the complex Langevin equation. In the lowest order, the minima are given by the saddle points of the action S. The next order removes the degeneracy. The same parameter is shown to count loops in a loop expansion of the stationary distributions (that satisfy Schwinger-Dyson equations). Therefore, we concluded that the complex Langevin equation must be sampling a stationary distribution that describes a field theory that is quantized around the

minimum of the complex Langevin equation effective action.

The work presented in this chapter should be viewed as a general statement on complex Langevin equations. To our knowledge, the path integral description of complex Langevin equations, which carries all the dynamic information about the process, has not been explored before. We feel that this may bring new conceptual insights to the problem at the very least, and it needs to be studied more. We hope that the novel approach we presented in this chapter will help in coming up with a scheme to control the complex Langevin process resulting in a good numerical scheme to solve realistic problems. Whatever this scheme is, we are sure that it will require a lot of work and will easily be the subject of independent studies.

As a final note, we want to mention that this construction can be used as a tool for studying symmetry breaking effects in stochastic quantization for complex actions [80].

Chapter Four

Dynamical Systems with Exact Statistics

Due to their sensitive dependence on initial conditions, the precise behavior of a chaotic dynamical system over very long times is unpredictable in practice, even though the underlying system is deterministic. However there is no fundamental obstruction to calculating statistical properties, in the form of long time averages over chaotic trajectories. Typically, statistical properties are calculated by direct numerical simulation, with the assumption that the statistics of the computer generated trajectory are accurate despite the accumulation of numerical errors in the solution. However this assumption depends on properties, such as 'shadowing' [7, 18, 50] which may not always be valid. Furthermore, direct simulation of systems with a very large number of degrees of freedom requires significant computational power which in many cases is not yet available. Such simulations, which are essentially experiments, are also of little theoretical value.

A much better approach to would be formulated entirely in terms of the quantities of interest, namely the statistics. One way to do so is to work with an equation due to Hopf [54, 31, 88], which governs the generating functional of equal time moments. In a few special instances, it is possible to exactly solve these equations, with their attendant boundary conditions, even for a large number of degrees of freedom (see for example [76]). The Fourier transform of the Hopf generating functional is a distribution which satisfies the Fokker-Planck equation [99]. The intent of this chapter is to further develop an inverse approach, proposed in [47], to construct chaotic systems starting with such a distribution. An infinite number of chaotic invariant sets can be constructed by the approach described in [47]. These are invariably dissipative in some regions of the phase space and non-dissipative in others. Although we have not attempted to construct an inverse approach based on the Hopf functional, rather than a distribution, such an approach might also generate globally dissipative chaotic invariant sets.

The fraction of time a chaotic trajectory spends in different regions of phase space is described by an invariant measure over the phase space $d\mu(\vec{x})$. If this measure can be described by a distribution over phase space, $d\mu(\vec{x}) = \rho(x_1 \cdots x_N)d^N x$, then $\rho(\vec{x})$ is the Fourier transform of the Hopf functional discussed above. For a deterministic chaotic system (with no stochastic component) ρ satisfies the static, zero-diffusion limit of the Fokker-Planck equation, $\vec{\nabla} \cdot (\rho\vec{v}) = 0$, where $d\vec{x}/dt \equiv \vec{v}(\vec{x})$ defines the dynamical system. Based on this equation, it was shown [47] that a large class of dynamical systems can be uniquely specified by a distribution ρ and a two-form $\mathcal{B} = \mathcal{B}_{ij}(x_1 \cdots x_N)dx^i \wedge dx^j$, which must be chosen carefully if the velocity field of the resulting dynamical system is to be polynomial in the phase space coordinates[1]. This is similar to the specification of Hamiltonian systems by a Hamiltonian and a symplectic form, although far more general. In particular there is no restriction to even number degrees of freedom or systems satisfying a Liouville theorem. Nor are there necessarily any conserved quantities.

Although ρ is, by construction, an invariant distribution of the dynamical system defined by ρ and $\mathcal{B}$, it does not necessarily describe the statistics of a chaotic trajectory. In other words, ρ is not necessarily ergodic, and may have a convex decomposition into other invariant distributions $\rho = x\rho_1 + (1-x)\rho_2$ with $0 < x < 1$. In some cases, for example, ρ may merely represent an arbitrary distribution over independent periodic orbits. However, as shown in [47], the dynamical system defined by ρ and $\mathcal{B}$ frequently exhibits a chaotic invariant set with statistics described by ρ, subject to certain constraints on its domain of support. We briefly review the construction of chaotic systems by the inverse method in section 4.2.

The purpose of this chapter is to generalize the analysis of [47] to compute unequal time correlation functions for chaotic systems generated by the inverse ap-

[1] A generalization to some stochastic systems was also discussed in [47].

proach. We will specifically consider auto-correlation functions, defined by

$$G_i(\Delta) \equiv < x_i(t)x_i(t+\Delta) > - < x_i(t) >^2 , \tag{4.1}$$

where <> denotes time averaging;

$$< f(t) > \equiv \lim_{T\to\infty} \frac{1}{T} \int_0^T dt\, f(t) . \tag{4.2}$$

We emphasize that our subsequent discussion is all readily generalizable to arbitrary un-equal time correlations, such as $< x_i(t)x_j(t+\Delta_1)x_k(t+\Delta_2) >$. For a chaotic orbit with an invariant measure $d\mu(\vec{x})$,

$$G_i(\Delta) = \int d\mu(\vec{X})\, x_i(0)\, x_i(\Delta) - \left(\int d\mu(\vec{X}) X_i \right)^2 , \tag{4.3}$$

where $\vec{x}(t)$ is a solution of the equations of motion with initial condition $\vec{x}(0) = \vec{X}$. If the invariant measure is known, as is the case for chaotic invariant sets generated by the inverse approach, $G_i(\Delta)$ can be computed by Monte-Carlo calculations, involving multiple simulations of the dynamical system over a duration Δ starting from randomly generated initial conditions. Since this is amenable to parallel computation, it can be done much faster than computations based on (4.1) which require a long run from a single initial condition. Due to the shorter run times, the Monte-Carlo approach may also be more reliable than long duration simulation. We give an example of such a computation in section 4.3, finding precise agreement with the result obtained by long duration simulation of the equations of motion.

Given the invariant measure of a chaotic trajectory , one can also write integral expressions for a Taylor-Mclaurin expansion of $G_i(\Delta)$, whose validity can be extended beyond the domain of convergence by Pade approximants. This approach

does not involve any direct simulation of the equations of motion. We perform such a calculation in section 4.4, for the same example discussed in section 4.3. The (4|4) Pade approximant gives good results for Δ well beyond the utility of the Taylor series in Δ, which we expect can be extended much further by considering higher order approximants.

Finally, in section 4.5, we make some remarks power spectra of dynamical systems obtained from Fourier decomposition of a signal within some time window. For a chaotic system, this approach is rife with ambiguities and pitfalls, unlike the Fourier transform of the auto-correlation function which is well defined. However these pitfalls are themselves interesting and can be well understood using the inverse approach.

4.1 Review of the inverse approach

We give a very brief review of the inverse method here. For details the reader is referred to [47]. We consider deterministic dynamical systems, with phase space coordinates $x_1(t) \cdots x_N(t)$ and equations of motion

$$\frac{dx_n}{dt} = v_n(x_1, \cdots x_N) \tag{4.4}$$

A distribution over initial conditions $\rho[x]$ which is left invariant by the time evolution is a solution of the zero diffusion limit of the static Fokker-Planck equation,

$$\vec{\nabla} \cdot (\rho \vec{v}) = 0\,, \tag{4.5}$$

For $N = 3$, this implies that $\rho\vec{v}$ can be written as the curl of a vector field,

$$\vec{v} = \frac{\vec{\nabla} \times \vec{A}}{\rho}\,, \tag{4.6}$$

and the inverse method amounts to choosing $\vec{A}$ and ρ, such that $\vec{v}$ is polynomial in the phase space coordinates x_n. For $N > 3$, it is convenient to use the language of differential forms, in which case (4.4) becomes

$$d^*(\rho v) = 0 \tag{4.7}$$

where v is the velocity one form $v_m dx^m$, d is the exterior derivative, and * indicates the Hodge dual. This implies that

$$v = \frac{{}^*d\mathcal{A}}{\rho} \tag{4.8}$$

where $\mathcal{A}$ is an $N-2$ form. The problem is then to choose ρ and $\mathcal{A}$ such that v is polynomial in x_n. This was done in [47] for a few increasingly complex analytic structures of ρ and $\mathcal{A}$.

Since ${}^*\mathcal{A}$ is a two-form (${}^*\mathcal{A} = \mathcal{B}$ in the notation of the introduction) which is more conveniently written down for large N than $\mathcal{A}$, it can be said that an invariant distribution and a two-form uniquely specify dynamical systems. This is very similar to the specification of Hamiltonian dynamical systems by a Hamiltonian and a symplectic form, although far more general. For example N need not be even and a Liouville theorem, $d^*v = 0$, need not apply, nor are there necessarily any conserved quantities.

Amongst the simplest distributions, so far as analytic structure is concerned, are polynomial distributions for which the real zeroes form a closed manifold inside of

which the polynomial is positive. For these,

$$\mathcal{A} = \rho^2 \Omega \tag{4.9}$$

were ρ is a polynomial, and Ω is a polynomial $N-2$ form, so that

$$v = {}^*(\rho d\Omega + 2d\rho \wedge \Omega) \tag{4.10}$$

Chaotic dynamical systems of this type are invariably repellers (see [47]). Chaotic attractors arise from distributions and two-forms with more complicated analytic structure, which are also discussed in [47].

Although a distribution ρ satisfying (4.4) is an invariant distribution over initial conditions, it does not necessarily describe the statistics of a single chaotic trajectory. It must be verified that the dynamics is chaotic and that ρ, or perhaps its projection to lower dimension, is an ergodic measure, having no convex decomposition into independent invariant measures $\rho \neq x\rho_1 + (1-x)\rho_2$ with $0 < x < 1$. In many instances discussed in [47], it was necessary to modify the domain of support of the initial distribution ρ for it to describe a chaotic invariant set. One mystery is that, for chaotic invariant sets with fractional information dimension, a function $\rho(x)$, with support in N dimensions can not be ergodic, yet the distributions discussed in [47] yield extremely accurate if not exact statistics. Since the information dimensions of the systems constructed in [47] have not yet been computed, it is difficult to draw specific conclusions. However, one possibility is that the initial invariant distribution in the inverse approach may still contain exact information about the statistics upon projection to lower integer dimension. This may be too strong, since an example was given in [47] for which ρ gave accurate connected correlation functions involving all phase space coordinates. Another possibility is that ρ may have the interpretation

as the Fourier transform of the generating functional of equal-time correlations, and therefore captures all polynomial moments. Of course it is also possible that the systems thus far constructed by the inverse method have information dimension which is very nearly N, in which case ρ yields, at worst, an extremely accurate approximation to the exact statistics.

Before continuing with our discussion, let us discuss an example to the inverse approach. Consider a specific chaotic system of the type (4.10) (studied in [47]) with

$$\begin{aligned} \rho &= 1 - x^4 - y^2 - z^6 \\ \Omega &= (xyz)dy + (y^2)dz\,. \end{aligned} \tag{4.11}$$

yielding

$$\begin{aligned} v_x &= 13z^6xy - 6y^3 - xy + 2y + yx^5 - 2yx^4 - 2yz^6 + y^3x\,, \\ v_y &= 8x^3y^2\,, \\ v_z &= -9x^4yz + yz - yz^7 - y^3z\,. \end{aligned} \tag{4.12}$$

Initial conditions with $\rho(x, y, z) > 0$, $y > 0$ and $z > 0$ give rise to chaotic trajectories whose statistics are described by an invariant distribution $\tilde{\rho} = \rho$ for $\rho(x, y, z) > 0$, $y > 0$, $z > 0$, up to a normalization, and $\tilde{\rho} = 0$ outside this domain. Long-time averages of this system were compared with Monte Carlo simulations of the invariant measure in [47] and a perfect agreement was found. In this chapter, we will generalize this system to "many lattice sites" with "nearest neighbor interactions".

We treat the dynamics (4.30) as a three degree of freedom sytem at a lattice site. Non-interacting generalization of this example to N non-interacting copies would

clearly be given by

$$\begin{aligned}\rho &= \prod_i \rho_i, \\ \rho_i &\equiv 1 - x_i^4 - y_i^2 - z_i^6, \qquad i = 1, \ldots, N.\end{aligned} \tag{4.13}$$

Now we define

$$\begin{aligned}\Omega_i &\equiv (x_i y_i z_i)\, dy_i + (y_i)^2\, dz_i, \\ {}^{*3}\Omega_i &\equiv (x_i y_i z_i)\, dz_i \wedge dx_i + (y_i)^2\, dx_i \wedge dy_i.\end{aligned} \tag{4.14}$$

Taking Ω to be

$${}^{*}\Omega = \sum_i \frac{{}^{*3}\Omega_i}{\prod_{j \neq i} \rho_j}, \tag{4.15}$$

it is easy to check that this selection of the invariant distribution and two-form given N independent copies of the original system.

This is not very interesting. We want to generalize this such that neghboring degrees of freedom interact, while keeping the velocity terms polynomial. The simplest way to do this is to include neares neighbor inteactions in the form

$$\rho = \prod_i \rho_i \prod_j \rho_{j,j+1}. \tag{4.16}$$

$\prod_j \rho_{j,j+1}$ is the interaction term. Let's choose it to have the simple form

$$\rho_{j,,j+1} \equiv 1 - \epsilon \left(\vec{x}_j - \vec{x}_{j+1}\right)^2. \tag{4.17}$$

and take

$$
\begin{aligned}
{}^{*}\Omega &\equiv \sum_i \frac{{}^{*3}\Omega_i}{\prod_{j\neq i}\rho_j \prod_{j\neq i,\, j+1\neq i}\rho_{j,j+1}}, \\
\tilde{\Omega}_i &\equiv {}^{*}\left({}^{*3}\Omega_i\right),
\end{aligned}
\tag{4.18}
$$

so that

$$
\begin{aligned}
v &= {}^{*}\left(\rho d\Omega + 2d\rho \wedge \Omega\right) \\
&= \sum_i {}^{*}\left(\rho_i\rho_{i-1,i}\rho_{i,i+1} d_i\tilde{\Omega}_i + 2d_i\left(\rho_i\rho_{i-1,i}\rho_{i,i+1}\right) \wedge \tilde{\Omega}_i\right).
\end{aligned}
\tag{4.19}
$$

This gives,

$$
\begin{aligned}
v_i &= {}^{*3}\left(\rho_i\rho_{i-1,i}\rho_{i,i+1} d_i\Omega_i + 2d_i\left(\rho_i\rho_{i-1,i}\rho_{i,i+1}\right) \wedge \Omega_i\right) \\
&= \rho_{i-1,i}\rho_{i,i+1} v_i^{(0)} + {}^{*3}\left(2\rho_i d_i\left(\rho_{i-1,i}\rho_{i,i+1}\right) \wedge \Omega_i\right),
\end{aligned}
\tag{4.20}
$$

where $v_i^{(0)}$ is the velocity for the uncoupled system

$$
v_i^{(0)} = {}^{*3}\left(\rho_i d_i\Omega_i + 2d_i\rho_i \wedge \Omega_i\right). \tag{4.21}
$$

Working out the details finally gives the dynamical system

$$\begin{aligned}
v_{i,x} &= \rho_{i,i+1}\rho_{i-1,i}v_{i,x}^{(0)} \\
&\quad - 4\epsilon\rho_i\left[\rho_{i-1,i}\left[\left(y_i - y_{i+1}\right)y_i^2 - \left(z_i - z_{i+1}\right)x_i y_i z_i\right]\right. \\
&\quad \left.+\rho_{i,i+1}\left[\left(y_i - y_{i-1}\right)y_i^2 - \left(z_i - z_{i-1}\right)x_i y_i z_i\right]\right], \\
v_{i,y} &= \rho_{i,i+1}\rho_{i-1,i}v_{i,y}^{(0)} \\
&\quad + 4\epsilon\rho_i\left[\rho_{i-1,i}\left(x_i - x_{i+1}\right) + \rho_{i,i+1}\left(x_i - x_{i-1}\right)\right]y_i^2, \\
v_{i,z} &= \rho_{i,i+1}\rho_{i-1,i}v_{i,z}^{(0)} \\
&\quad - 4\epsilon\rho_i\left[\rho_{i-1,i}\left(x_i - x_{i+1}\right) + \rho_{i,i+1}\left(x_i - x_{i-1}\right)\right]x_i y_i z_i,
\end{aligned} \tag{4.22}$$

where

$$\begin{aligned}
\rho_i &= 1 - x_i^4 - y_i^2 - z_i^6, \\
\rho_{i-i+1} &= 1 - \epsilon\left(\vec{x}_i - \vec{x}_{i+1}\right)^2, \\
v_{i,x}^{(0)} &= 13z_i^6 x_i y_i - 6y_i^3 - x_i y_i + 2y_i + y_i x_i^5 - 2y_i x_i^4 - 2y_i z_i^6 + y_i^3 x_i, \\
v_{i,y}^{(0)} &= 8x_i^3 y_i^2, \\
v_{i,}^{(0)} &= -9x_i^4 y_i z_i + y_i z_i - y_i z_i^7 - y_i^3 z_i.
\end{aligned} \tag{4.23}$$

We performed a simulation of this system with $N = 150$ and a Monte Carlo simulation of the associated probability distribution. In Table 4.1, we compare these results and find perfect agreement. As expected, one was able to engineer a dynamical system with a given invariant measure.

One thing to note about this approach is that nowhere in our derivation did we specify the domain of the invariant distribution. The domain is specified by the attractor of the derived dynamical system. In the example above, we note that there

Table 4.1: Comparison of long runs to Monte Carlo simulations

	Long Run	Monte Carlo
y_{110}	0.3475	0.3420
$\frac{1}{N}\sum_i < y_i >$	0.3406	0.3450
z_1	0.4045	0.4157
$\frac{1}{N}\sum_i < z_i >$	0.4031	0.4129
$< x_1^2 >$	0.1966	0.1983
$\frac{1}{N}\sum_i < x_i^2 >$	0.1981	0.1979
$< y_{100}^2 >$	0.1703	0.1694
$\frac{1}{N}\sum_i < y_i^2 >$	0.1701	0.1712
$< y_5 y_6 >$	0.1332	0.1425
$\frac{1}{N}\sum_i < y_i y_{i+1} >$	0.1179	0.1196
$< x_{33} z_{37} >$	0.0010	-0.0010
$\frac{1}{N}\sum_i < x_i z_{i+4} >$	0.0005	0
$< z_7 y_8 >$	0.1360	0.1387
$\frac{1}{N}\sum_i < z_i y_{i+1} >$	0.1405	0.1384
...		

For these simulations $N = 150$ and periodic boundary conditions are applied. $\epsilon = 0.1$ and is chosen such that the probability distribution never becomes negative. Comparisons are made with averages over lattice sites as well as individual lattice sites. Results suggest translational invariance. Long runs start from $t = 0$ and end at $t = 20000$, with time steps $\Delta t = 0.001$. Monte Carlo simulation are done by the Metropolis algorithm with 2000000 sweeps.

is no crossing in the dynamics across $y_i = 0$ and $z_i = 0$ axes. Therefore we restrict ourselves to the domain in which $y_i > 0$ and $z_i > 0$ and $\rho > 0$.

We emphasize that the results in this chapter are not restricted to chaotic dynamical systems generated by the inverse method. In fact, they may be applied to any chaotic system for which there is known information about the invariant measure over phase space or equal time moments. This information can be used to facilitate the computation of time dependent statistics, such as auto-correlation functions.

4.2 Monte-Carlo computation of the auto-correlation and power spectrum

Power spectra are useful signatures of dynamical systems derived from time series data. The 'energy spectral density' associated with a signal $x(t)$ is defined as the squared amplitude of the Fourier transform of $x(t)$. However, if the system is chaotic the Fourier transform of $x(t)$ is is not well defined, since $x(t)$ is a-periodic and does not fall of as $t \to \pm\infty$. The 'power spectral density', on the other hand, is well defined;

$$\tilde{G}(\omega) \equiv \int_{-\infty}^{\infty} d\Delta \, e^{i\omega\Delta} G(\Delta) \,, \tag{4.24}$$

where $G(\Delta)$ is the auto-correlation function,

$$G(\Delta) \equiv < x(t)x(t+\Delta) > - < x(t) >^2 \ . \tag{4.25}$$

Due to the tendency of chaotic systems to 'forget' their initial conditions, $G(\Delta)$ falls off with large Δ sufficiently rapidly that the Fourier transform (4.24) is well defined. The total power between frequencies ω and $\omega + d\omega$ is given by $\tilde{G}(\omega)d\omega$.

Time averages of functions of phase space over an ergodic chaotic trajectory are equal to averages with respect to an invariant measure over phase space;

$$< f(\vec{x}(t)) >= \int d\mu(\vec{X}) f(\vec{X}) \,. \tag{4.26}$$

Noting that $\vec{x}(t+\Delta)$ is a function of $\vec{x}(t)$, the auto-correlation of a phase space

variable x_i can be written as

$$G_i(\Delta) = \int d\mu(\vec{X}) f_\Delta(\vec{X}) - \left(\int d\mu(\vec{X}) X_i \right)^2 , \tag{4.27}$$

where

$$f_\Delta(\vec{X}) \equiv X_i x_i(\Delta) , \quad \text{with } \vec{x}(0) = \vec{X} . \tag{4.28}$$

When the exact invariant measure is known, as is the case for chaotic invariant sets generated by the inverse approach, the auto-correlation functions can be computed by Monte-Carlo methods. This entails multiple fixed time simulations of the dynamical system of duration Δ, starting from initial conditions generated randomly according to the invariant distribution $\rho(\vec{X})$.

4.3 An example

We consider a specific chaotic invariant set found in [47], with dynamics of the type (4.10) with polynomial ρ and Ω given by

$$\begin{aligned} \rho &= 1 - x^4 - y^2 - z^6 , \\ \Omega &= (xyz)dy + (y^2)dz , \end{aligned} \tag{4.29}$$

yielding

$$\begin{aligned} v_x &= 13z^6xy - 6y^3 - xy + 2y + yx^5 - 2yx^4 - 2yz^6 + y^3x\,, \\ v_y &= 8x^3y^2\,, \\ v_z &= -9x^4yz + yz - yz^7 - y^3z\,. \end{aligned} \tag{4.30}$$

Initial conditions with $\rho(x,y,z) > 0$, $y > 0$ and $z > 0$ give rise to chaotic trajectories whose statistics are described by an invariant distribution $\tilde{\rho} = \rho$ (up to normalization) within the domain $\rho(x,y,z) > 0$, $y > 0$, $z > 0$ and $\tilde{\rho} = 0$ elsewhere.

Consider the auto-correlation $G_x(\Delta)$ for the variable x on these chaotic trajectories. The auto-correlation can be evaluated by a long duration numerical simulation of the equations of motion, taking the time average of $x(t)x(t+\Delta)$. Alternatively, it can be evaluated using (4.27);

$$G_x(\Delta) = \int dX dY dZ \tilde{\rho}(X,Y,Z)\, f_\Delta(X,Y,Z) - \left(\int dX dY dZ \tilde{\rho}(X,Y,Z)\, X \right)^2 , \tag{4.31}$$

where

$$F_\Delta(X,Y,Z) \equiv X x(\Delta)\,, \tag{4.32}$$

with

$$x(0) = X,\ y(0) = Y,\ z(0) = Z\,. \tag{4.33}$$

Evaluating (4.31) by Monte Carlo simulation amounts to generating initial conditions X, Y, Z randomly according to the distribution $\tilde{\rho}$, and simulating the time evolution from each of these points over a duration Δ. The results of both the Monte-Carlo

calculation and a direct long-duration numerical simulation of (4.30) are shown in figure 4.1, showing extremely good agreement.

The example we have given is a small dimension system, with $N = 3$, so there is little computational advantage to the Monte-Carlo approach over a direct long duration simulation. The advantage comes at large N, for which the Monte-Carlo approach will be far faster, as it is amenable to parallel computation. Furthermore, we would be more inclined to trust the results of a Monte-Carlo calculation, since it involves shorter run times with less error accumulation due to sensitivity to initial conditions.

4.4 Calculating the auto-correlation without direct numerical simulation.

Using (4.27), the auto-correlation function $G_i(\Delta)$ can be expanded as a power series in Δ. To do so let us first expand (4.28) in Δ:

$$F_\Delta(\vec{X}) \sim x_i(0)\left(x_i(0) + \Delta\dot{x}_i(0) + \frac{1}{2}\Delta^2\ddot{x}_i(0)\cdots\right), \text{ with } \vec{x}(0) = \vec{X}\,. \tag{4.34}$$

Note that $x_i\frac{d^n x_i}{dt^n}$ can be written as a total time derivative for odd n:

$$x_i\frac{dx_i}{dt} = \frac{d}{dt}\left(\frac{1}{2}x_i^2\right), \quad x_i\frac{d^3x_i}{dt^3} = \frac{d}{dt}\left(x_i\frac{d^2x_i}{dt^2} - \frac{1}{2}\left(\frac{dx_i}{dt}\right)^2\right), \text{ etc} \tag{4.35}$$

For even n, $n = 2m$,

$$x_i\frac{d^n x_i}{dt^n} = \frac{d}{dt}(g_n) + (-1)^m\left(\frac{d^m x_i}{dt^m}\right)^2 \tag{4.36}$$

where we will not bother to specify g_n, since total time derivatives vanish when averaged over a chaotic trajectory[2]. Thus

$$G(\Delta) = \langle F_\Delta \rangle \sim \sum_{m=0}^{\infty} \alpha_m \Delta^{2m} \tag{4.37}$$

$$\alpha_m \equiv (-1)^m \frac{1}{2m!} \left\langle \left(\frac{d^m x_i}{dt^m} \right)^2 \right\rangle \tag{4.38}$$

Using the equations of motion

$$\frac{dx_i}{dt} = v_i(\vec{x})$$

the terms $(d/dt)^m x_i$ can be related to functions on phase space. For example

$$\frac{d^2 x_i}{dt^2} = \frac{dv_i}{dt} = \sum_j v_j(\vec{x}) \frac{\partial v_i(\vec{x})}{\partial x_j}$$

so that

$$\alpha_2 = \left\langle \left(\frac{d^2 x_i}{dt^2} \right)^2 \right\rangle = \int d\mu(\vec{X}) \left(\sum_j v_j(\vec{X}) \frac{\partial v_i(\vec{X})}{\partial X_j} \right)^2$$

Since $F_\Delta(\vec{X})$ can not have singularities on the real axis (the real solutions of the equations of motion are assumed to be non-singular), the series (4.37) has a finite radius of convergence. We propose to evaluate $G(\Delta)$ by Monte-Carlo integration to evaluate the coefficients α_m, followed by a Pade resummation of (4.37).

For the dynamical system (4.30), the moments α_m are evaluated with respect to the measure $d\mu(\vec{x}) = dxdydz\tilde{\rho}(\vec{x})$, with

$$\begin{aligned} &\tilde{\rho} = 1 - x^4 - y^2 - z^6 \text{ for } x^4 + y^2 + z^6 < 1,\ y > 0,\ z > 0, \\ &\tilde{\rho} = 0 \text{ elsewhere}, \end{aligned} \tag{4.39}$$

up to normalization. We have calculated the coefficients $\alpha_0 \cdots \alpha_8$ associated with the

[2]We are assuming a bounded system with no explicit time dependence in the equations of motion.

auto-correlation $G_x(\Delta)$ using computer algebra and Monte-Carlo simulation. The corresponding (4|4) Padé approximant is a ratio of polynomials of degree 4 whose first 9 Taylor-Maclaurin series coefficients are $\alpha_0 \cdots \alpha_8$. The (4|4) Padé approximant to $G_x(\Delta)$ is plotted in figure 4.2, along with the 9'th order Taylor-Maclaurin series result and the result of direct numerical simulation by a long run of the dynamical system. Note that the 9-th order Taylor-Maclaurin series begins to differ markedly from the result of direct numerical simulation at $\Delta \sim 0.35$, well before the first zero, whereas the (4|4) Padé approximant gives accurate result for much larger values of Δ, and is an acceptable approximation up to a neighborhood of the first zero, $\Delta \sim 2$. Higher order Padé approximants are needed to obtain more real zeros and provide a good approximation for larger values of Δ. This requires more computing power than we have presently applied to the problem. Nevertheless, the initial results are very encouraging, suggesting that the auto-correlation may be computed without any direct simulation of the dynamical system. This approach is probably not as computationally efficient as combining Monte-Carlo simulation with short duration direct numerical simulation. However it has the advantage of replacing an 'experimental' approach to calculating auto-correlation functions with a purely theoretical approach based on exact integral expressions for their Taylor-Mclaurin expansion. As such, it has the potential to yield general insights which were previously out of reach, particularly if one can determine the large order behavior of the Taylor-Mclaurin expansion.

Chaotic power spectra are expected to have a non-zero exponentially small component at high frequency [32, 105], $\tilde{G}(\omega) \sim \exp(-\alpha\omega)$. The time-scale α is determined by the proximity of the nearest singularity of the auto-correlation $G(\Delta)$ to the real Δ axis. Note that there can not be any singularities on the real Δ axis, as it is assumed that the time evolution of the dynamical system does not encounter any

singularities. Due to the tendency of chaotic systems to 'forget' their intial conditions, one expects singularities of $G(\Delta)$ near the real axis to occur for small values of $Re(\Delta)$. This suggest that the high frequency behavior of the power spectral density can be extracted from the small Δ behavior of the auto-correlation. It may therefore be possible to use a relatively low order Padé approximant to the auto-correlation to get an estimate of the parameter α. Some care must be taken, since the poles of the Padé approximant do not necessarily correspond to the true analytic structure. In fact the (4|4) Padé approximant we have computed here has two poles which are likely both spurious, including one on the positive real axis which must be spurious. These poles are extremely close to zeros of the Padé approximant. There is one pole which is not near any zero, at $\Delta = 1.24i$, suggesting $\alpha \approx 1.24$ as a crude first approximation.

It is interesting to note that the dependance of un-equal time correlations, such as the auto-correlation, on the two-form used in the inverse approach is rather different from that of the equal time moments. Equal time moments are determined by the invariant distribution, subject to constraints on the domain of support required for ergodicity. The dependence of these constraints on the two-form appears topological in character, as smooth variations of the two-form do not necessarily change the constraints. On the other hand, un-equal time correlation depend directly on the two-form as well as the invariant distribution, through the dependence of $\vec{v}(\vec{x})$ on these quantities. In general, smooth variations of the two-form change the un-equal time correlations, if not the equal-time moments.

4.5 Remarks on the Fourier transform of a chaotic signal

The Fourier transform of a chaotic trajectory,

$$\tilde{x}(\omega) = \int_{-\infty}^{\infty} dt\, e^{-i\omega t} x(t)\,, \tag{4.40}$$

is not well defined since $x(t)$ is a-periodic and does not fall off at $t \to \pm\infty$. Nevertheless, it is common to take the Fourier (or discrete Fourier) transform of chaotic time series with some window of fixed duration, squaring the amplitude to give a kind of 'energy' spectral density. The result is very sensitive to the initial conditions and the duration of the time series, but nevertheless bears some resemblance to the (well defined) power spectral density. Although somewhat peripheral to the main thrust of this chapter, it is interesting to attempt to quantify this resemblance using tools similar to those discussed above.

Let us consider a function on phase space $f_\omega(\vec{X})$, defined by

$$f_\omega(\vec{X}) = \frac{\omega}{2\pi} \int_0^{2\pi/\omega} dt\, x_i(t) e^{-i\omega t}, \quad \text{with } \vec{x}(0) = \vec{X}\,, \tag{4.41}$$

Next consider the time average of $f_\omega(\vec{X})$ over a chaotic trajectory $\vec{X}(t)$; $< f_\omega(\vec{X}(t)) >$. We assume that the average can be computed by summing over values of $f_\omega(\vec{X}(t))$ at arbitrary regular time intervals Δt, yielding a result which is independent of the interval. If one chooses the interval $\Delta t = 2\pi/\omega$, one arrives at the formal result

$$< f_\omega(\vec{x}(t)) >= \lim_{T\to\infty} \frac{1}{T} \int_0^T dt\, e^{-i\omega t} x_i(t)\,. \tag{4.42}$$

In terms of the invariant measure $d\mu(\vec{X})$ on the phase space of a chaotic system,

ergodicity implies

$$< f_\omega(\vec{x}(t)) >= \int d\mu(\vec{X}) f_\omega(\vec{X})\,. \tag{4.43}$$

Note that different initial conditions $\vec{x}(0)$ which are different points on the same chaotic trajectory lead to a different overall phase in (4.42). On the other hand, (4.43), to which (4.42) is formally equivalent, has no reference to an initial condition. This is consistent only if $< f_\omega(\vec{x}(t)) >= 0$.

It is interesting to try to compute (4.43) by Monte-Carlo simulation. Note that any non-zero result is pure error, which we shall see is closely related to the power spectral density. The Monte-Carlo calculation amounts to generating a set of n initial conditions randomly, according to the distribution of the chaotic invariant set, and then running the dynamical system from each initial condition for a duration $2\pi/\omega$. Given the chaotic 'loss of information' about initial conditions with time, one expects this to yield a very similar result to direct numerical simulation from a single initial condition over a duration $2\pi n/\omega$.

As stated above, any non-zero result of a Monte-Carlo calculation of (4.43) is pure error, The size of the error, on the average, is determined by the variance of the Monte-Carlo result, which is $1/n$ times the variance of $f_\omega(\vec{X})$. The variance of $f_\omega(\vec{X})$ can be expressed in terms of the auto-correlation function $G_x(\Delta)$, since

$$< |f_\omega(\vec{x}(t)) - < f_\omega(\vec{x}(t)) > |^2 >= \int_0^{2\pi/\omega} dt \int_0^{2\pi/\omega} dt' \int d\mu(\vec{X}) x(t) x(t') e^{i\omega(t-t')}$$
$$\text{with } \vec{x}(0) = \vec{X}\,, \tag{4.44}$$

so that

$$< |f_\omega - < f_\omega > |^2 >= \int_0^{2\pi/\omega} dt \int_0^{2\pi/\omega} dt' G_x(t-t') e^{i\omega(t-t')} \,. \tag{4.45}$$

Note that (4.45) is very similar to the expression for the power spectral density, with the exception of the boundaries of integration.

We have calculated an 'energy' spectral density for a chaotic trajectory of the dynamical system defined by (4.29), defined as the square of the amplitude of a discrete Fourier transform within some time window. This can be compared with the result obtained by a Monte-Carlo approximation to $< f_\omega >$. The results of both calculations are plotted in figure 4.3.

Due to the tendency of chaotic systems to 'forget' their initial conditions, on might expect the Fourier transform of a run of finite but long duration to be qualitatively similar to the Monte-Carlo result, which involves shorter runs from randomly generated initial conditions. Indeed the results plotted in figure 4.3 have some crude qualitative equivalence. In some sense, both these results can in be viewed as nothing but finite total simulation time errors, the exact result vanishing identically, where the error is related to a quantity (4.45) similar, but not equivalent, to the power spectral density.

4.6 Discussion of Results

Direct numerical simulation of chaotic dynamical systems is a viable method to compute their statistics. However it is difficult to obtain theoretical insight from such an approach. Furthermore, direct simulation places extreme or prohibitive

demands on computational resources for systems with a very large number of degrees of freedom. The intent of this work has been to further develop an inverse method, introduced in [1], which yields statistical quantities of a certain class of chaotic systems without the use of long duration numerical simulation.

Determining the statistics of a chaotic systems has for the most part been an experimental problem; one simulates the equations of motion for a long time and observes what happens on the average. The inverse approach turns this into a theoretical problem of reverse engineering the system of interest by the right choice of an invariant distribution and two-form. If one succeeds in doing this, one obtains exact integral expressions for equal time correlations and for the series expansions of unequal time correlations, which may generally be re-summable by Padé approximants. It is interesting, and perhaps advantageous, to note that the inverse approach leads to a mathematical description of the statistics which is quite familiar in quantum field theory.

A systematic procedure to reverse engineer a given chaotic dynamical system, assuming it is one for which an invariant distribution exists, by the right choice of two-form and invariant distribution has yet to be developed. Initial steps were made in [1], in which chaotic systems with polynomial velocity fields were constructed from two-forms and distributions with increasingly complex analytic structure. Given the success of the inverse method in producing precise statistics of chaotic systems, demonstrated both here and in [47], we believe that developing such a procedure is an important problem. While the systems we have considered so far are low dimensional, the practical power of the inverse method will come for a very large number of degrees of freedom, since statistical information is given from the outset. Moreover correlation functions can be computed by parallel Monte-Carlo algorithms involving short duration simulations of the equations of motion. We do not anticipate

any great obstruction in extending the inverse approach to large dimensionality.

In its present form, the inverse approach can not generate chaotic invariant sets which are globally dissipative, since no invariant distribution exists for such systems. However it may be possible to construct a variant of the inverse approach based upon the Hopf characteristic functional rather than an invariant distribution. The Fourier transform of the Hopf functional, being an invariant distribution, can not exist in globally dissipative cases. It would be very interesting to examine the conditions under which the Fourier transform of the Hopf functional does not exist. Presumably, these conditions are closely related to properties of strange attractors such as the fractional information dimension.

The method described here generates dynamical systems with given invariant distributions. If this method were to be used for modelling experiments, one also would like to capture correlation functions to desired order. We have given examples of dynamical systems with the same invariant distributions but differing autocorrelation functions. Reverse engineering a dynamical system that has given correlation functions and a given invariant distribution is yet to be done.

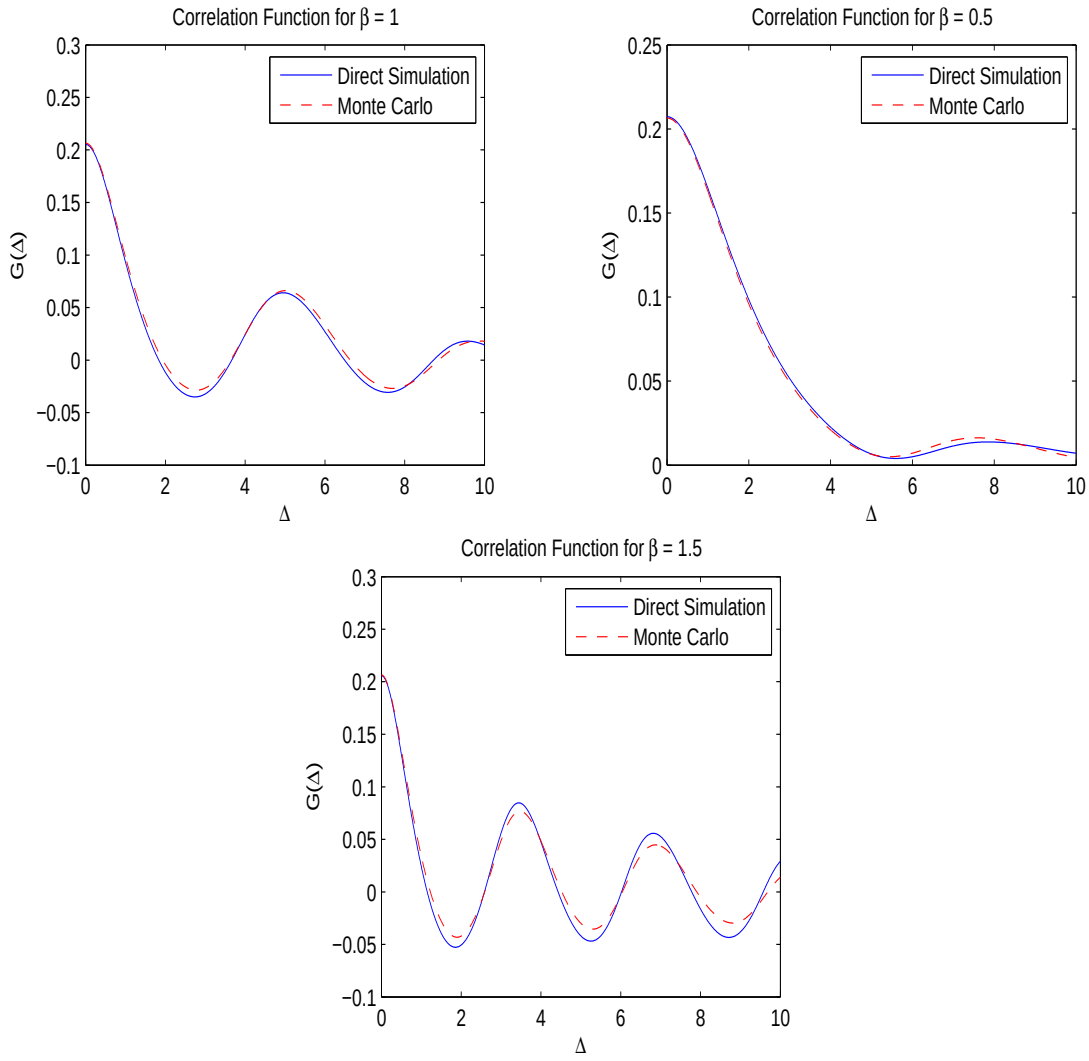

Figure 4.1: Auto-correlation functions calculated by Monte-Carlo simulation and direct long-duration simulation.
Dahed line shows Monte Carlo simulation and solid line shows direct long-duration simulation. The dimensionless number β parameterizes a variation of the dynamical system (4.30), obtained from $\rho = 1 - x^4 - y^2 - z^6$, $\Omega = (xyz)dy + \beta(y^2)dz$.

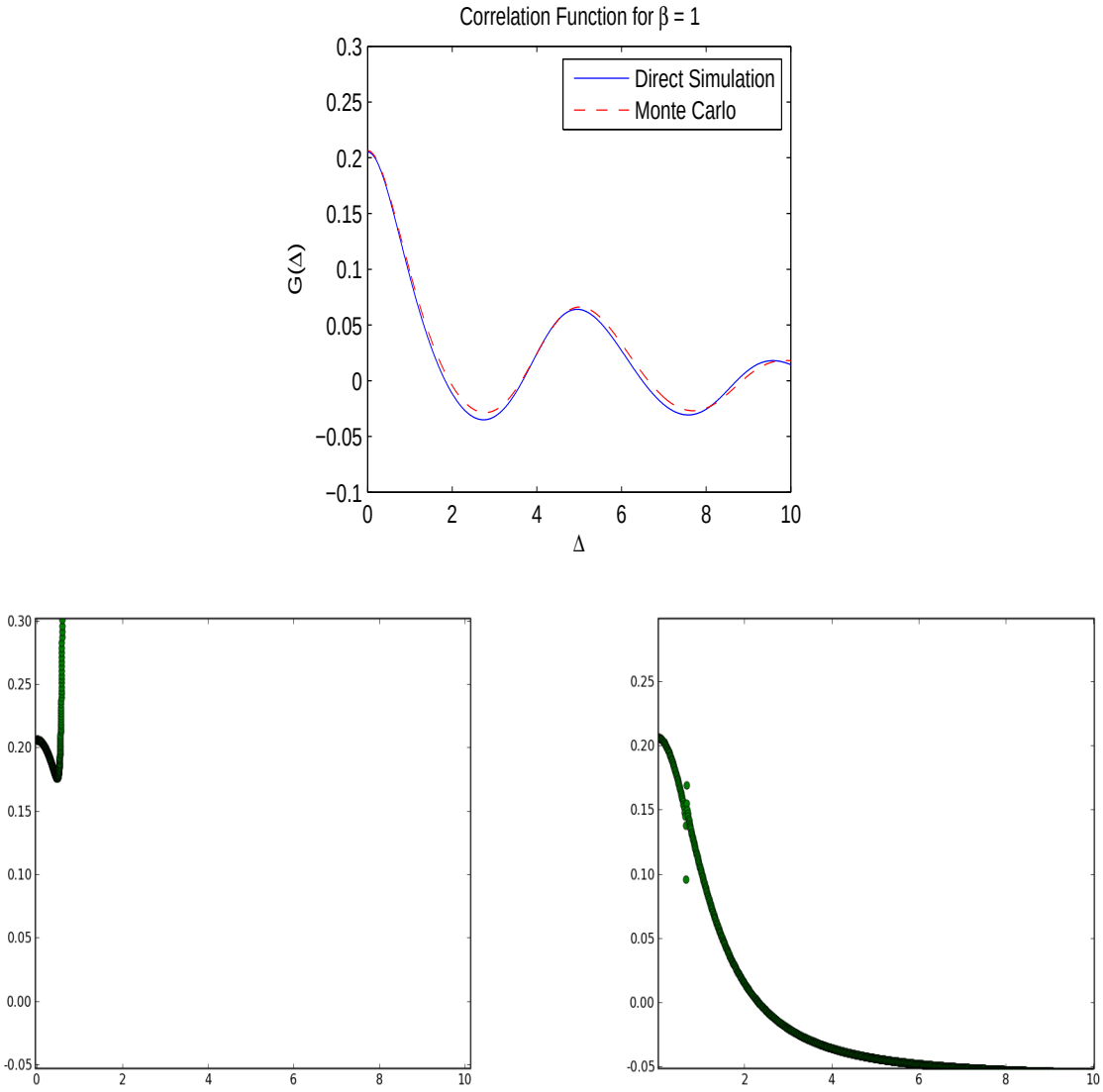

Figure 4.2: Auto-correlation function.
The auto-correlation calculated by long-run numerical simulation and by Monte-Carlo short run simulations (top), by 9'th order Monte-Carlo/Taylor-Maclaurin series (bottom left) , and by Monte-Carlo/(4|4) Pade approximant (bottom right). The Pade result is a smooth continuous curve, with the exception of a very small neighborhood of the point $\Delta = 0.6529$, at which there is a spurious pole.

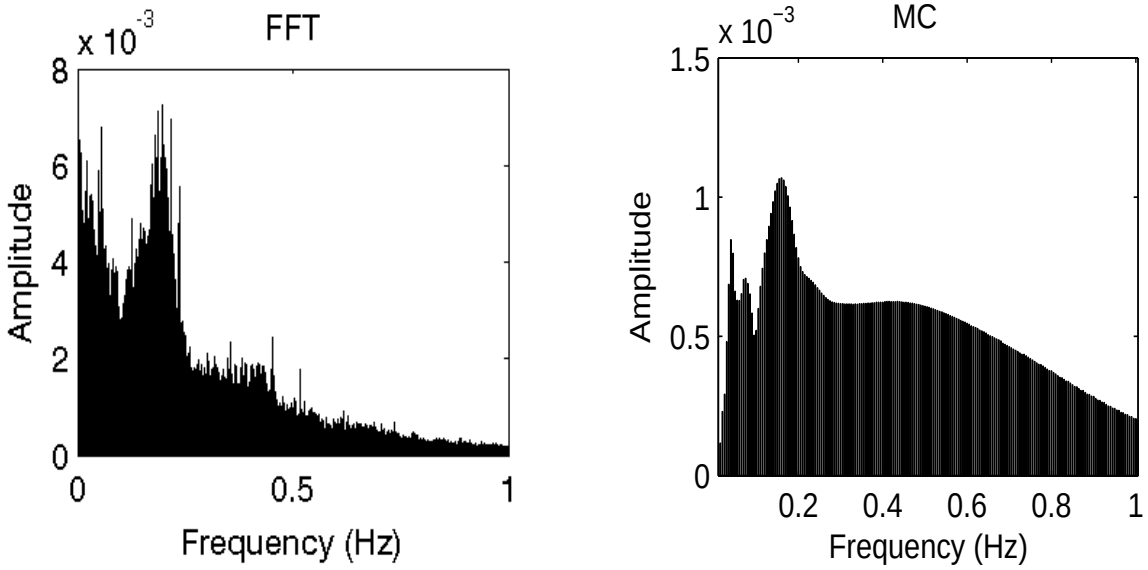

Figure 4.3: 'Power spectrum' computed by Fast Fourier Transform of a chaotic signal (on the left) and by Monte-Carlo simulation (on the right).

Chapter Five

Chiral Phase Transition via AdS/CFT

A variant of the holographic (AdS/CFT) duality relating strongly coupled large N gauge theories to a semiclassical limit of string theory in an asymptotically Anti-deSitter spacetime [74, 114, 41] may provide a useful tool to solve previously intractable problems in QCD. One advantage of the AdS approach is that it is possible to study non-equilibrium dynamics, which is not accessible to Euclidean lattice QCD. Of particular interest is the dynamical passage of a cooling quark-gluon plasma, such as that created in RHIC [104], through the chiral phase transition.

The Euclidean AdS description of first order phase transitions akin to the chiral phase transition in QCD have been described in [9, 70, 65, 8, 3, 77, 94, 2]. The generic feature of the relevant string theory backgrounds is the presence of a Euclidean black hole in an asymptotically AdS space, in which probe D-branes end either at or away from the horizon, depending on whether the temperature is above or below the critical temperature. The degrees of freedom of the embedded D-branes are dual to operators involving fundamental fields (quarks)[58]. Moreover, the change in the topology of the embedding corresponds to a jump in the expectation value of the chiral condensate at the phase transition.

Since we ultimately wish to study the non-equilibrium dynamics of passage through the phase transition, it is necessary to consider a Lorentzian signature background. As a starting point, we discuss properties of static D-brane embedding solutions in a static Lorentzian signature AdS black hole. These are essentially the same as Euclidean solutions, except that space-time no-longer ends at the horizon. In the high temperature phase, the D-branes fall through the horizon. There are then two possibilities; the D-branes can either extend all the way to the the singularity or not. For the $\mathcal{N} = 2$ gauge theory considered in [9], we find that the D-branes end, via annihilation into closed strings, before reaching the singularity.

The fact that the D-branes end before reaching the singularity could have been guessed on physical grounds. If the D-branes reached the singularity, it would not be obvious how they "pull out" of the black hole in a an expanding plasma which cools through the phase transition. However if the D-branes annihilate before reaching the singularity, there is an obvious way for the D-branes to pull out as the plasma cools: the point of annihilation simply moves toward the horizon with increasing coordinate time. Of course nothing really pulls out of the black hole. Rather, the parts of the D-brane behind the horizon annihilate into gravitons, etc. Moreover one can associate a trapped energy with the component the D-brane behind the horizon, which (for a temperatures just above T_c) we propose is related to the latent heat.

The latent heat associated with the first order phase transition is another interesting matter. We look for a description of the latent heat in terms of the stress-energy tensor of the brane. The strategy here is to make use of the AdS/CFT correspondence in Hamiltonian formalism, which amounts to equating the energy of the supergravity theory to the dual gauge theory. We find that, as also noted in [61], the Hamiltionian of the brane do not contain all the energy to subleading order in large N_c expansion, there is also a contribution from the backreacted metric. Moreover, the latent heat is identified as a purely backreaction contribution. During this discussion, we clarify several points that were overlooked in the literature, such as the holographic renormalization of the stress-energy tensor.

A time-dependent AdS black hole solution which is dual to an expanding-cooling purely gluonic plasma has been found in an expansion for large times [57] and points far from the horizon[1]. The leading order in this expansion corresponds to a relativis-

[1]Naively taking the asymptotic solution of [57], which was stated in Fefferman-Graham coordinates as given in equation (5.124), as a globally valid metric, one finds a curvature singularity, where one should have had a horizon. Later, through the use of Eddington-Finkelstein coordinates it was shown that the geometry dual described by [57] is regular with an apparent horizon that covers the singularity[52, 63, 64, 29]. The curvature singularity turned out to be an artifact of

tic perfect fluid, while the subleading part [56] yields a shear viscosity to entropy ratio which is consistent with other calculations [97], as well as present observations at RHIC [103]. We will describe a simple background derived from phenomenological considerations with correct asymptotics for large times[2] and compare it to the metric of [57]. We find that both metrics are related by a coordinate transformation. Although not an exact solution of Einstein's equations, this background provides a simple starting point to study the dynamics of a chiral phase transition in a strongly coupled expanding cooling plasma. We numerically show that this background allows a D7-brane evolution from an infalling configuration to a non-infalling configuration.

We start by reviewing the AdS/CFT description of the equilibrium thermodynamics of the $\mathcal{N} = 2$ super Yang-Mills theory obtained by coupling an $\mathcal{N} = 4$ multiplet to N_f, $\mathcal{N} = 2$ hypermultiplet in the fundamental representation of the gauge group $SU(N_c)$. We review elements of AdS/CFT conjecture as needed. We also show details of some calculations that have not appeared in the literature. Before studying the time evolution of a D7-brane, we describe the D7-brane embeddings in Lorentzian signature AdS black hole background. We find that, for infalling embeddings, the brane ends before reaching the singularity. We calculate the stress-energy tensor of the brane, compare it to the thermodynamical internal energy and discuss the latent heat. Next, we introduce our time dependent background. Finally, we perform a numerical simulation of the D7-brane in the time dependent background and show that this background allows for a D7-brane to evolve from an infalling configuration to a non-infalling configuration, thus signalling the chiral phase transition.

Fefferman-Graham coordinates. This issue will be discussed in more detail.

[2] In [17] the early time behavior of a dual background to boost invariant dynamics of a strongly coupled conformal plasma is studied. A numerical study of boost invariant flow in $N = 4$ super Yang-Mills theory is done in[22], where a time dependent boundary metric is used to source the background.

5.1 Equilibrium thermodynamics

We first consider the $\mathcal{N} = 2$ super Yang-Mills theory obtained by coupling an $\mathcal{N} = 4$ multiplet to N_f, $\mathcal{N} = 2$ hypermultiplet in the fundamental representation of the gauge group $SU(N_c)$. Moreover, we consider the large N_c limit with N_f fixed and large t'Hooft coupling $\lambda = g^2 N_c >> 1$. In this limit the theory is conformal[3]. The phase diagram and spectroscopy of this theory has been studied in great detail using AdS/CFT duality. Of particular note is a first order phase transition as T/M is varied, akin to the chiral phase transition in QCD [9, 65, 77, 3]. A more detailed discussion of the $\mathcal{N} = 2$ super Yang-Mills theory and similarities to QCD will be discussed in the coming pages.

Static finite temperature thermodynamic quantities in this theory can be computed from the dual string theory description of this theory, which involves a background which is the direct product of the five-dimensional flat AdS-blackhole times a five-sphere

$$ds^2 = -\frac{1}{R^2}\left(r^2 - \frac{r_H^4}{r^2}\right)dt^2 + R^2\frac{dr^2}{r^2 - \frac{r_H^4}{r^2}} + \frac{r^2}{R^2}d\vec{x}^2 + R^2 d\Omega_5^2. \tag{5.1}$$

The $AdS_5 \times S^5$ radius is related to the 't Hooft coupling of the dual gauge theory through $R^4 = g_{YM}^2 N_c \alpha'^2 = \lambda \alpha'^2$. The Hawking temperature is given by the horizon radius of the blackhole $r_H = \sqrt{\lambda}\alpha'\pi T$ and it is the temperature of the dual field theory. Some basic AdS/CFT dictionary:

$$\begin{aligned} &R^4 = g_{YM}^2 N_c \alpha'^2 = \lambda \alpha'^2 = \lambda l_s^4 = 4\pi g_s N_c \alpha'^2, \qquad r_H = \sqrt{\lambda}\alpha'\pi T \\ &g_{YM}^2 = 4\pi g_s, \qquad \lambda = g_{YM}^2 N_c, \qquad \alpha' = l_s^2. \end{aligned} \tag{5.2}$$

[3]For finite N_c, this theory is not asymptotically free and requires an ultraviolet completion.

We will primarily use this metric in z coordinates, where $z = 1/r$, and $r_H = b$,

$$ds^2 = \frac{1}{R^2 z^2}\left[-(1-b^4z^4)dt^2 + d\vec{x}^2\right] + \frac{R^2}{z^2}\frac{dz^2}{1-b^4z^4} + R^2 d\Omega_5^2. \tag{5.3}$$

It is convenient to write the five-sphere metric as

$$dS_5^2 = d\theta^2 + \sin^2\theta d\psi^2 + \cos^2\theta dS_3^2\,. \tag{5.4}$$

This space-time is defined for $z \leq 1/b$ and is smooth and complete if the Euclidean time t is compactified on a circle of radius $R^2\pi/b$. We will call z coordinates Schwarzschild coordinates, even though it is the r coordinates that are Schwarzschild-like. Perhaps a better terminology would be inverse-Schwarzschild-like.

The inclusion of the $N_f = 2$ hypermultiplets (quarks) corresponds to the addition of N_f D7-branes to this background, embedded on a surface [58]

$$\psi = 0, \qquad \theta = \theta(z) \tag{5.5}$$

The induced metric on the D7-brane worldvolume is

$$\begin{aligned} ds^2_{D7} = \frac{1}{R^2 z^2}\left[-(1-b^4z^4)dt^2 + d\vec{x}^2\right] + \left[\frac{R^2}{z^2(1-b^4z^4)} + R^2\theta'(z)^2\right]dz^2 \\ + \cos^2\theta(z) d\Omega_3^2. \end{aligned} \tag{5.6}$$

Then the action is

$$\begin{aligned} I_{D7} &= -N_f T_{D7}\Omega_3 \left(\int d^4x\right)\int dz\,\frac{\cos^3\theta}{z^5}\sqrt{1+z^2(1-b^4z^4)\theta'^2} \\ &= -N_f T_{D7}\Omega_3 b^4 \left(\int d^4x\right)\int dz'\,\frac{\cos^3\theta}{z'^5}\sqrt{1+z'^2(1-z'^4)\theta'^2}. \end{aligned} \tag{5.7}$$

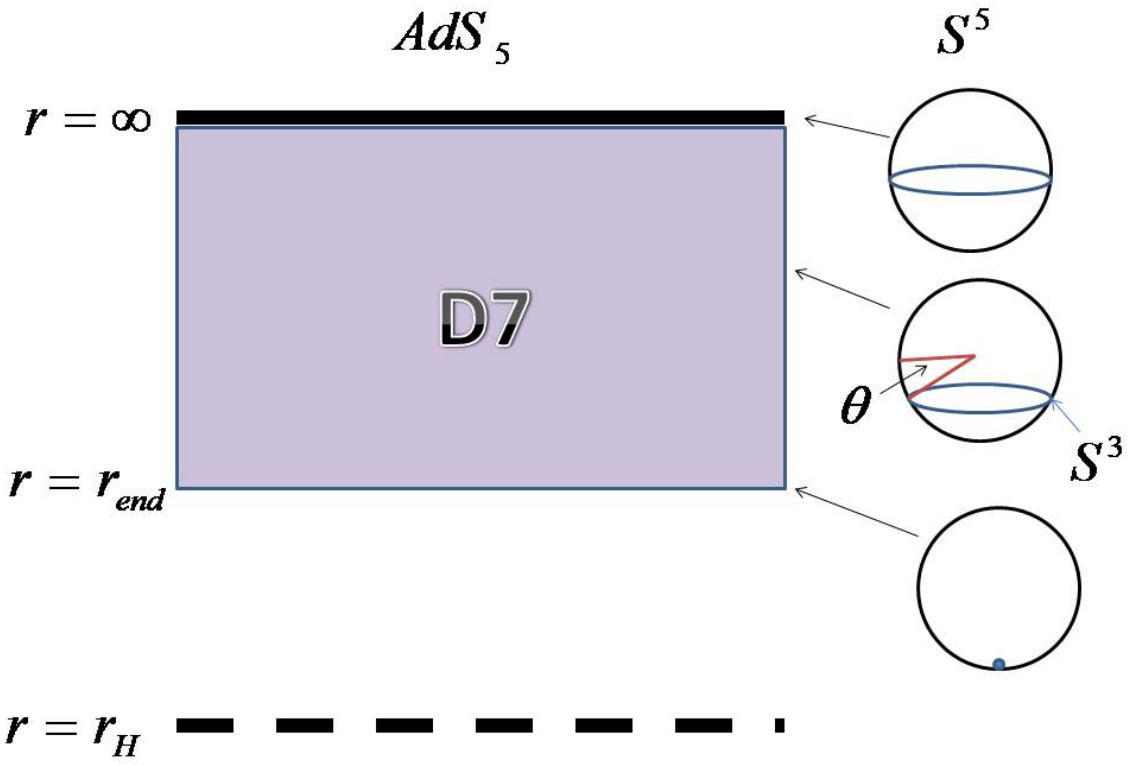

Figure 5.1: An illustration of the D7-brane embedding discussed in the text.

$T_{D7} = 1/(2\pi)^7 \alpha'^4 g_s$ is the brane tension and $b = r_H$. z' is dimensionless, $z' = bz$. $\Omega_3 = 2\pi^2$. The equation of motion that follows from the action is

$$\theta''(z') = \frac{3\tan\theta(z')}{z'^2(z'^4-1)} - \frac{(3+z'^4)}{z'(z'^4-1)}\theta'(z') \\ - 3\tan\theta(z')\,\theta'(z')^2 + 2z'(2-z'^4)\theta'(z')^3 \tag{5.8}$$

Here $'$ denotes differentiation with respect to z'. We want to analyze the solution around $z' = 0$. Following [59], we assume the most general power series expansion for $\theta(z')$

$$\theta(z') = \theta_0 + \sum_{i=1}^{\infty}\theta_i z'^i + \sum_{i=1}^{\infty}\psi_i z'^i \ln z' + \sum_{i=1}^{\infty}\sum_{j=2}^{p}\Psi_{i,j} z'^i (\ln z')^j. \tag{5.9}$$

Authors of [59] worked in Fefferman-Graham coordinates, which are related to our coordinates as

$$\begin{aligned} z' &= u\left(1+\frac{u^4}{4}\right)^{-1/2} \\ &\implies u = \frac{\sqrt{2}}{z'}\sqrt{1-\sqrt{1-z'^4}} \sim z' + \mathcal{O}(z'^5) \\ &\implies \ln u \sim \ln z' + \mathcal{O}(z'^4). \end{aligned} \tag{5.10}$$

Note that the series given in (5.9) has to be truncated at some finite p, otherwise the $\theta(z')$ would not have a series expansion in powers of z'. We truncated z' powers at z'^8 and $p = 8$ and found that the leading order terms that are important for our discussion are

$$\theta(z) \approx \theta_1 bz + \theta_3 b^3 z^3 + \mathcal{O}(b^5 z^5) = \theta_1 z' + \theta_3 z'^3 + \theta_5 z'^5 + \mathcal{O}(z'^7). \tag{5.11}$$

Note that the series expansion does not set θ_3 however θ_5 can be solved in terms of θ_1 and θ_3.

$$\theta_5 = \frac{\theta_1}{8} - \frac{7\theta_1^5}{40} + \frac{3}{2}\theta_1^2\theta_3. \tag{5.12}$$

At this stage θ_3 is a free parameter. However, as we will see later for the solutions that have physical interpretation, θ_3 is a function of θ_1. That we cannot deduce such a relation at this expansion is an artifact of the nonlinearity of the differential equation at hand. In the following, we will take $\theta_3 = \theta_3(\theta_1)$.

Using this asymptotics, one sees that the action is divergent.

$$\int_0 dz' \, \frac{\cos^3\theta}{z'^5}\sqrt{1+z'^2(1-z'^4)\theta'^2} \sim \int_0 dz' \, \left[\frac{1}{z'^5} - \frac{\theta_1^2}{z^3} + \mathcal{O}(z)\right]. \tag{5.13}$$

The renormalization procedure (called "the holographic renormalization") for bulk fields where developed in [60, 106, 10]. The procedure to cancel this particular divergence was worked out in [59]. One first introduces at cut-off ϵ and introduces counterterms at $z' = \epsilon$ slice. These counterterms are made of geometric invariants of the induced brane metric at $z' = \epsilon$ slice. The authors of [59] calculated these counterterms in Euclidean signature. In Fefferman-Graham coordinates, the counterterms are given by (R is set to 1)

$$\begin{aligned}
L_1 &= -\frac{1}{4}\sqrt{\gamma}, \\
L_2 &= -\frac{1}{48}\sqrt{\gamma}\, R_\gamma, \\
L_3 &= -\ln u_\epsilon \sqrt{\gamma}\, \frac{1}{32}\left(R_{ij}R^{ij} - \frac{1}{3}R_\gamma^2\right), \\
L_4 &= \frac{1}{2}\sqrt{\gamma}\, \theta(x, u_\epsilon)^2, \\
L_5 &= -\frac{1}{2}\ln u_\epsilon \sqrt{\gamma}\, \theta(x, u_\epsilon)\left(\Box_\gamma + \frac{1}{6}R_\gamma\right)\theta(x, u_\epsilon) \\
L_F &= -\frac{5}{12}\sqrt{\gamma}\, \theta(x, u_\epsilon)^4.
\end{aligned} \tag{5.14}$$

γ_{ij} is the induced brane metric on $u = u_\epsilon$ slice. R_{ij} and R are made of γ_{ij}. The counterterms are found by figuring out the geometric invariants at the $u = u_\epsilon$ slice that cancel the divergences. Note that L_F is a finite term, it is introduced to preserve supersymmetry at zero temperature, by setting the condensate to zero at zero temperature. When one transforms these counterterms to the coordinates we use, γ_{ij} is now the induced metric in $z' = \epsilon$ slice and

$$\ln u_\epsilon = \ln \epsilon + \frac{\epsilon^4}{8} + \mathcal{O}(\epsilon^8). \tag{5.15}$$

We will use the counterterms listed above stated in z' coordinates and in Lorentzian signature. In [107], examples were given in which the Euclidean counterterms, when

adjusted for the $(-)$ signs, succesfully cancelled the divergences in the Lorentzian case. One should be careful to apply these counterterms to the dimensionless integral, there will be an overall dimensionful factor. There will be extra $(-)$ signs needed to be added as we go along. We will deal with these extra factors when the time comes. Note also that the counterterms given in equation (5.14) are to be formed of the AdS_5 part of the metric. The γ_{ij} metric is

$$\gamma_{ij}dx^i dx^j = \frac{1}{\epsilon^2}\left[-(1-\epsilon^4)dt^2 + d\vec{x}^2\right], \tag{5.16}$$

Here an overall factor of b^2/R^2 is omitted to match [59] conventions. These factors will be inserted back when necessary. Hence

$$\gamma = -\frac{1-\epsilon^4}{\epsilon^8}, \qquad R_{ij} = 0, \qquad R_\gamma = 0. \tag{5.17}$$

Furthermore, $\partial_i\theta(x,\epsilon) = 0$. Then the only relevant counterterms (in Lorentzian signature) are

$$\begin{aligned}
L_1 &= \frac{1}{4\epsilon^4}\sqrt{1-\epsilon^4}, \\
L_4 &= -\frac{1}{2\epsilon^4}\sqrt{1-\epsilon^4}\left(\theta_1\epsilon + \theta_3\epsilon^3 + \mathcal{O}(\epsilon^5)\right)^2, \\
L_F &= \frac{5}{12\epsilon^4}\sqrt{1-\epsilon^4}\left(\theta_1\epsilon + \theta_3\epsilon^3 + \mathcal{O}(\epsilon^5)\right)^4, \\
L_1 + L_4 + L_F &= \frac{1}{4\epsilon^4} - \frac{\theta_1^2}{2\epsilon^2} - \frac{1}{8} + \frac{5\theta_1^4}{12} - \theta_1\theta_3 + \mathcal{O}(\epsilon^2)
\end{aligned} \tag{5.18}$$

These counterterms precisely cancel the divergence in the action, which is given by

$$\lim_{\epsilon\to 0} -\int_\epsilon dz' \, \frac{\cos^3\theta}{z'^5}\sqrt{1 + z'^2(1-z'^4)\theta'^2} \sim \lim_{\epsilon\to 0} -\frac{1}{4\epsilon^4} + \frac{\theta_1^2}{2\epsilon^2} + \mathcal{O}(\epsilon^2). \tag{5.19}$$

There is an extra finite piece in the counterterms (5.18). The purpose of this finite piece will be apparent in the following paragraphs. For the sake of completeness, we

insert the following equation here,

$$\frac{-I_{D7,\mathrm{ren}}}{N_f T_{D7}\Omega_3 b^4\left(\int d^4x\right)} = \lim_{\epsilon\to 0}\int_{\epsilon}^{z_{\mathrm{end}}} dz'\,\frac{\cos^3\theta}{z'^5}\sqrt{1+z'^2(1-z'^4)\theta'^2} - L_1 - L_4 - L_F. \tag{5.20}$$

Next, we apply the AdS/CFT dictionary to match sources and operators of the dual gauge theory to asymptotics of the $\theta(z)$ field. We are looking for the field theory operator that is dual to $\theta(z)$, which is a scalar field in the bulk. The leading asymptotic value θ_0 is, up to some constant, the hypermultiplet mass M.

$$M = \frac{1}{2}\sqrt{\lambda}T\theta_1 \tag{5.21}$$

This follows from dimensional matching in both sides of the correspondence [58]. In the AdS/CFT prescription [114, 41], the leading value of the bulk field acts as a source for the dual operator. In the weak form of the AdS/CFT conjecture ($N_c \to \infty$, $\lambda \equiv g^2_{YM}N_c$ finite but $\lambda >> 1$), the precise statement would be as follows. Let ϕ be some SUGRA field, $\bar{\phi}$ a particular solution to the SUGRA equations of motion and $\bar{\phi}_0$ the leading asymptotic behavior of this solution near the boundary. The AdS/CFT prescription is then

$$\left\langle e^{i\int d^4x \mathcal{O}\bar{\phi}_0}\right\rangle_{\mathcal{N}=4\,SYM} = e^{iS_{IIB\,SUGRA}[\bar{\phi}\to\bar{\phi}_0]}. \tag{5.22}$$

The exact form of the operator that is dual to the θ field is given in [68]. For our purposes, we will continue to denote the dual operator as $\langle\bar{q}q\rangle$. We vary M keeping C and T constant and calculate the change in the on-shell action, which will give us the expectation value of the dual operator according to the AdS/CFT correspondence.

Then we are considering the variation, given in terms of dimensionful parameters

$$\delta M = \frac{1}{2}\sqrt{\lambda}T\delta\theta_1, \qquad \delta\theta = \delta\theta_1 z, \tag{5.23}$$

Then

$$\begin{aligned} -C \equiv \langle\bar{q}q\rangle &= \frac{1}{\int d^4x}\frac{dI_{D7,\text{ren}}}{dM} \\ &= \lim_{\epsilon\to 0} -\frac{2N_f T_{D7}\Omega_3 b^4}{\sqrt{\lambda}T}\left(\frac{\cos^3\theta}{z'^5}\frac{z'^2(1-z'^4)\theta'}{\sqrt{1+z'^2(1-z'^4)\theta'^2}}\frac{d\theta}{d\theta_1}\bigg|_{z=\epsilon}^{z=z_{\text{end}}}\right. \\ &\qquad \left. +\frac{\theta_1}{\epsilon^2} - \frac{5\theta_1^3}{3} + \theta_3 + \theta_1\frac{d\theta_3}{d\theta_1}\right) \\ &= -\frac{2N_f T_{D7}\Omega_3 b^4}{\sqrt{\lambda}T}\left(-2\theta_3 + \frac{\theta_1^3}{3}\right) \\ &= -\frac{1}{8}N_f N_c T^3\sqrt{\lambda}\left(-2\theta_3 + \frac{\theta_1^3}{3}\right). \end{aligned} \tag{5.24}$$

In the derivation above, the temperature is kept constant. Note that this result matches the one given in [78]. Another note: M depends on T, hence b. Let's discuss why the $z = z_{\text{end}}$ term dissapears in the third line above. As seen by numerical solutions, the brane either ends at the horizon or before reaching the horizon. This was shown in [9] by a shooting method. For embeddings that end at the horizon, θ and θ' are expected to be continuous, which can be shown by numerically continuing the solution behind the horizon. Then $(1-z'^4)$ term sets the boundary term to zero. How about embeddings that end before reaching the horizon? Numerical solutions show that non-infalling embeddings end with $\theta(z_{\text{end}}) = \pi/2$, $\theta'(z_{\text{end}}) = \infty$. Then the singularity in the denominator cancels the singularity in the numerator and $\cos^3\pi/2$ sets the boundary contribution to zero.

For the sake of completeness, let's investigate the equation of motion (5.8) for non-infalling configurations. Clearly $\tan\theta$ and θ' are divergent. We look for consistent

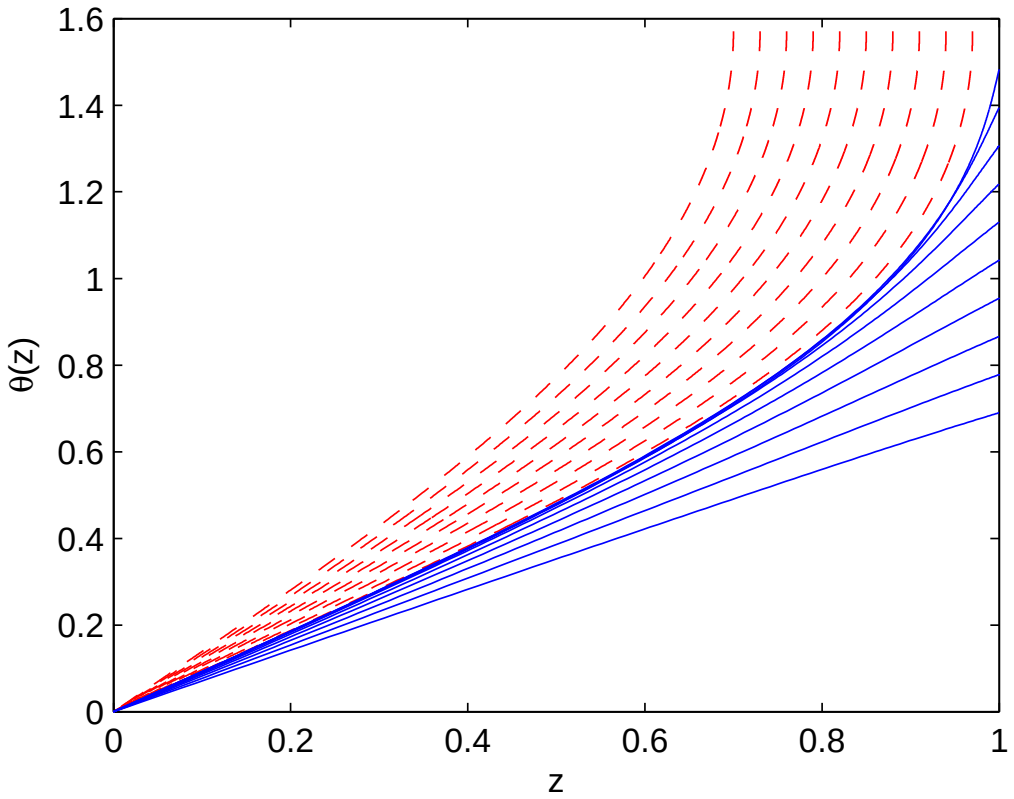

Figure 5.2: Static D7-brane embeddings in the Euclidean black hole background. $b = 1$. Blue (solid) lines plot embeddings that extend to the horizon and red (dashed) lines plot embeddings that do not extend to the horizon.

asymptotics. Define $\alpha = z'_{\rm end} - z'$. Assume $\pi/2 - \theta \sim \mathcal{O}(\alpha^k)$, where $0 < k \leq 1$. I assume the existence of logarithmic terms also. Then the equation of motion gives

$$\mathcal{O}(\alpha^{k-2}) = \mathcal{O}(\alpha^{-k}) + \mathcal{O}(\alpha^{k-1}) + \mathcal{O}(\alpha^{k-2}) + \mathcal{O}(\alpha^{3k-3}). \tag{5.25}$$

This will give a consistent result either if $k - 2 > 3k - 3$, which implies $k < 1/2$, or $k - 2 = 3k - 3$, which implies $k = 1/2$. On the other hand, there should be integer increments between the powers of α.

Let me comment a little more on the numerical integration that we used to generate figures 5.2 and 5.3. The topology of a constant z slice of the D7-brane for

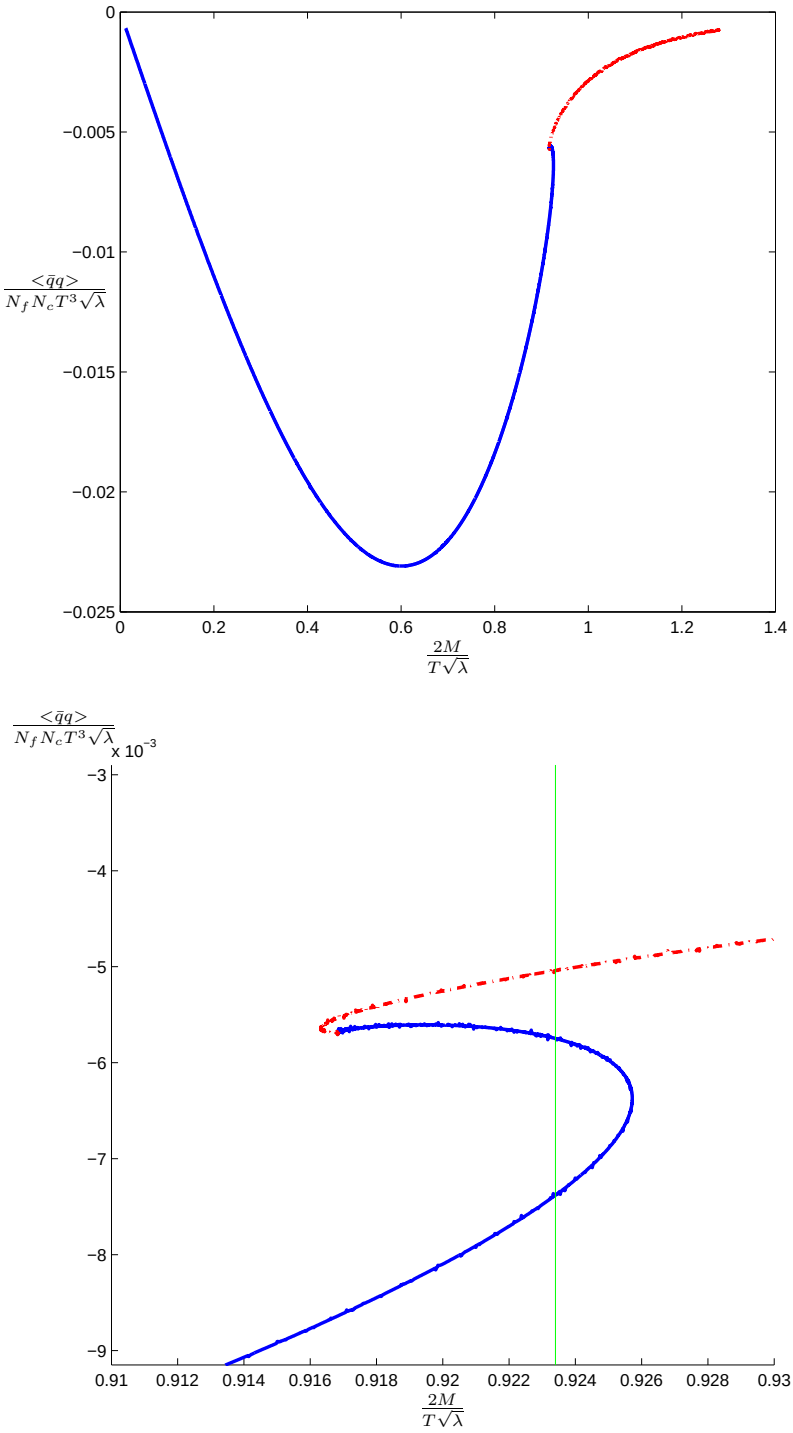

Figure 5.3: Quark condensate as a function of M/T that arises from the D7-brane embeddings.
$b = 1$. Blue (solid) lines plot embeddings that extend to the horizon and red (dashed) lines plot embeddings that do not extend to the horizon. On the bottom is the multivalued part of the curve. The green (vertical) line shows the critical mass at which the condensate's vev jumps discontinously, at which $\frac{2M}{T\sqrt{\lambda}} = 0.9234$. This value was found by equating the area between the green (vertical) line and the C–M curve on both sides of the green (vertical) line [3].

$z \to 0$ is $R^3 \times S^1 \times S^3$. The D7-brane can end at $z_{\rm end} < 1/b$ if the S^3 contracts to zero size, with $\theta(z_{\rm end}) = \pi/2$ and $\theta'(z_{\rm end}) = \infty$, so that the end is smooth rather than a conical singularity. If on the other hand $z_{\rm end} = 1/b$, the S^1 of the space-time in which the D7-brane is embedded contracts to zero and the boundary condition $\theta' = \frac{3}{4}\tan\theta$ follows from the equations of motion (5.8). We briefly discuss boundary conditions involved briefly. In the following, we set $b = 1$.

For the infalling case, the boundary conditions are set at $z' = 1$, the horizon. We set the angle at the horizon to some value $\theta(1) = \theta_0$. We get another initial condition by evaluating the above equation at $z' = 1$,

$$0 = -3\sin\theta_0 + 4\cos\theta_0\,\theta'(1) \implies \theta'(1) = \frac{3}{4}\tan\theta_0. \tag{5.26}$$

Of course, numerically it is not possible to set boundary conditions at $z' = 1$. Therefore, we set boundary conditions at z'_0 very close to $z' = 1$. Then,

$$\begin{aligned} &\epsilon = 1 - z'_0, \\ &\theta(z'_0) \approx \theta_0 - \epsilon\theta'(1) \\ &\theta'(z'_0) \approx \theta'(1) - \epsilon\theta''(1). \end{aligned} \tag{5.27}$$

To calculate $\theta''(1)$, we differentiate equation (5.8) with respect to z and evaluate at $z = 1$,

$$\theta''(1) = \theta'(1)^3 - \tan\theta_0\,\theta'(1)^2 - \frac{5}{8}\theta'(1). \tag{5.28}$$

For the non-infalling case, the boundary condition is set at $z_{\rm end} < 1$ as $\theta(z'_{\rm end}) =$

$\pi/2$. To get the other boundary condition, we start with the ansatz

$$\theta(z'_{\text{end}} - \epsilon) = \frac{\pi}{2} - a\sqrt{\epsilon} + \mathcal{O}(\epsilon). \tag{5.29}$$

We will try to find this constant a. Note the following:

$$\begin{aligned}
\theta'(z'_{\text{end}} - \epsilon) &\approx \frac{a}{2\sqrt{\epsilon}} \\
\theta''(z'_{\text{end}} - \epsilon) &\approx \frac{a}{4\epsilon^{3/2}} \\
\tan\theta(z'_{\text{end}} - \epsilon) &\approx \tan(\pi/2 - a\sqrt{\epsilon}) \approx \frac{1}{a\sqrt{\epsilon}}.
\end{aligned} \tag{5.30}$$

Plugging these into (5.8) and looking at the leading singularity gives $a = \frac{2}{\sqrt{z'_{\text{end}}(2 - z'^4_{\text{end}})}}$, therefore:

$$\begin{aligned}
\theta(z'_{\text{end}} - \epsilon) &\approx \pi/2 - 2\sqrt{\frac{\epsilon}{z'_{\text{end}}(2 - z'^4_{\text{end}})}} \\
\theta'(z'_{\text{end}} - \epsilon) &\approx -\frac{1}{\sqrt{\epsilon z'_{\text{end}}(2 - z'^4_{\text{end}})}}.
\end{aligned} \tag{5.31}$$

These conditions were used in setting up boundary conditions for the calculation given in Figure 5.2.

The thermodynamics is to be calculated in Euclidean signature. The free energy is given by $F = TI_{D7,\text{Euclidean}}$. The free energy density, i.e. $\mathcal{F} = F/\int d^3x$. Note that in Euclidean signature, the time direction is periodic and $\int dt = \beta = 1/T = \sqrt{\lambda}\alpha'\pi/b$. Then the following hold

$$\begin{aligned}
\mathcal{F} &= N_f T_{D7}\Omega_3 b^4 \int dz' \, \frac{\cos^3\theta}{z'^5}\sqrt{1 + z'^2(1 - z'^4)\theta'^2} + \text{counterterms} \\
\left.\frac{d\mathcal{F}}{dM}\right|_{T=\text{const}} &= C \implies d\mathcal{F} = -SdT = CdM.
\end{aligned} \tag{5.32}$$

Here, our parameters are $b = r_H = \sqrt{\lambda}\alpha'^2\pi T$ and $M = \frac{1}{2}\sqrt{\lambda}T\theta_0$. We do not change λ which is related to g_sN_c nor α'. Note that there is no work in this system. Even though we treat it as an external source when calculating the quark condensate through AdS/CFT correspondence, in the thermal description we do not consider it as an external parameter that can lead to mechanical work.

Using the condition above, we can calculate the other thermodynamic quantities. We will write $\mathcal{F} = \mathcal{F}(M,T)$. Now, note that the dimensionless integral

$$\lim_{\epsilon\to 0}\int_{\epsilon}^{z'_{\rm end}} dz' \,\frac{\cos^3\theta}{z'^5}\sqrt{1+z'^2(1-z'^4)\theta'^2} + \text{counterterms} = \tilde{\mathcal{F}}(M/T), \tag{5.33}$$

depends on $\theta_1 = \frac{2M}{\sqrt{\lambda}T}$ only. We keep $\sqrt{\lambda}$ constant and $z'_{\rm end} = z'_{\rm end}(\theta_1)$. Then

$$\begin{aligned}
&\mathcal{F} = \#T^4\tilde{\mathcal{F}}(M/T), \qquad \# = \frac{1}{16}N_fN_c\lambda \\
&\implies \left.\frac{d\mathcal{F}}{dM}\right|_{T=\text{const}} = \#T^3\tilde{\mathcal{F}}' = C \\
&\implies \left.\frac{d\mathcal{F}}{dT}\right|_{M=\text{const}} = 4\#T^3\tilde{\mathcal{F}} - \#T^2M\tilde{\mathcal{F}}' = -S \\
&\implies \tilde{\mathcal{F}}' = \frac{16C}{N_fN_c\lambda T^3}, \qquad S = \frac{1}{16}N_fN_c\lambda\left(-4T^3\tilde{\mathcal{F}} + T^2M\tilde{\mathcal{F}}'\right). \\
&\implies U(M,T) = F + TS = \frac{1}{16}N_fN_c\lambda T^4\left(-3\tilde{\mathcal{F}} + T^3M\tilde{F}'\right).
\end{aligned} \tag{5.34}$$

Using these relations one can calculate the thermodynamic functions using the numerical static D7-brane embededings generated above. Figure 5.4 shows the free energy.

The figures 5.2, 5.3 and 5.4 show an interesting behavior. The $C - M$ curve is multivalued, as well as the free energy curve. This is very much like the Van der Waals gas system and the associated first order phase transition[4]. Using the Maxwell equal

[4]The thermodynamic description of gasses include a work term PdV. Van der Waals equation of state leads to a multivalued Gibbs free energy. In our description of the brane systems there is

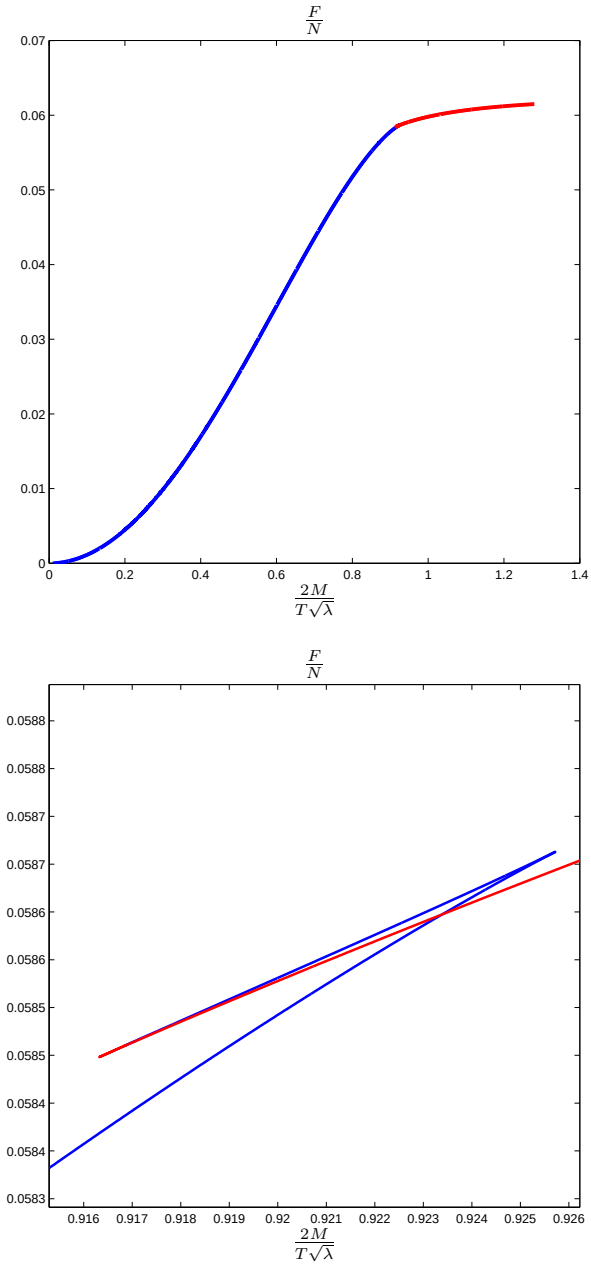

Figure 5.4: Free energy of static D7-brane embeddings.
$b = 1$. Blue (solid) lines plot embeddings that extend to the horizon and red (dashed) lines plot embeddings that do not extend to the horizon. The figure is generated from integrating the Figure 5.3. The bottom figure zooms into the free energy where the C–M curve that arises from the D7-brane embeddings is multivalued. The free energy is shifted to 0 for supersymmetric embeddings and and scaled by $1/2$ to match the figure of [3]. This arises from our definition of C.

area rule, one can deduce the equilibrium states. This is equivalent to choosing the minimum free energy states among the multivalued states, since as discussed above $d\mathcal{F} = -SdT = CdM$. Hence one arrives at a first order phase transition, in which the first derivative of the free energy is discontinuos. This happens at the critical value of the parameter $\frac{2M}{T\sqrt{\lambda}} = 0.9234$. There is a latent heat associated with this transition and it is given by the heat absorbed during the phase transition. Below we calculate this latent heat using dimensional arguments. We note that "before" refers to the state right before the phase transition and "after" refers to the state right after the phase transition.

$$\begin{aligned} L = T\Delta S = & -T\frac{d\mathcal{F}}{dT}\Big|_{\text{after}}^{\text{before}} \\ = & -T\#\left(4T^3\tilde{F} - MT^2\tilde{F}'\right)\Big|_{\text{after}}^{\text{before}}. \end{aligned} \tag{5.35}$$

There is no discontinuity in the free energy, the discontinuity is in the derivative of the free energy. Then the latent heat density is given by,

$$L = \#MT^3\tilde{F}'\Big|_{\text{after}}^{\text{before}} = M\frac{d\mathcal{F}}{dM}\Big|_{\text{after}}^{\text{before}} = M(C_{\text{after}} - C_{\text{before}}). \tag{5.36}$$

Using the numerical values of C and M, we calculated this latent heat density to be

$$L = 0.0011\,\lambda T^4 N_f N_c. \tag{5.37}$$

What physical process does this transition correspond to in the dual gauge theory? When the brane configurations are non-infalling, the small oscillating modes of the scalar fields around the classical embedding are interpretted as meson fields in the dual theory and one can calculate the masses of the associated mesons. This

no mechanical work. Therefore there is no difference between the Helmhotz free energy and the Gibbs free energy. Hence we use the term "free energy".

was done in [9, 69, 78]. When the embeddings become infalling, the induced metric on the brane has a horizon and the modes decay since one can now set infalling boundary conditions. This fact was used to calculate meson decay widths in [20]. Therefore this transition is related to meson melting in the dual gauge theory. The topology change in the gravitational theory corresponds to a phase transition in the dual gauge theory.

5.1.1 Comparison to QCD

Let us comment briefly on similarities to QCD chiral phase transition. Consider the Lagrangian of massless QCD,

$$\mathcal{L}_{QCD,\,m=0} = -\frac{1}{4}F^a_{\mu\nu}F^{a\mu\nu} + \sum_f \bar{\psi}_{L,f}\not{D}\psi_{L,f} + \sum_f \bar{\psi}_{R,f}\not{D}\psi_{R,f}. \tag{5.38}$$

Of course in QCD mass terms are present. However, if we are interested in hadron physics below ~ 1 GeV, we can ignore charm, top and bottom quarks. Then our flavor index f counts up down and strange, $f = 1, 2, 3$. Remembering that $\Lambda_{QCD} \sim 0.2$ GeV, we will treat up and down quarks as massless which are much lighter than $\Lambda_{\rm QCD}$. We will set the the mass of the strange quark to zero also, although this approximation is not as justified. This detail is not central to our discussion below, however one could proceed by only two massless quarks. $a = 1, \ldots, 8$. Here we projected the Dirac spinor into its chiral components

$$\psi_{R,L} = \frac{1}{2}(1 \pm \gamma^5)\psi. \tag{5.39}$$

The classical massles QCD Lagrangian has, $U(3)_L \times U(3)_R$ symmetry. The left-handed and right-handed spinors transform separately as,

$$\psi_L \to \exp\left(-i\alpha_L \cdot \lambda - i\beta_L I\right)\psi_L, \qquad \psi_R \to \exp\left(-i\alpha_R \cdot \lambda - i\beta_R I\right)\psi_R, \tag{5.40}$$

where λ^a are the $SU(3)$ Gell-Mann matrices and I is the 3-by-3 identity matrix. We can rewrite the $U(3)_L \times U(3)_R$ symmetry as $U(1)_L \times SU(2)_L \times U(1)_R \times SU(2)_R$ and further $U(1)_L \times U(1)_R = U(1)_V \times U(1)_A$, where the vector and axial $U(1)'$s would correspond to

$$\psi \to \exp\left(-i\beta_V I\right)\psi, \qquad \psi \to \exp\left(-i\beta_A \gamma^5\right)\psi, \tag{5.41}$$

where $\beta_V = (\beta_L + \beta_R)/2$ and $\beta_A = (\beta_L - \beta_R)/2$. It turns out that in the quantum theory $U(1)_A$ is anomalous. This happens because the axial current

$$J^\mu_A = \bar{\psi}\gamma^\mu\gamma^5\psi \tag{5.42}$$

is not conserved, $\partial_\mu J^\mu_A \neq 0$, due to triangle quark loop graph. However, when $N_f << N_c$, which is the limit that we are considering the $\mathcal{N} = 2$ SYM theory, the quark loops are subleading in the $1/N_c$ expansion and $U(1)_A$ symmetry is present. $U(1)_V$ is baryon number.

The QCD chiral symmetry is spontaneously broken - the strong dynamics gives a vev to the operator $\langle\bar{\psi}\psi\rangle$ (called the chiral condensate), see e.g. [109]. In terms of the symmetry group this means $SU(3)_L \times SU(3)_R \to SU(3)_V$. Spontaneous breaking of global symmetries lead to massless bosons for each spontaneously broken generator. This is known as the Goldstone theorem. The 8 Goldstone bosons which correspond to 8 generators of $SU(3)_A$ are quark bound states $\pi^\pm$, π^0, $K^\pm$, K^0, $\bar{K}^0$ and the η. In

the large N_c limit $U(1)_A$ symmetry is restored as mentioned above, but it also gets spontaneously broken. The associated Goldstone boson is η'.

This was the story for zero temperature. At high temperatures chiral symmetry is restored. The order parameter for this transition is the chiral condensate, which is zero at high temperatures and non-zero at low temperatures. This phase transition is first order and $U(1)_A$ is also restored [96].

Inclusion of the mass terms breaks the chiral symmetry explicitly, the Goldstone bosons acquire mass to become pseudo-Goldstone bosons. At high temperatures, there is still a phase transition, however it is not a genuine symmetry breaking phase transition. Chiral condensate is still an order parameter. See [110] for a review of QCD phase diagram.

Now we discuss a little more about the $\mathcal{N} = 2$ SYM theory and identify the particular symmetry that is associated with the phase transition in our model. The Lagrangian for this theory in $\mathcal{N} = 1$ superspace formalism is given in [8]. Let's review some properties of the theory, mostly relying on the summary given in [59, 89]. Recall that $\mathcal{N} = 4$ SYM theory has an $SU(4) \simeq SO(6)$ R-symmetry, which is dual to the $SO(6)$ isometry of S_5. $\mathcal{N} = 2$ SYM has all the fields of $\mathcal{N} = 4$ SYM, but also has fields in the fundamental representation. The $\mathcal{N} = 2$ hypermultiplet has 2 complex scalars and 2 Weyl fermions of opposite chirality. In $\mathcal{N} = 2$ SYM, the R-symmetry is broken to $SO(4) \times SO(2)$, which can easily be seen by the D7-brane wrapping an S_3 inside the S_5. This $SO(2) \simeq U(1)_R$ acts as a chiral rotation on the "quarks", 2 Weyl fermions of the hypermultiplet have opposite charges. $U(1)_R$ of $\mathcal{N} = 2$ SYM is a lot like $U(1)_A$ of QCD. It is anomalous at finite N_c but symmetry is restored at $N_c \to \infty$ limit. At finite mass, the symmetry is explicitly broken. As we saw above, at high temperature there is a phase transition for which the chiral condensate is an order

parameter. A couple of more words needed to compare QCD to $\mathcal{N} = 2$ SYM theory. $\mathcal{N} = 4$ SYM is conformal, including the hypermultiplet breaks the conformality. At high temperatures, the supersymmetry is broken. For more details refer to [89].

5.2 Stress-Energy Tensor and Internal Energy - A Hamiltonian Approach to AdS/CFT

In this section we will look at the stress-energy tensor of the D7-brane. We will form a conserved current out of this tensor, which will give us the energy density and energy flux. The energy density thus formed is also the Hamiltonian of the system. This quantity is important, because as noted in [114] the AdS/CFT correspondence identifies the Hilbert space of the dual gauge theory to the Hilbert space of supergravity (or string theory). Every state in the field theory must map to a state in the bulk theory. This means that the expectation values of conserved charges such as energy and momentum must agree between the bulk theory and the boundary theory [61]. In particular, we can simply calculate the total energy of the SUGRA theory and equate it with the total energy of the dual field theory.

Now we switch to the Lorentzian signature and calculate the stress-energy tensor of the D7 brane. One would naively hope that the stress-energy tensor component corresponding to the Hamiltonian would describe the thermodynamic internal energy. This turns out not to be true. The way to see this would be to notice that the action of the whole gravitational system would be given schematically by

$$S = N_c^2 S_{\text{AdS background}} + N_f N_c S_{\text{probe brane}}. \tag{5.43}$$

The action of the D7-brane is suppressed by a factor N_f/N_c. The backreaction of the brane on the background geometry is suppressed by the same factor. This does not cause a problem in calculation of the (Euclidean) action because the variation of the background action gives Einstein equations of motion and evaluated on the AdS blackhole background this contribution vanishes. Therefore to order $N_f N_c$, $S_{\text{AdS background}}$ does not get a correction from the backreaction. Therefore the free energy of the theory can be calculated reliably in the probe approximation using the Euclidean action. When it comes to internal energy things are more complicated. Aside from the energy of the probe brane, the gravitational background carries energy. A stress-energy tensor for the gravitational backgrounds was constructed in [10]. The backreaction will increase the energy in the gravitational background and this will be of order N_f/N_c, the same order as the stress-energy tensor of the brane. Therefore the subleading order correction to the internal energy will have two components, the stress-energy tensor of the D7-brane and theN_f/N_c correction to the gravitational background. This fact was observed in [61] as it was suggested that the gravitational contribution to the internal energy is related to the portion of the brane extending behind the horizon, because this part only could increase the area of the horizon. Below we will agree that this is not true, simply because there is a backreaction contribution to the internal energy even in the case of non-infalling configurations.

Below we will study the details of this effect for the D3-D7 system we are considering. Through our analysis, we will idenity the latent heat in the first order phase transition to be a totally backreaction contribution. Before doing so, let's look at a toy model to demonstrate what we have described above.

5.2.1 A Simple Model

To increase our understanding of the thermodynamics in the probe approximation, we look at a simple model proposed by Karch et. al. in [61]. Their model in $d = 4$ is

$$S = \frac{1}{16\pi G}\int_M d^5x\sqrt{-g}\left(R + \frac{12}{L^2} - T_0\right) - \frac{1}{8\pi G}\int_{\partial M} d^4x\sqrt{-\gamma}K + S_{\rm ct}, \qquad (5.44)$$

where the D brane tension is $\frac{T_0}{16\pi G}$, T_0/G is a small parameter of order N_f/N_c and K is the etrinsic curvature. $S_{\rm ct}$ stands for counterterms and their specific definition will be given below[5][6]. This model is interesting because the T_0 term can be treated as a cosmological constant term as well as a space-filling brane.

In the absence of the brane ($T_0 = 0$) the solution is AdS black hole

$$ds^2 = g_{MN}dx^m dx^n = -h(r)dt^2 + \frac{dr^2}{h(r)} + \frac{r^2}{L^2}d\vec{x}^2, \qquad h(r) = \frac{r^2}{L^2} - \frac{r_h^4}{L^2 r^2}. \qquad (5.47)$$

The radial coordinate runs from the horizon at $r = r_h$ to the boundary at $r - \infty$[7].

[5] A note on the convention. Capital Latin indices run over AdS_5 coordinates, greek indices run over boundary coordinates, i.e. no r.

[6] A reminder on sign conventions in continuation to Euclidean space. We do this by substituting $t \to -it$,

$$Z = \int \mathcal{D}\phi\, e^{iS[\phi]} \longrightarrow Z = \int \mathcal{D}\phi\, e^{-S_E[\phi]}, \qquad (5.45)$$

which means

$$e^{-\beta F} = \int \mathcal{D}\phi\, e^{-S_E[\phi]}. \qquad (5.46)$$

[7] For later reference, let us list the non-vanishing Cristoffel symbols

$$\Gamma^r_{rr} = -\Gamma^t_{tr} = \frac{r_h^4 + r^4}{r_h^4 r - r^5}, \qquad \Gamma^r_{xx} = \Gamma^r_{yy} = \Gamma^r_{zz} = \frac{r_h^4 - r^4}{L^4 r}$$
$$\Gamma^r_{tt} = \frac{r_h^8 - r^8}{L^4 r^5}, \qquad \Gamma^x_{xr} = \Gamma^y_{yr} = \Gamma^z_{zr} = \frac{1}{r}. \qquad (5.48)$$

The Ricci tensor, Ricci scalar, and temperature associated with this geometry are

$$R_{MN} = -\frac{4}{L^2} g_{MN}, \qquad R = -\frac{20}{L^2}, \qquad T = \frac{1}{\beta} = \frac{r_H}{\pi L^2}. \tag{5.49}$$

The free energy density is given by the Euclidean on-shell action (divided by β and the volume $\int d\vec{x}$) calculated in the Euclidean signature. The action is

$$-S_E = \lim_{r_{\max}\to\infty} \frac{\beta \int d\vec{x}}{16\pi G} \int_{r_h}^{r_{\max}} dr\, \frac{r^3}{L^3} \left(-\frac{20}{L^2} + \frac{12}{L^2} \right) - \frac{1}{8\pi G} \int d^4x \sqrt{\gamma} K + S_{ct} \tag{5.50}$$

Now we calculate the extrinsic curvature. Remembering that

$$\begin{aligned} K^{\mu\nu} &= -\frac{1}{2} \left(\nabla^\mu \hat{\eta}^\nu + \nabla^\nu \hat{\eta}^\mu \right) \\ K = K^\mu_\mu &= -\nabla_\mu \hat{\eta}^\mu = -\gamma_{\mu\nu} \nabla^\mu \hat{\eta}^\nu, \end{aligned} \tag{5.51}$$

where $\hat{\eta}^\mu$ is the unit outward normal to the boundary, i.e $\hat{\eta}^\mu = \sqrt{h(r)}\delta^\mu_r$, we get

$$K = -\nabla_\mu \hat{\eta}^\mu = -\sqrt{h(r)} \Gamma^\mu_{\mu r} = -\frac{3}{L} \sqrt{1 - \frac{r_h^4}{r^4}} - \frac{1}{L} \frac{1 + r_h^4/r^4}{\sqrt{1 - r_h^4/r^4}}. \tag{5.52}$$

Note that the induced metric at a constant r slice is

$$\gamma_{\mu\nu} dx^\mu dx^\nu = h(r) dt^2 + \frac{r^2}{L^2} d\vec{x}^2. \tag{5.53}$$

Also

$$\gamma = \frac{r^8}{L^8} \left(1 - \frac{r_h^4}{r^4} \right). \tag{5.54}$$

Then

$$
\begin{aligned}
-\frac{1}{8\pi G}\int d^4x\sqrt{\gamma}K &= \frac{\beta\int d^3\vec{x}}{8\pi G}\frac{r^4}{L^4}\left(1-\frac{r_h^4}{r^4}\right)^{1/2}\left(\frac{3}{L}\sqrt{1-\frac{r_h^4}{r^4}}+\frac{1}{L}\frac{1+r_h^4/r^4}{\sqrt{1-r_h^4/r^4}}\right)\\
&= \frac{\beta\int d^3\vec{x}}{8\pi G}\frac{r^4}{L^4}\left[\frac{3}{L}\left(1-\frac{r_h^4}{r^4}\right)+\frac{1}{L}\left(1+\frac{r_h^4}{r^4}\right)\right]\\
&= \frac{\beta\int d^3\vec{x}}{8\pi GL^5}\left(4r^4-2r_h^4\right) \qquad (5.55)
\end{aligned}
$$

Putting everything together

$$
\begin{aligned}
-S_E &= \frac{\beta\int d^3\vec{x}}{8\pi GL^5}\lim_{r_{\max}\to\infty} -4\int_{r_h}^{r_{\max}} dr\, r^3+4r_{\max}^4-2r_h^4+\text{c.t.}\\
&= \frac{\beta\int d^3\vec{x}}{8\pi GL^5}\lim_{r_{\max}\to\infty} 3r_{\max}^4-r_h^4+\text{c.t.} \qquad (5.56)
\end{aligned}
$$

The counterterms are defined again by the holographic renormalization, especially [10]. We form geometric invariants of the induced metric on $r=r_{\max}$ and subtract them to cancel the divergences. At the cut-off boundary $\sqrt{\gamma}\sim r_{\max}^4$. Note that $R_{(\gamma)}=0$. Then the only possible counterterm is a suitably normalized $\sqrt{\gamma}$,

$$
\sqrt{\gamma}=\frac{r_{\max}^4}{L^4}\sqrt{1-\frac{r_h^4}{r_{\max}^4}}\approx\frac{r_{\max}^4}{L^4}-\frac{r_h^4}{2L^4}+\mathcal{O}(r_{\max}^{-4}).\implies S_{ct}=-\frac{3}{8\pi GL}\sqrt{\gamma}. \qquad (5.57)
$$

Then

$$
\begin{aligned}
-S_E &= \frac{\beta\int d^3\vec{x}}{8\pi GL^5}\lim_{r_{\max}\to\infty} 3r_{\max}^4-r_h^4-3\sqrt{\gamma}=\frac{r_h^4\beta\int d^3\vec{x}}{16\pi GL^5}\\
&\implies f=-\frac{S_E}{\beta\int d^3\vec{x}}=-\frac{r_h^4}{16\pi GL^5}=-\frac{\pi^3}{16G}L^3T^4 \qquad (5.58)
\end{aligned}
$$

This matches the result of [61].

Then we can calculate the other thermodynamic quantities, entropy density (s)

and energy density (ϵ)

$$\begin{aligned} Ts &= -T\frac{\partial f}{\partial T} = -4f \\ \epsilon &= f + Ts = -3f. \end{aligned} \tag{5.59}$$

The energy density can also be calculated from the stress-energy tensor of the gravitational background. We switch to Minkowski signature. The stress-energy tensor is defined by [10]

$$\langle T^{\mu\nu}(x)\rangle = \lim_{r\to\infty} \frac{2}{\sqrt{-\eta}}\frac{\delta S}{\delta \eta_{\mu\nu}} = \lim_{r\to\infty} \frac{r^6}{L^6}\frac{2}{\sqrt{-\gamma}}\frac{\delta S}{\delta \gamma_{\mu\nu}}, \tag{5.60}$$

where $\eta_{\mu\nu}$ is the normalized boundary metric, i.e. $\eta_{\mu\nu} = \frac{L^2}{r^2}\gamma_{\mu\nu}$. This definition is equivalent to the Brown-York definition of energy [19]. Here the action is the full on-shell action including the counterterms. The variation with respect to the boundary metric means $\gamma'_{\mu\nu} = \gamma_{\mu\nu} + \delta\gamma_{\mu\nu}$ and $g'_{MN} = g_{MN} + \delta g_{MN}$ such that $\delta g(\epsilon, x)_{\mu\nu} = \delta\gamma_{\mu\nu}$. The Einstein-Hilbert action does not contribute anything, since its variation vanishes on-shell. The contributions come from the counterterms and the boundary action. First, let's derive the variation of the boundary action. We get [10]

$$\frac{\delta}{\delta\gamma_{\mu\nu}}\int d^4x\sqrt{-\gamma}K = \frac{\sqrt{-\gamma}}{2}\gamma^{\mu\nu}K - \frac{\sqrt{-\gamma}}{2}K^{\mu\nu}. \tag{5.61}$$

Putting this all together

$$\frac{2}{\sqrt{-\gamma}}\frac{\delta S}{\delta\gamma_{\mu\nu}} = \frac{1}{8\pi G}\left[K^{\mu\nu} - K\gamma^{\mu\nu} - 3\frac{\gamma^{\mu\nu}}{L}\right]. \tag{5.62}$$

We can calculate this for the problem at hand. We are interested in $\langle T^{tt}\rangle$, which is

the energy.

$$\begin{aligned}
\gamma^{tt} &= -\frac{1}{h(r)}, \\
K^{tt} &= -\nabla^t \hat{\eta}^t = -\gamma^{tt}\nabla_t \hat{\eta}^t = \frac{1}{h(r)}\left(\partial_t \hat{\eta}^t + \Gamma^t_{t\mu}\hat{\eta}^\mu\right) = \frac{1}{\sqrt{h(r)}}\Gamma^t_{tr}, \\
K\gamma^{tt} &= \frac{1}{\sqrt{h(r)}}\Gamma^\mu_{\mu r} \\
&\implies 8\pi G \frac{2}{\sqrt{-\gamma}}\frac{\delta S}{\delta \gamma_{tt}} = -\frac{3}{r\sqrt{h(r)}} + \frac{3}{Lh(r)} = \frac{3}{2}\frac{Lr_h^4}{r^6} + \mathcal{O}(r^{-8}) \\
&\implies \left\langle T^{tt}\right\rangle = \frac{3}{16\pi G}\frac{r_h^4}{L^5},
\end{aligned} \tag{5.63}$$

which is exactly the energy calculated above directly from the free energy.

Now we include the brane and calculate the backreaction contribution to the background energy. While we do this, we keep the temperature constant, since this in true in the probe approximation which we will compare the results to. To calculate the backreaction, we notice that the effect of the brane is to shift the curvature radius L with a new curvature subject to the relation

$$\frac{12}{L^2} - T_0 = \frac{12}{l^2}, \tag{5.64}$$

or, expanding to leading order in the dimensionless parameter $\tau = T_o L^2$,

$$\begin{aligned}
l &= \frac{L}{\sqrt{1-\tau/12}} \\
l &= L\left(1 + \frac{\tau}{24} + \mathcal{O}(\tau)\right).
\end{aligned} \tag{5.65}$$

Correspondingly, the shift in the thermodynamic quantities are

$$\delta f = \frac{\tau}{8} f, \qquad \delta\epsilon = -3\delta f, \qquad T\delta s = -4\delta f. \tag{5.66}$$

We calculate these first by calculating the shift in the free energy and then using the thermodynamic relations. Note that the energy of the gravitational background calculated in (5.63), when accounted for the backreaction contribution, totally reproduces this shift in the energy. An important point to note is that it seems like the thermodynamic relation $dE = TdS$ seems to be violated. This is not true of course, the missing component as we will see below comes from the stress-energy tensor of the probe brane.

We want to see if one can calculate these quantities from the probe approximation. The free energy density is given by the normalized on-shell D-brane action. The counterterms are again formed by geometric invariants on the boundary surface.

$$\begin{aligned} -\delta S_{\text{probe,Euclidean}} &= \lim_{r_{\max}\to\infty} -\frac{T_0\beta\int d^3x}{16\pi G}\int_{r_h}^{r_{\max}} dr\,\frac{r^3}{L^3} + \underbrace{\frac{1}{4}\frac{T_0 L\beta\int d^3x}{16\pi G}\sqrt{\gamma}}_{\text{counterterm}} \\ &= \frac{\tau}{8}\frac{\beta\int d^3x\, r_h^4}{16\pi G L^5} \\ \implies \delta f_{\text{probe}} &= \frac{\tau}{8} f = \delta f \end{aligned} \tag{5.67}$$

This result matches the exact correction calculated above. It also matches [61]. Using this result, one can calculate the other thermodynamic quantities by the standart manipulations and check that it matches the above result. The problem arises if one wants to calculate the change in energy using the stress-energy tensor of the D-brane probe. We switch back to the Lorentzian signature. The stress-energy tensor is given by

$$T^{MN}_{\text{probe}} = \frac{2}{\sqrt{-g}}\frac{\delta S_{\text{probe}}}{\delta g_{MN}} = -\frac{T_0}{16\pi G}g^{MN} + \frac{1}{2\sqrt{-g}}\frac{T_0 L}{16\pi G}\frac{\delta}{\delta g_{MN}}\int d^4x\sqrt{-\gamma} \tag{5.68}$$

Note that $\gamma_{\mu\nu}$ can be written as a five dimensional metric,

$$\gamma_{MN} = g_{MN} - \hat{\eta}_M \hat{\eta}_N, \tag{5.69}$$

where $\hat{\eta}_M$ is again the outward unit vector to the boundary, i.e. $\hat{\eta}_M = \sqrt{g_{rr}}\delta^r_M$. Then, in the setup we are working

$$\begin{aligned}\frac{\delta}{\delta g_{MN}} \int d^4x \sqrt{-\gamma} &= \frac{\delta}{\delta g_{MN}} \int d^5x \sqrt{-\det \gamma_{MN}}\, \delta(r - r_{\max}) \\ &= \begin{cases} \frac{1}{2}\sqrt{\gamma}\gamma^{MN}\delta(r - r_{\max}) & \text{if } M \neq 0 \text{ and } N \neq 0 \\ 0 & \text{if } M = 0 \text{ or } N = 0 \end{cases} .\end{aligned} \tag{5.70}$$

We need to compute the energy density, which is given by

$$\begin{aligned}\delta\epsilon_{\text{probe}} &= -\int_{r_h}^{\infty} dr \sqrt{-g}\, \delta^t_\mu T^\mu_\nu \delta^\nu_t \\ &= \lim_{r_{\max}\to\infty} \frac{T_0}{16\pi G} \int_{r_h}^{r_{\max}} dr \sqrt{-g} - \frac{1}{4}\frac{T_0 L}{16\pi G}\sqrt{-\gamma} \\ &= \frac{T_0}{16\pi G} \lim_{r_{\max}\to\infty} \frac{r^4}{4L^3}\bigg|_{r_h}^{r_{\max}} - \frac{r_{\max}^4}{4L^3} + \frac{r_h^4}{8L^3} + \mathcal{O}(r_{\max}^{-4}) \\ &= -\frac{1}{8}\frac{t\, r_h^4}{16\pi G L^5} = \delta f = \delta\epsilon + 4\delta f.\end{aligned} \tag{5.71}$$

We have $4|\delta f|$ missing! This is exactly the contribution of the backreaction on the $T\delta s$ term in equation (5.66).

As we have anticipated, the total energy of the system is given by the backreaction contribution and the stress-energy tensor of the brane. The authors of [61] speculated that the missing energy, which is the backreaction contribution, should be attributed to the part of the brane that extends behind the horizon. Later, we will study this point in detail.

5.2.2 Stress-energy tensor of the D7-brane

Now consider a time dependent embedding in an AdS black hole background. The action becomes

$$\begin{aligned} I_{D7} &= -\mathcal{N}\int dtdz\,\frac{\cos^3\theta}{z^5}\sqrt{1+z^2(1-b^4z^4)\theta'^2-\frac{z^2R^4\dot{\theta}^2}{1-b^4z^4}}, \\ &= -\mathcal{N}b^3R^2\int dt'dz'\,\frac{\cos^3\theta}{z'^5}\sqrt{1+z'^2(1-z'^4)\theta'^2-\frac{z'^2\dot{\theta}^2}{1-z'^4}}. \\ \mathcal{N} &\equiv N_fT_{D7}\Omega_3\left(\int d^3x\right), \\ \mathcal{L}- &\equiv \frac{\cos^3\theta}{z'^5}\sqrt{1+z'^2(1-z'^4)\theta'^2-\frac{z'^2\dot{\theta}^2}{1-z'^4}}. \end{aligned} \tag{5.72}$$

Here we defined the dimensionless coordinates and parameters

$$z' = bz, \qquad t' = \frac{tb}{R^2}. \tag{5.73}$$

The stress-energy tensor is given by

$$\begin{aligned} T^{AB}(x) &= \frac{2}{\sqrt{-g}}\frac{\delta I_{D7}}{\delta g_{AB}} \\ &= -N_fT_{D7}\frac{1}{\sqrt{-g}}\int d^8\xi\,\delta^{10}(x-X(\xi))\sqrt{-h}h^{ij}\partial_iX^A\partial_jX^B. \end{aligned} \tag{5.74}$$

Here h_{ij} is the induced metric. Given a killing vector ξ^A, one can define conserved currents

$$\partial_A\left(\xi^B\sqrt{-g}\,T^A_{\ B}\right) = 0. \tag{5.75}$$

We choose the killing vector $\xi^A\partial_A = \frac{\partial}{\partial t}$. Then $T^A{}_t = g_{tt}T^{At}$.

$$
\begin{aligned}
-\frac{\sqrt{-g}\,T^t{}_t}{N_f T_{D7}} &= \delta(\psi)\delta(\theta-\Theta(z,t))\det\Omega_3 \frac{\cos^3\theta}{z^5}\frac{1+z^2(1-b^4z^4)\theta'^2}{\sqrt{1+z^2(1-b^4z^4)\theta'^2-\frac{z^2R^4\dot\theta^2}{1-b^4z^4}}} \\
-\frac{\sqrt{-g}\,T^z{}_t}{N_f T_{D7}} &= \delta(\psi)\delta(\theta-\Theta(z,t))\det\Omega_3 \frac{\cos^3\theta}{z^5}\frac{-z^2(1-b^4z^4)\theta'\dot\theta}{\sqrt{1+z^2(1-b^4z^4)\theta'^2-\frac{z^2R^4\dot\theta^2}{1-b^4z^4}}}.
\end{aligned}
\tag{5.76}
$$

$\Theta(z,t)$ is the classical trajectory. We checked on Mathematica $\partial_A\sqrt{-g}\,T^A{}_t = 0$. As expected, for static configurations $\sqrt{-g}\,T^z{}_t$ vanishes. One can then define a conserved energy associated with the probe D7-brane.

$$
\begin{aligned}
U_{D7} &= -\int dz d^3x d\ldots\ \sqrt{-g}\,T^t{}_t \\
&= \mathcal{N}\int dz\,\frac{\cos^3\Theta}{z^5}\frac{1+z^2(1-b^4z^4)\Theta'^2}{\sqrt{1+z^2(1-b^4z^4)\Theta'^2-\frac{z^2R^4\dot\Theta^2}{1-b^4z^4}}}
\end{aligned}
\tag{5.77}
$$

which satisfies

$$
\begin{aligned}
\frac{dU_{D7}}{dt} &= \int d^3x d\ldots\ \sqrt{-g}\,T^z{}_t\big|_{z=z_{\rm end}} - \int d^3x d\ldots\ \sqrt{-g}\,T^z{}_t\big|_{z=z_0} \\
\Delta U_{D7} &= \int dt d^3x d\ldots\ \sqrt{-g}\,T^z{}_t\big|_{z=z_{\rm end}} - \int dt d^3x d\ldots\ \sqrt{-g}\,T^z{}_t\big|_{z=z_0}.
\end{aligned}
\tag{5.78}
$$

Recalling that $-\sqrt{-g}\,T^z{}_t$ is the energy flow through a constant z surface in the positive z direction. The equation above is saying that the increase in energy is given by the flow of energy from both ends of the brane. Later, we will be interested in the energy that flows into the horizon at the end of the brane. This will require us to look at $-\sqrt{-g}\,T^z{}_t$ at $z_{\rm end} = 1/b$.

Holographic Renormalization of the Time-Dependent Action

Now, we discuss the remormalization of the energy. The action for the static case was divergent, as we will see it is divergent for the time-dependent case also. The treatment of these divergences is a straightforward generalization of the static case and was treated in [59]. We will calculate the renormalized currents later on.

We start by extracting the divergent terms in the action. Rewriting the induced metric

$$ds^2_{D7} = \left[-\frac{1-b^4z^4}{R^2z^2} + R^2\dot{\theta}^2\right]dt^2 + 2R^2\theta'\dot{\theta}dzdt + \left[\frac{R^2}{z^2}\frac{1}{1-b^4z^4} + R^2\theta'^2\right]dz^2 + \frac{d\vec{x}^2}{R^2z^2} + R^2\cos^2\theta(t,z)d\Omega_3^2. \tag{5.79}$$

The equation of motion that follows from the action, in terms of the dimensionless coordinates is

$$\begin{aligned} 0 &= 3(1-z'^4)\tan\theta - z'(1-z'^4)(3+z'^4)\theta' + 3z'^2(1-z'^4)^2\tan\theta\,\theta'^2 \\ &- 3z'^2\tan\theta\,\dot{\theta}^2 + 2z'^3(2+z'^4)\dot{\theta}^2\theta' - 2z'^3(1-z'^4)(z'^8-3z'^4+2)\theta'^3 \\ &+ 2z'^4(1-z'^4)\dot{\theta}\theta'\dot{\theta}' + z'^2(1-z'^4)^2\theta'' - \beta^4z'^4(1-z'^4)\dot{\theta}^2\theta'' \\ &- z'^2\ddot{\theta} - z'^4(1-z'^8)\theta'^2\ddot{\theta}. \end{aligned} \tag{5.80}$$

Again, following [59], we assume an asymptotic expansion of the form

$$\theta(t',z') = \sum_{i=1}^{\infty}\theta_i(t')z'^i + \sum_{i=1}^{\infty}\psi_i(t')z'^i\ln z' + \sum_{i=1}^{\infty}\sum_{j=2}^{p}\Psi_{i,j}(t')z'^i(\ln z')^j. \tag{5.81}$$

We truncate at $i = 8$ and $p = 8$ and found that the leading order terms important

for our discussion is

$$\theta(t', z') = \theta_1(t')z' + \theta_3(t')z'^3 + \frac{1}{2}\ddot{\theta}_1(t')z'^3 \ln z' + \mathcal{O}(z'^5) \tag{5.82}$$

A logarithmic term appeared which was missing in the static case. When plugged into the action, the divergence of the integrand around $z' = 0$ id given by

$$\frac{1}{z'^5} - \frac{\theta_1(t')^2}{z'^3} + \frac{\theta_1\ddot{\theta}_1 - \dot{\theta}_1^2}{2z'} + O(z') \tag{5.83}$$

The $1/z'$ term is new and does not appear in the static case.

To renormalize, we will again introduce a finite cut-off at $z' = \epsilon$ slice and use counterterms given in (5.14). Let's first look at the induced metric at $z' = \epsilon$ slice

$$\begin{aligned} \gamma_{ij}dx^i dx^j &= -R^2\frac{1-\epsilon^4}{\epsilon^2}dt'^2 + \frac{b^2 d\vec{x}^2}{R^2\epsilon^2} \\ \gamma &= -\frac{b^6}{R^4\epsilon^8}\left(1-\epsilon^4\right) \end{aligned} \tag{5.84}$$

Note that γ_{ij} is flat, i.e. $R_\gamma = 0$ and $R_{ij}R^{ij} = 0$. We will suppress the dimensionful constant in front of γ. The only relevant counterterms are (dimensionful constants

suppressed)

$$
\begin{aligned}
L_1 &= \frac{1}{4\epsilon^4}\sqrt{1-\epsilon^4}, \\
L_4 &= -\frac{1}{2\epsilon^4}\sqrt{1-\epsilon^4}\,\theta(t',\epsilon)^2, \\
L_5 &= \frac{1}{2}\left(\ln\epsilon + \frac{\epsilon^4}{8} + \mathcal{O}(\epsilon^8)\right)\theta(t',\epsilon) \\
&\qquad \times \frac{\partial}{\partial t'}\left[\frac{1}{\epsilon^4}\left[-\frac{1-\epsilon^4}{\epsilon^2}\right]^{-1}\sqrt{1-\epsilon^4}\,\dot{\theta}(t',\epsilon)\right], \\
L_F &= \frac{5}{12\epsilon^4}\sqrt{1-\epsilon^4}\,\theta(t',\epsilon)^4, \\
&\implies L_1 + L_4 + L_5 + L_F = \frac{1}{4\epsilon^4} - \frac{\theta_1^2}{\epsilon^2} - \theta_1\ddot{\theta}_1\ln\epsilon - \frac{1}{8} - \theta_1\theta_3 + \frac{5}{12}\theta_1^4. \qquad (5.85)
\end{aligned}
$$

These counterterms cancel the divergence in the action. Note that the logarithmic terms does not cancel precisely but it gives a total time derivative term which is to be integrated over time:

$$
-\frac{\theta_1\ddot{\theta}_1 - \dot{\theta}^2}{2}\ln\epsilon + \theta_1\ddot{\theta}_1\ln\epsilon = \frac{1}{2}\frac{\partial}{\partial t}\left(\theta\dot{\theta}\right)\ln\epsilon \qquad (5.86)
$$

Another way to deal with this divergence would be to deal with the total derivative at the counterterm level and rewrite L_5 as

$$
\begin{aligned}
L_5 &= \frac{1}{2}\ln u_\epsilon\,\theta\partial_i\sqrt{-\gamma}\gamma^{ij}\partial_j\theta \\
&\to -\frac{1}{2}\sqrt{-\gamma}\gamma^{ij}(\partial_i\theta)(\partial_j\theta) \\
&\implies -\frac{1}{2}\ln u_\epsilon\sqrt{-\gamma}(\partial_i\theta)(\partial^i\theta) \\
&\implies L_1 + L_4 + L_5 + L_F = \frac{1}{4\epsilon^4} - \frac{\theta_1^2}{\epsilon^2} - \frac{\theta_1\ddot{\theta}_1 - \dot{\theta}_1^2}{2}\ln\epsilon - \frac{1}{8} - \theta_1\theta_3 + \frac{5}{12}\theta_1^4. \qquad (5.87)
\end{aligned}
$$

Now the cancelation is precise. Combining these results

$$-\frac{I_{D7,\mathrm{ren}}}{\mathcal{N}b^3R^2} = \lim_{\epsilon\to 0}\left[\int_\epsilon^{z'_{\mathrm{end}}} dz' \int dt' \,\frac{\cos^3\theta}{z'^5}\sqrt{1+z'^2(1-z'^4)\theta'^2 - \frac{z'^2\dot{\theta}^2}{1-z'^4}}\right.$$
$$\left. - \int dt' \,(L_1+L_4+L_5+L_F)\right]. \tag{5.88}$$

Next we calculate the time dependent quark condensate using the AdS/CFT dictionary. The mass is again given by

$$M(t) = \frac{1}{2}\sqrt{\lambda}T\theta_1(t). \tag{5.89}$$

The prescription for calculating the condensate is [106, 59]

$$\begin{aligned}\langle\bar{q}q\rangle &= \frac{\delta I_{D7,\mathrm{ren}}}{\delta M(t)} = \frac{2}{\sqrt{\lambda}T}\frac{\delta I_{D7,\mathrm{ren}}}{\delta\theta_1(t)} = \frac{2}{\sqrt{\lambda}T}\lim_{\epsilon\to 0}\frac{1}{\epsilon^3}\frac{1}{\sqrt{-\gamma}}\frac{\delta I_{D7,\mathrm{ren}}}{\delta\theta(t,\epsilon)}\\ &= \frac{2}{\sqrt{\lambda}T}\frac{b}{R^2}\lim_{\epsilon\to 0}\frac{1}{\epsilon^3}\frac{1}{\sqrt{-\gamma}}\frac{\delta I_{D7,\mathrm{ren}}}{\delta\theta(t',\epsilon)}.\end{aligned} \tag{5.90}$$

Now

$$\frac{1}{N_f T_{D7}\Omega_3 b^3R^2}\frac{\delta I_{D7,\mathrm{reg}}}{\delta\theta(t',\epsilon)} = \int dt''\,\delta(t''-t')\,\frac{\partial\mathcal{L}}{\partial\theta'}\frac{\partial\theta(t'',z';\theta(\epsilon))}{\partial\theta(t'',\epsilon)}\bigg|_\epsilon^{z'_{\mathrm{end}}}$$
$$+\int dz''\,\delta(z''-\epsilon)\,\frac{\partial\mathcal{L}}{\partial\dot{\theta}}\frac{\partial\theta(t',z'';\theta(t',\epsilon))}{\partial\theta(t',\epsilon)}\bigg|_{t_i}^{t_f}. \tag{5.91}$$

The boundary term at the z_{end} boundary vanishes due to the boundary conditions that make the variational problem well defined. It would be nice to verify this through an asymptotic analysis of the solutions to the equation of motion. The boundary contributions at t_i and t_f do not vanish. We will assume that t_i and t_f are at past and future infinity and fields vanish there. This will be sufficient for our purposes. A more detailed analysis can be found at [75]. Then, the only contribution

is from the ϵ boundary which will be cancelled by the counterterms:

$$\begin{aligned}
&-\frac{1}{N_f T_{D7}\Omega_3 b^3 R^2}\frac{\delta I_{D7,\text{reg}}}{\delta\theta(t',\epsilon)} \\
&\qquad = -\frac{\cos^3\theta(t',\epsilon)}{\epsilon^5}\frac{\epsilon^2(1-\epsilon^4)\theta'(t',\epsilon)}{\sqrt{1+\epsilon^2(1-\epsilon^4)\theta'(t',\epsilon)^2-\frac{\epsilon^2\dot\theta(t',\epsilon)^2}{1-\epsilon^4}}} \\
&\qquad = -\frac{\theta_1}{\epsilon^3}+\frac{1}{\epsilon}\left(2\theta_2^3-3\theta_3-\frac{1}{2}\ddot\theta_1-\frac{3}{2}\ddot\theta_1\ln\epsilon\right)+\mathcal{O}(\epsilon).
\end{aligned} \tag{5.92}$$

The counterterm contributions are

$$\begin{aligned}
&\frac{\delta}{\delta\theta(\epsilon)}\int d\vec{x}dt'\left(L_1+L_4+L_5+L_F\right) \\
&\qquad = -\sqrt{-\gamma}\theta(\epsilon)+\ln u_\epsilon\,\gamma^{t't'}\sqrt{-\gamma}\,\partial_{t'}^2\theta+\frac{5}{3}\sqrt{-\gamma}\theta(\epsilon)^3 \\
&\qquad = -\frac{\theta_1}{\epsilon^3}+\frac{1}{\epsilon}\left(\frac{5\theta_1^3}{3}-\theta_3-\frac{3}{2}\ddot\theta_1\ln\epsilon\right).
\end{aligned} \tag{5.93}$$

Putting everything together

$$\begin{aligned}
\langle\bar q q\rangle &= -N_f T_{D7}\Omega_3 b^3 R^2\frac{2}{\sqrt{\lambda}T}\frac{b}{R^2}\left(-2\theta_3+\frac{\theta_1^3}{3}-\frac{1}{2}\ddot\theta_1(t')\right) \\
&= -\frac{2N_f T_{D7}\Omega_3 b^4}{\sqrt{\lambda}T}\left(-2\theta_3+\frac{\theta_1^3}{3}-\frac{1}{2}\frac{R^4}{b^2}\ddot\theta_1(t)\right) \\
\langle\bar q q\rangle(t) &= -\frac{1}{8}N_f N_c T^3\sqrt{\lambda}\left(-2\theta_3+\frac{\theta_1^3}{3}-\frac{1}{2\pi^2T^2}\ddot\theta_1(t)\right).
\end{aligned} \tag{5.94}$$

Note that the 1/2 factor in front of $\ddot\theta_1$ is missing in [59].

Holographic Renormalization of the Bulk Stress-Energy tensor

Having done this, we now proceed to renormalize the stress-energy tensor. The most natural way to renormalize $T^t{}_t$ would be to take the renormalized action, which includes the counterterms, and vary with respect to the boundary metric. One hopes

that the variation of the action counterterms will give the correct counterterms for the stress-energy tensor component at hand. We will find that this is not true, and propose another way to fix the counterterms. The necessity of another method is already presented by the fact that variations of the action counterterms with respect to the bulk metric components whose indices include the radial or angular directions, vanish. Therefore, by variation with respect to the bulk metric, one will not be able to set the counterterms for all components of the bulk stress-energy tensor. Let's demonstrate this explicitly.

First, let's write down the divergent terms in $T^t{}_t$:

$$-\frac{\sqrt{-g}\,T^t{}_t(\epsilon)}{N_f T_{D7}} \sim \frac{1}{\epsilon^5} - \frac{b^2\theta_1^2}{\epsilon^3} + \frac{b^2R^4\dot{\theta}_1^2 + b^2R^4\theta_1\ddot{\theta}_1}{2\epsilon} + \mathcal{O}(\epsilon). \tag{5.95}$$

This is almost the same divergence as in the action, however the $\dot{\theta}^2$ term reverses sign. Now we look at the variation of the counterterms and see if they really cancel the divergence. Since we are interested in the bulk stress-energy tensor, therefore we will do variations with respect to the boundary metric. This requires variations of γ_{ij} with respect to $g_{\mu\nu}$. Note that γ_{ij} is induced from the AdS part of $g_{\mu\nu}$. Let's do one sample variation explicitly:

$$\begin{aligned} 2\,\frac{\delta}{\delta g_{\mu\nu}(x)}\int d^4x\sqrt{-\gamma} &= \\ &= \frac{\delta}{\delta g_{\mu\nu}(x)}\int d^4x d\bar{z}\ldots\,\delta(\bar{z}-\epsilon)\delta(\bar{\psi})\delta(\bar{\theta}-\Theta(t,z))\delta^3(\ldots)\sqrt{-\gamma} \\ &= \delta(z-\epsilon)\delta(\psi)\delta(\theta-\Theta(t,z))\delta^3(\ldots)\sqrt{-\gamma}\gamma^{ij}\delta_i^\mu\delta_j^\nu \end{aligned} \tag{5.96}$$

Here we switched to the notation in which capital Θ denotes a particular solution to the equation of motion. So unless μ and ν are in the directions of the boundary, no contribution will be made from the counterterms. Remembering that $g_{tt}(\epsilon)\gamma^{tt} = 1$,

L_1, L_4 and L_F carry over directly up to the delta functions. This is convenient because the divergence is almost the same as the divergence in the action. The difference is in the $\dot{\theta}^2$ term, which was cancelled by the L_5 counterterm. Let's look at is variation carefully:

$$\begin{aligned} &- 2g_{tt}\frac{1}{2}\ln u_\epsilon \frac{\delta}{\delta g_{tt}(x)}\int d^4x\,\sqrt{-\gamma}\gamma^{ij}(\partial_i\Theta)(\partial_j\Theta) \\ &\quad = -\frac{3}{2}\delta^6(\ldots)\ln u_\epsilon\,\sqrt{-\gamma}\gamma^{tt}(\partial_t\Theta)^2. \end{aligned} \tag{5.97}$$

This does not cancel the divergence! The variations of the counterterms give

$$\frac{1}{4\epsilon^4} - \frac{b^2\theta_1^2}{2\epsilon^2} + \frac{b^4}{8} - \frac{5b^4\theta_1^4}{12} + b^4\theta_1\theta_3 + \frac{3}{2}\ln(bz)\dot{\theta}_1^2 - \frac{1}{2}\ln(bz)\theta_1\ddot{\theta}_1 + \mathcal{O}(\epsilon), \tag{5.98}$$

which is not the integral of (5.95). Why did this method not work? Is this a serious problem for the holographic renormalization procedure? These questions deserves attention of their own, which we do not do here. We hope to come back to this point and investigate it further in the future.

We still need to renormalize the stress-energy tensor. The variation method did not succeed, hence we turn to the other definition of $-\sqrt{-g}\,T^t{}_t$: it is the Hamiltonian of the system!

$$\begin{aligned} P_\theta &= \frac{\partial\mathcal{L}}{\partial\dot{\theta}} = \frac{\cos^3\theta}{z^5}\frac{\frac{z^2R^4\dot{\theta}}{1-b^4z^4}}{\sqrt{1+z^2(1-b^4z^4)\theta'^2 - \frac{z^2R^4\dot{\theta}^2}{1-b^4z^4}}}, \\ \mathcal{H} &= P_\theta\dot{\theta} - \mathcal{L} = \frac{\cos^3\theta}{z^5}\frac{1+z^2(1-b^4z^4)\theta'^2}{\sqrt{1+z^2(1-b^4z^4)\theta'^2 - \frac{z^2R^4\dot{\theta}^2}{1-b^4z^4}}}. \end{aligned} \tag{5.99}$$

We can use this to definition to calculate the counterterms. L_1, L_4 and L_F simply reverses sign. For L_5, one gets a contribution from the P_θ, since L_5 also contains a

time derivative of θ. Putting thing together, the renormalized $T^t{}_t$ is

$$
\begin{aligned}
-\frac{\sqrt{-g}\,T^t{}_{t,\mathrm{ren}}}{N_f T_{D7}} = \\
&\lim_{\epsilon\to 0}\Bigg\{\delta(\psi)\delta(\theta-\Theta(z,t))\det\Omega_3\frac{\cos^3\theta}{z^5}\frac{1+z^2(1-b^4z^4)\theta'^2}{\sqrt{1+z^2(1-b^4z^4)\theta'^2-\frac{z^2R^4\dot\theta^2}{1-b^4z^4}}} \\
&-\delta(z-\epsilon)\delta(\psi)\delta(\theta-\Theta(t,z))\delta^3(\ldots)R^4\Omega_3\sqrt{-\gamma} \\
&\qquad\times\left[\frac{1}{4}-\frac{1}{2}\theta^2+\frac{5}{12}\theta^4+\frac{R^2}{2}\ln u_\epsilon\,\gamma^{tt}(\partial_t\theta)^2\right]\Bigg\}
\end{aligned}
\tag{5.100}
$$

Here γ_{ij} is the induced metric on $z=\epsilon$ slice, i.e. $\sqrt{-\gamma}=\frac{1}{R^4}\frac{\sqrt{1-b^4z^4}}{z^4}$. One can check that when the above statement is integrated in z, the divergence at the $z=\epsilon$ slice cancels up to the finite term

$$
\frac{b^4}{8}-\frac{5b^4\theta_1^4}{3}+b^4\theta_1\theta_3+\mathcal{O}(bz). \tag{5.101}
$$

We will take equation (5.100) as the correctly renormalized $-\sqrt{-g}\,T^t{}_t$.

We also need to calculate renormalized $-\sqrt{-g}\,T^z{}_t$. One might question the necessity of this, since this component of the stress-enery tensor is to be integrated over constant z slices, hence no integration over z is done. We will be interested in the flow of enery to the brane from the boundary, and this requires an integration of $-\sqrt{-g}\,T^z{}_t$ at $z=0$ boundary. In this limit, $-\sqrt{-g}\,T^z{}_t$ is divergent. To find the consistent counterterms, one again needs to be creative since variation of the action will give no counterterms as discussed above. To fix the counterterms here, we will use the continuity equation, $\partial_\mu\sqrt{-g}\,T^\mu_t=0$. Let's repeat here the previously defined

energy relations:

$$
\begin{aligned}
U_{D7} &= -\int dz d^3x d\ldots \sqrt{-g}\, T^t{}_t \\
\frac{dU_{D7}}{dt} &= \int d^3x d\ldots \sqrt{-g}\, T^z{}_t\big|_{z=z_{\rm end}} - \int d^3x d\ldots \sqrt{-g}\, T^z{}_t\big|_{z=0}\,.
\end{aligned}
\tag{5.102}
$$

From this statement, the procedure is very clear. The time derivative of the $-\sqrt{-g}\,T^t{}_t$ counterterms should renormalize $-\sqrt{-g}\,T^z{}_t$. Doing that, one gets

$$
\begin{aligned}
&-\frac{\sqrt{-g}\,T^z{}_{t,\rm ren}(z=0)}{N_f T_{D7}} = \\
&\quad \lim_{\epsilon\to 0}\Bigg\{ \delta(\psi)\delta(\theta-\Theta(t,\epsilon))\det\Omega_3 \frac{\cos^3\theta}{\epsilon^5}\frac{-\epsilon^2(1-b^4\epsilon^4)\theta'\dot\theta}{\sqrt{1+\epsilon^2(1-b^4\epsilon^4)\theta'^2-\frac{\epsilon^2R^4\dot\theta^2}{1-b^4\epsilon^4}}} \\
&\quad - \delta(\psi)\delta(\theta-\Theta(t,\epsilon))\delta^3(\ldots)R^4\Omega_3\sqrt{-\gamma} \\
&\qquad \times\left[-\theta\dot\theta+\frac{5}{3}\theta^3\dot\theta+R^2\ln u_\epsilon\,\gamma^{tt}\dot\theta\ddot\theta\right]\Bigg\} \\
&\quad = \delta(\psi)\delta(\theta-\Theta(t,\epsilon))\delta^3(\ldots)\Omega_3\left[\frac{b^4}{3}\dot\theta_1\theta_1^3-2b^4\dot\theta_1\theta_3-\frac{b^2R^4}{2}\dot\theta_1\ddot\theta_1\right].
\end{aligned}
\tag{5.103}
$$

This implies

$$
\begin{aligned}
\Delta U_{D7} &= \int dt d^3x d\ldots \sqrt{-g}\, T^z{}_t\big|_{z=z_{\rm end}} \\
&\qquad - N_f T_{D7} b^4\Omega_3 \int dt d^3x \left[\frac{1}{3}\dot\theta_1\theta_1^3-2\dot\theta_1\theta_3-\frac{R^4}{b^2 2}\dot\theta_1\ddot\theta_1\right] \\
&= \int dt d^3x d\ldots \sqrt{-g}\, T^z{}_t\big|_{z=z_{\rm end}} + \int dt d^3x\, M(t)\,\langle\bar q q\rangle\,(t).
\end{aligned}
\tag{5.104}
$$

This is the most general form of the flow equation. In the coming pages, we will look at quasistatic processes in more detail.

Eddington-Finkelstein Coordinates

Before discussing more about the time-dependent brane embeddings, let's discuss the system in Eddington-Finkelstein coordinates which is more suitable for these calculations. To go to EF coordinates, we define the new time direction

$$v = t - \int^z dz' \, \frac{R^2}{1 - b^4 z'^4}, \tag{5.105}$$

so that the new metric is

$$ds^2 = \frac{1}{R^2 z^2} \left[-(1 - b^4 z^4) dv^2 - 2R^2 dv dz + d\vec{x}^2 \right] + R^2 d\Omega_5^2. \tag{5.106}$$

The induced metric is

$$\begin{aligned} ds^2_{D7} = &- \left(\frac{1}{R^2 z^2} - \frac{b^4 z^2}{R^2} - R^2 (\partial_v \theta)^2 \right) dv^2 + 2 \left(R^2 \partial_z \theta \partial_v \theta - \frac{1}{z^2} \right) dv dz \\ &+ (\partial_z \theta)^2 R^2 dz^2 + \frac{1}{R^2 z^2} d\vec{x}^2 + R^2 \cos^2 \theta d\Omega_3^2. \end{aligned} \tag{5.107}$$

The DBI action becomes

$$I_{D7} = -\mathcal{N} \int dv dz \, \frac{\cos^3 \theta}{z^5} \sqrt{1 + z^2 (1 - b^4 z^4)(\partial_z \theta)^2 - 2R^2 z^2 \, \partial_z \theta \, \partial_v \theta}. \tag{5.108}$$

For later use, let's note a couple of relations. We denote tensor components in EF coordinates by a bar above the quantity.

$$\begin{aligned} \xi^t &= \bar{\xi}^v + \frac{R^2}{1 - b^4 z^4} \bar{\xi}^z & \qquad \xi_z &= -\frac{R^2}{1 - b^4 z^4} \bar{\xi}_v + \bar{\xi}_z \\ \bar{\xi}^v &= \xi^t - \frac{R^2}{1 - b^4 z^4} \xi^z & \qquad \bar{\xi}_z &= \frac{R^2}{1 - b^4 z^4} \xi_t + \xi_z. \end{aligned} \tag{5.109}$$

What happens to the conserved currents? In EF coordinates, $\bar{\xi}^A\bar{\partial}_A = \frac{\partial}{\partial v}$ is a timelike Killing vector. This is just the Killing vector in Schwarzchild coordinates $\xi^A\partial_A = \frac{\partial}{\partial t}$, written in a different coordinate system ($\xi^A = \delta^A_t$ which transforms to $\bar{\xi}^A = \delta^A_v$). Therefore, we can use conserved quantities w.r.t. this vector and derive conclusions about Schwarzchild coordinates.

Using the definition of the stress-energy tensor given above, let's calculate the conserved currents. $\bar{T}^A{}_v = g_{vv}\bar{T}^{Av} + g_{zv}\bar{T}^{Az}$.

$$
\begin{aligned}
-\frac{\sqrt{-g}\,\bar{T}^v{}_v}{N_f T_{D7}} &= \\
&\delta(\psi)\delta(\theta-\Theta(v,z))\det\Omega_3\frac{\cos^3\theta}{z^5}\frac{1+z^2(1-b^4z^4)(\partial_z\theta)^2 - R^2z^2\,\partial_v\theta\,\partial_z\theta}{\sqrt{1+z^2(1-b^4z^4)(\partial_z\theta)^2 - 2R^2z^2\,\partial_v\theta\,\partial_z\theta}} \\
-\frac{\sqrt{-g}\,\bar{T}^z{}_v}{N_f T_{D7}} &= \\
&\delta(\psi)\delta(\theta-\Theta(z,t))\det\Omega_3\frac{\cos^3\theta}{z^5}\frac{-z^2(1-b^4z^4)\partial_v\theta\,\partial_z\theta + R^2z^2(\partial_v\theta)^2}{\sqrt{1+z^2(1-b^4z^4)(\partial_z\theta)^2 - 2R^2z^2\,\partial_v\theta\,\partial_z\theta}}
\end{aligned}
\tag{5.110}
$$

Using these, one can again define an energy. However, note that this energy will be different than the energy of Schwarzschild coordinates! The current is the same but the space-like surface that we integrate over differ.

$$
\begin{aligned}
\bar{U}_{D7} &= -\int dz d^3x d\ldots\,\sqrt{-g}\,\bar{T}^v{}_v \\
&= \mathcal{N}\int dz\,\frac{\cos^3\Theta}{z^5}\frac{1+z^2(1-b^4z^4)(\partial_z\Theta)^2 - R^2z^2\,\partial_v\Theta\,\partial_z\Theta}{\sqrt{1+z^2(1-b^4z^4)(\partial_z\Theta)^2 - 2R^2z^2\,\partial_v\Theta\,\partial_z\Theta}}
\end{aligned}
\tag{5.111}
$$

For comparison, we also write down the energy defined in the previous section, equation (5.77), in EF coordinates. In other words, we take the integral in equation

(5.77) and change parameters from $(t, z) \to (v, z)$.

$$\begin{aligned} U_{D7} &= -\int dz d^3x d\ldots \sqrt{-g}\, T^t{}_t \\ &= \mathcal{N}\int dz\ \frac{\cos^3\Theta}{z^5}\frac{1+z^2(1-b^4z^4)(\partial_z\Theta)^2-2R^2z^2\,\partial_v\Theta\,\partial_z\Theta+\frac{R^4z^2(\partial_v\theta)^2}{1-b^4z^4}}{\sqrt{1+z^2(1-b^4z^4)(\partial_z\Theta)^2-2R^2z^2\,\partial_v\Theta\,\partial_z\Theta}}\Bigg|_{v=v(t,z)} \end{aligned} \tag{5.112}$$

Note that this integral is to be taken at a constant t slice, which means v in the integrand is a function of t and z. $U_{D7} \neq \bar{U}_{D7}$. This is to be expected. Even though the currents are the same in both cases, we are integrating through different surfaces, constant t slice for the former and constant v slice for the latter. On the other hand, energy flow thorugh a constant z slice will be the same, since constant z slice describes the same surface in both coordinate systems. Consider a surface $z = z_s$. The energy flow through this surface is

$$\begin{aligned} \Delta\bar{U}_{D7,z_s} &= -\int dv d^3x d\ldots \sqrt{-g}\, T^z{}_v\big|_{z=z_s} \\ &= \mathcal{N}\int dv d^3x d\ldots \frac{\cos^3\Theta}{z^5}\frac{-z^2(1-b^4z^4)\partial_v\Theta\,\partial_z\Theta+R^2z^2(\partial_v\Theta)^2}{\sqrt{1+z^2(1-b^4z^4)(\partial_z\Theta)^2-2R^2z^2\,\partial_v\Theta\,\partial_z\Theta}}\Bigg|_{z=z_s} \end{aligned} \tag{5.113}$$

Also

$$\begin{aligned} \Delta U_{D7,z_s} &= -\int dt d^3x d\ldots \sqrt{-g}\, T^z{}_t\big|_{z=z_s} \\ &= \mathcal{N}\int dt d^3x d\ldots \frac{\cos^3\Theta}{z^5}\frac{-z^2(1-b^4z^4)\Theta'\dot{\Theta}}{\sqrt{1+z^2(1-b^4z^4)\Theta'^2-\frac{z^2R^4\dot{\Theta}^2}{1-b^4z^4}}}\Bigg|_{z=z_s} \\ &= \mathcal{N}\int dv d^3x d\ldots \frac{\cos^3\Theta}{z^5}\frac{-z^2(1-b^4z^4)\partial_v\Theta\,\partial_z\Theta+R^2z^2(\partial_v\Theta)^2}{\sqrt{1+z^2(1-b^4z^4)(\partial_z\Theta)^2-2R^2z^2\,\partial_v\Theta\,\partial_z\Theta}}\Bigg|_{z=z_s} \end{aligned} \tag{5.114}$$

$\Delta U_{D7,z_s} = \Delta\bar{U}_{D7,z_s}$ as expected.

EF coordinates reveal another property of the D7-brane. The DBI action in EF coordinates look exactly the same as DBI action in Schwarzschild coordinates for static embeddings. Consider a static embedding in Schwarzschild coordinate system $\theta(t,z) = \theta(z)$. For the moment let us denote the EF coordinates by $(v,\bar{z})$. Then $\theta(t,z) = \theta(v(t,z),\bar{z})$. A constant time slice embedding in Schwarzschild coordinates do not live on a constant v slice. However

$$\frac{\partial\theta(t,z)}{\partial t} = 0 \qquad \Longrightarrow \qquad \frac{\partial\theta(v,\bar{z})}{\partial v} = 0. \tag{5.115}$$

This means $\theta(z) = \theta(\bar{z})$ and one should remember that $\bar{z} = z$. The static D7-brane embeddings outside the blackhole would look exactly the same in both coordinate systems. In EF coordinates, we could extend this embedding inside the horizon. We plot these embeddings in figure 5.5. To find these embeddings, we used exactly the same procedure we used for Euclidean embeddings. To continue our solutions across the horizon, we used the continuity of the solution.

The important point to note here that the D7-brane embeddings end before reaching the singularity. This is an important observation, because it allows a nice description of the dual field theory going through the first order phase transition. Towards the end of this chapter, we will use this idea to simulate a D7-brane dynamically going through a topological phase transition.

Quasistatic process

Let's consider a processes in which the temperature is varied slowly. This will require one to change the background geometry. We assume that the process is quasi-static, that is is infinitely slow, such that at each instant the system is in equilibrium. The

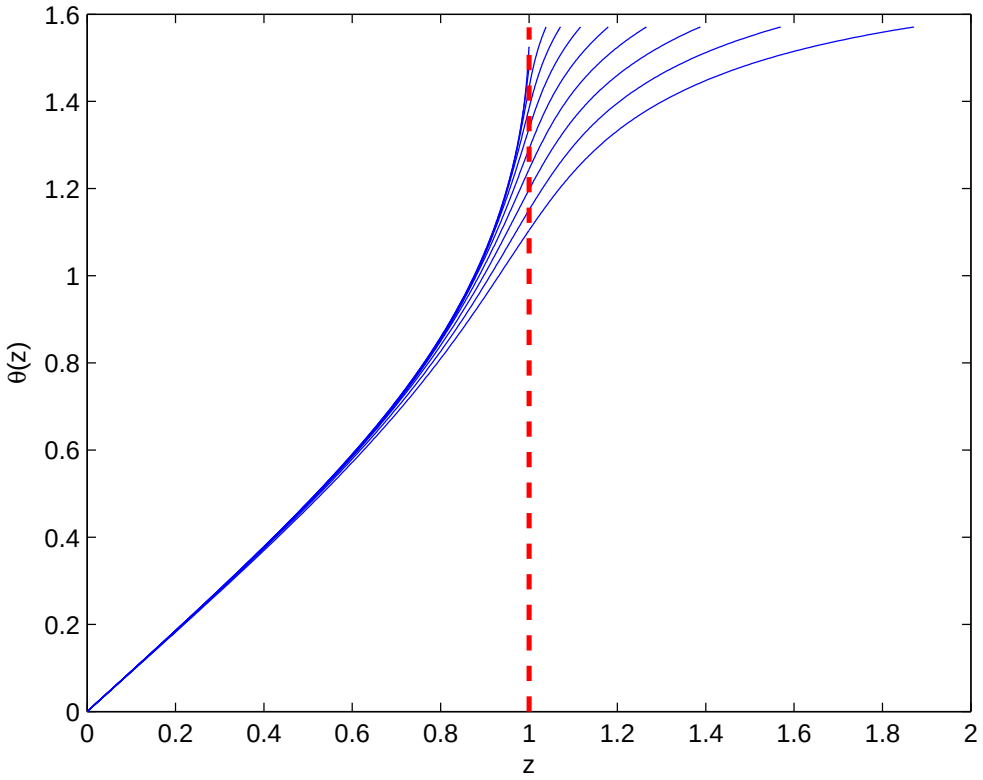

Figure 5.5: Static D7-brane embeddings in EF coordinates continued behind the horizon.
The red (dashed) line shows the location of the horizon.

background geometry is always changed first, allowed to come to equilibrium and then the brane moves. Then $\dot{\Theta} \to 0$. Let's look at energy flow an both ends of the brane.

First the $z = z_{\rm end}$ contribution for non-infalling embeddings.

$$\begin{aligned} &- \int dt d^3x d\ldots \sqrt{-g} T^z{}_t \big|_{z=z_{\rm end}} \\ &\quad = \mathcal{N} \int dt \left[\frac{\cos^3\Theta}{z^5} \frac{-z^2(1-b^4z^4)\Theta'\dot{\Theta}}{\sqrt{1+z^2(1-b^4z^4)\Theta'^2}} + \mathcal{O}(\dot{\Theta}^2) \right] \Bigg|_{z=z_{\rm end}} \\ &\quad = \mathcal{N} \int d\Theta \left. \frac{\cos^3\Theta}{z^5} \frac{-z^2(1-b^4z^4)\Theta'}{\sqrt{1+z^2(1-b^4z^4)\Theta'^2}} \right|_{z=z_{\rm end}} = 0 \end{aligned} \tag{5.116}$$

Note that the statement is integrated over static configurations. Let me discuss why this integral is zero. For non-infalling configurations, we know from the equations of motion that $\Theta \sim \pi/2 + a\sqrt{z_{\rm end} - z}$. The singularity in the square root cancels the singularity from $\Theta'(z_{\rm end})$ and $\cos^3 \frac{\pi}{2}$ sets the integrand to 0.

For infalling configurations, (t, z) coordinates is not appropriate. Let's look at the EF coordinates. The energy flow through the horizon is given by equation (5.113), where $z_s = 1/b$. Also note that $\dot{\Theta} \to 0 \implies \partial_v \Theta \to 0$. Then

$$\Delta U_{D7, z=1/b} = \mathcal{N} \int dv d^3x d\ldots \left. \frac{\cos^3\Theta}{z^5} \frac{R^2 z^2 (\partial_v\Theta)^2}{\sqrt{1 - 2R^2z^2\,\partial_v\Theta\,\partial_z\Theta}} \right|_{z=1/b} \sim 0, \tag{5.117}$$

since leading contribution is of order $\mathcal{O}\left((\partial_v\Theta)^2\right)$. Another thing to note is that this quantity is positive, which signals that energy can only flow into the horizon.

How about the tip of the brane inside the horizon? Is there any flow through there? To answer this question we require a definition of energy for the embedding behind the horizon. The Schwarzschild definition of energy cannot be continued

behind the horizon, since the coordinates do not extend there. However, Eddington-Finkelstein definition of energy does. Here the problem of course is that these energies differ since constant t and v surfaces are different. However for static embeddings the energy definition agrees, in the sense that for the part of the embedding outside the horizon the integral of $\sqrt{-g}T^t{}_t$ over a constant t slice equals to the integral of $\sqrt{-g}T^v{}_v$ over a constant v slice. One can then perhaps use $\sqrt{-g}T^v{}_v$ as a definition of energy behind the horizon.we again work in EF coordinates. Another observation that helps this suugestion is that static configurations in Schwarzschild coordinates correspond to static configurations in EF coordinates. In fact, equations of motion in both coordinates look the same for $\dot{\theta} = \partial_v \theta = 0$ case.

We solved the static equations of motion in a power series around the tip of the brane, assuming that θ is regular there,

$$\theta(z) = \frac{\pi}{2} + \sum_{n=1}^{\infty} a_n (z'_{\rm end} - z')^n \tag{5.118}$$

The first six coefficients are fixed by the equation of motion, a_7 is free. As far as we experimented, remaining coefficients can be solved in terms of a_7. Now, what is interesting is, if one looks at the quasistatic flow at the tip

$$\begin{aligned} &- \int dv d^3x d\ldots \sqrt{-g}T^z{}_v\big|_{z=z_{\rm end}} \\ &\quad = \mathcal{N} \int d\Theta \ \frac{\cos^3\Theta}{z^5} \frac{-z^2(1-b^4z^4)\partial_z\Theta}{\sqrt{1+z^2(1-b^4z^4)(\partial_v\Theta)^2}}\bigg|_{z=z_{\rm end}} \\ &\quad = \mathcal{N} \int d\theta \ \left(f(z_{\rm end}, a_7) + \mathcal{O}(z_{\rm zend} - z)\right)\big|_{z=z_{\rm zend}} \end{aligned} \tag{5.119}$$

The function f is complicated, but nevertheless there is a flow! The coeffiecients and the function $f(z_{\rm end}, a_7)$ are listed in an appendix.

Finally, we check the flow at the AdS boundary. Let's look at the energy flow at $z = 0$. The renormalized form was given in equation (5.104).

$$\begin{aligned} &- \int dv d^3x d\ldots \sqrt{-g} T^z{}_{t,\mathrm{ren}}\big|_{z=0} \\ &\quad = -N_f T_{D7} b^4 \Omega_3 \int dt d^3x \left[\frac{1}{3}\dot{\theta}_1\theta_1^3 - 2\dot{\theta}_1\theta_3 - \frac{R^4}{b^2 2}\dot{\theta}_1\ddot{\theta}_1\right] \\ &\quad \approx -N_f T_{D7} b^4 \Omega_3 \int d\theta_1 d^3x \left[\frac{1}{3}\theta_1^3 - 2\theta_3\right] \\ &\quad \approx \int dM d^3x\, C \end{aligned} \tag{5.120}$$

Now let's interpret these results. First of all, we note that the statement for the static U_{D7} is exactly the same as the free energy F. Here we are looking at the embedding in Schwarzschild coordinates and ignoring the embedding inside the horizon, since in Schwarzschild coordinates do not extend beyond the horizon. This is all consistent with the flows we calculated, for quasistic processes the only boundary energy flow to the embedding is at the AdS boundary, and this flow is exactly $CdM = d\mathcal{F}$. There is no flow across the horizon. We also know that

$$U = U_{D7} + U_b. \tag{5.121}$$

where U_b stands for energy in the backreaction. Then for static configurations

$$U = \mathcal{F} + TS = U_{D7} + U_b \implies U_b = TS \qquad U_{D7} = \mathcal{F}. \tag{5.122}$$

So we deduced the energy contribution of the backreaction! Note that during the phase transition T is constant and $\mathcal{F}$ is constant. The change in the energy during the transition is the latent heat. From the equalities above, we see that the latent

heat is totally a bacreaction contribution!

$$L = T\Delta S = \Delta U_b. \tag{5.123}$$

Now, this observation is interesting because one could argue that the increase in the backreaction contribution to the energy, which is totally related to an increase in entropy, therefore the mass of the blackhole should be related to the energy of the embedding behind the horizon. After all, the embedding behind the horizon should increase the energy of the black hole. Similar statements were made in [61]. Our results falsify this statement. First of all, even for embeddings that do not extend beyond the horizon there is a contribution to the energy from the backreaction. We also noted that for quasistatic processes, there is no flow across the horizon. The energy of the brane embedding behind the horizon comes in from the tip. One could interpret this as energy flowing into the brane from the blackhole mass, however to an outside observer this energy is still behind the horizon and this process does not lead to an increase in blackhole mass. The backreaction contribution due to the embedding outside the horizon however is increasing the blackhole area and leading to increased gravitational energy. One consistency check of the above argument would be to calculate the inflow of energy at the tip of the brane and compare it to the energy of the embedding behind the horizon.

5.3 Dynamics of an expanding plasma

One of the great potential advantages of AdS/CFT duality over lattice gauge theory is the possibility of simulating time dependent, non-equilibrium processes in a

strongly gauge theory. An approximate Lorentzian signature solution of Einstein's equations corresponding to an expanding $\mathcal{N}=4$ Yang-Mills plasma found in [57] is, in Fefferman Graham coordinates,

$$ds^2 = \frac{1}{\bar{z}^2}\left[-\frac{\left(1-\frac{e_0}{3}\frac{\bar{z}^4}{\bar{\tau}^{4/3}}\right)^2}{1+\frac{e_0}{3}\frac{\bar{z}^4}{\bar{\tau}^{4/3}}}d\bar{\tau}^2+\left(1+\frac{e_0}{3}\frac{\bar{z}^4}{\bar{\tau}^{4/3}}\right)(\bar{\tau}^2 d\eta^2+dx_\perp^2)\right]+\frac{d\bar{z}^2}{\bar{z}^2}\,, \qquad (5.124)$$

where $\bar{\tau}, \eta, x_\perp$ are the coordinates of the the Yang-Mills theory and of the AdS boundary at $z \to 0$. These are the natural coordinates for a relativistic heavy ion collision where, for a collision along the x^3 axis, $\bar{\tau}^2 \equiv t^2-(x^3)^2$, $\eta = \frac{1}{2}\ln\frac{t-x^3}{t+x^3}$ (the rapidity), and $x_\perp = x^1, x^2$. Homogeneity of the solution in $x_\perp$, as if the initial collision was between pancakes infinitely extended in $x_\perp$, is a reasonable assumption so long as one only considers the mid-rapidity region. The asymptotic $z \to 0$ expansion of the metric yields the expectation value of the Yang-Mills theory stress energy tensor, via $g_{\mu\nu} = g^{(0)}_{\mu\nu} + \bar{z}^4 < T_{\mu\nu} > + \cdots$. The stress energy tensor derived from (5.124) corresponds to a relativistic perfect fluid with boost invariant initial conditions [57], with energy density

$$\varepsilon(\tau) = \frac{e_0}{\tau^{4/3}} \qquad (5.125)$$

The reasoning of [57] in deriving the metric (5.124) was actually motivated by asymptotic behavior of D7-brane embeddings that we discussed above. They noticed that plugging a series expansion to the static equation of motion (5.8) did not fix θ_3. Given a $\theta_1 \sim M/T$, each θ_3 defines a solution, however only one particular θ_3 leads to a non-singular solution, which gives the physical value of the quark condensate. They applied this reasoning to the boundary metric and stress-energy tensor. They found that enforcing non-singularity one ended up with the time dependent metric

(5.124), and the dual stress-energy tensor described Bjorken hydrodynamics [24], whose characteristic result is given by the $\bar{\tau}^{-4/3}$ fall in energy density, equation (5.125).

The metric (5.124) above is actualy the leading term in a late time expansion in terms of a scaling variable $s = \bar{\tau}^{-1/3}$, such that $g_{\mu\nu} = g^{(0)}_{\mu\nu}(s) + \mathcal{O}(\bar{\tau}^{-2/3})$. Other authors calculated higher order terms in this expansion and found that the regularity condition was violated [51]. This turned out to be an artifact of Fefferman-Graham coordinates and was resolved by using Eddington-Finkelstein coordinates [52, 63].

We are heading towards a time-dependent description of a D7-brane in a cooling plasma. As we have found above, branes extend behind the horizon. Therefore, we need to use another metric than (5.124) that is valid through the horizon. We could of course take the metric above and transform it into another set of coordinates. We will take an alternative approach and try to "guess" a metric from phenomenological arguments. Later on, we will relate our metric to (5.124).

5.3.1 Proposed Background

In this section we introduce our proposed background using phenomenological arguments. Later on we compare to the metric of Janik and Peschanski, (5.124), and show that both metrics are related by a coordinate transformation.

Before making our educated guess, let us note that the solution (5.124) closely resembles an AdS-black hole in Fefferman-Graham coordinates,

$$ds^2 = \frac{1}{\bar{z}^2}\left[-\frac{(1-b^4\bar{z}^4/4)^2}{1+b^4\bar{z}^4/4}dt^2 + (1+b^4\bar{z}^4/4)d\vec{x}^2\right] + \frac{d\bar{z}^2}{\bar{z}^2}\,, \tag{5.126}$$

where $d\vec{x}^2$ is replaced with the metric on a constant τ surface in the Yang-Mills theory, $\tau^2 d\eta^2 + d\vec{x}_\perp^2$, and b depends on τ.

We require a Lorentzian signature solution which is valid from the boundary through the horizon. As a starting point consider the metric of a static AdS black hole in another set of coordinates that we have been using all along,

$$ds^2 = \frac{1}{z^2}\left(-(1-b^4z^4)dt^2 + \frac{1}{1-b^4z^4}dz^2 + d\vec{x}^2\right), \tag{5.127}$$

which like the Fefferman-Graham form is valid only outside the horizon. The coordinate transformation that relates both coordinate systems is

$$z = \frac{\bar{z}}{\sqrt{1+b^4\bar{z}^4/4}} \tag{5.128}$$

To avoid this problem, one can first write the static AdS black hole metric as

$$ds^2 = \frac{1}{z^2}\left(-dt_r^2 + (dz - b^2z^2dt_r)^2 + d\vec{x}^2\right) \tag{5.129}$$

where t_r is related to t in (5.127) by[8]

$$t_r = t - \int^z \frac{b^2z'^2}{1-b^4z'^4}dz'\,. \tag{5.130}$$

Being motivated by the analogy between (5.126) and (5.124), we now let b depend on time.

Since b is proportional to the temperature of the Yang-Mills plasma, a naive background dual to an expanding cooling plasma would have b decreasing with time, which can not be viable in the space-time (5.130) since it would give a decreasing

[8]These coordinates are similar to the "river model" or Gullstrand-Painleve coordinates of a Schwarzchild black hole in an asymptotically Minkowski space [42, 91].

horizon area. However, assuming boost invariance, the isentropic surfaces of the expanding plasma are not constant t, but constant $\tau^2 = t^2 - (x^3)^2$, on which the metric is $\tau^2 d\eta^2 + dx_\perp^2$. Thus a more natural guess for the form of the metric is

$$ds^2 = \frac{1}{z^2}\left(-d\tau^2 + (dz - b^2 z^2 d\tau)^2 + \tau^2 d\eta^2 + d\vec{x}_\perp^2\right) . \tag{5.131}$$

This form looks like a AdS black hole solution with horizon moving in the bulk according to $z_h = \tau^{1/3}$. With an abuse of terminology, we call this surface a horizon, even though it needs a lot of work to establish a surface as an event horizon. For slowly varying $b(\tau)$, the volume form on the horizon is

$$\mathcal{A} = b(\tau)^3 \tau d\eta \wedge dx^2 \wedge dx^3. \tag{5.132}$$

It is not clear whether one can assign an entropy to an evolving gravitational background, however if we extend the statement from the static case to the metric above, the volume corresponds to an entropy per unit rapidity per unit transverse area $S(\tau) = b(\tau)^3\tau$, which must increase or remain constant with increasing τ. If the expansion is isentropic, then $b(\tau) \sim \tau^{-1/3}$. The metric (5.131) then agrees with (5.124) for large τ and small z. The metric (5.124) is the leading term in a large τ, small z asymptotic expansion of a solution of Einstein's equations, which is consistent with a perfect fluid in the dual Yang-Mills theory[9]. The advantage of the metric (5.131) which we propose is that it extends through the horizon can therefore be used to study chiral dynamics near the phase transition. While we did not obtain (5.131) by solving Einstein's equations in a controlled expansion, we propose to use it as a simple model in which to study the chiral phase transition. Later in this chapter, we will numerically simulate the evolution of a D7-brane in the proposed background.

[9]Sub-leading corrections to the large τ behavior[56] are consistent with the small shear-viscosity computed by other means in [97].

For the sake of completeness, let us rewrite our proposed metric

$$ds^2 = \frac{1}{z^2}\left[-\left(1-\frac{4e_0}{3}\frac{z^4}{\tau^{4/3}}\right)d\tau^2 - 2\sqrt{\frac{4e_0}{3}}\frac{z^2}{\tau^{2/3}}dzd\tau + dz^2 + \tau^2 d\eta^2 + d\vec{x}_\perp^2\right]. \tag{5.133}$$

Is there a relation between our proposed metric (5.131) and the metric (5.124) of Janik and Peschanski? It is not hard to see that the following change of coordinates

$$z = \bar{z}\frac{1}{\sqrt{1+\bar{s}^4/4}}, \qquad \tau = \bar{\tau}\left(1+\frac{\tau_2(\bar{s})}{\bar{\tau}^{2/3}}\right), \tag{5.134}$$

where $\bar{s} = \left(\frac{4e_0}{3}\right)^{1/4}\bar{z}\bar{\tau}^{-1/3}$ and

$$\tau_2(\bar{s}) = -\left(\frac{4e_0}{3}\right)^{-1/4}\int^s d\bar{s}'\,\frac{\bar{s}'^2}{\left(1+\bar{s}'^4/4\right)^{1/2}\left(1-\bar{s}'^4/4\right)} \tag{5.135}$$

transforms between our proposal and (5.124) to leading order in the $\bar{\tau}^{-2/3}$ expansion of [57].

This suggests that our metric may also be derived from a controlled approximation using equations of general relativity, where the expansion terms are functions of $s \sim z\tau^{-1/3}$ in a series of $\tau^{-2/3}$. This idea is enhanced by the following observation, the Ricci scalar of our proposed metric is

$$R = -20 - \frac{8}{3}\left(\frac{4e_0}{3}\right)^{1/2} z^3\tau^{-5/3} = 20 + \frac{8}{3}\left(\frac{4e_0}{3}\right)^{-1/4}\frac{s^3}{\tau^{2/3}} \tag{5.136}$$

which exactly has the proposed analytic form. Also note that the leading order term is the Ricci scalar of AdS (or AdS black hole) space, which is the only surviving term as $\tau \to \infty$ keeping s constant. This expansion is valid for late times, early τ requires another asymptotic study. Another interesting curvature invariant is $R^{\mu\nu\rho\sigma}R_{\mu\nu\rho\sigma}$,

which is

$$\begin{aligned} R^{\mu\nu\rho\sigma}R_{\mu\nu\rho\sigma} &= 40 + 72\left(\frac{4e_0}{3}\right)^2 \frac{z^8}{\tau^{8/3}} + 32\left(\frac{4e_0}{3}\right)^{\frac{3}{2}} \frac{z^7}{\tau^3} \\ &\quad + \frac{32}{3}\left(\frac{4e_0}{3}\right)^{\frac{1}{2}} \frac{z^3}{\tau^{5/3}} + \frac{64}{9}\frac{4e_0}{3}\frac{z^6}{\tau^{10/3}} \\ &= 40 + 72s^4 + \frac{32}{\tau^{2/3}}\left(\frac{4e_0}{3}\right)^{-\frac{1}{4}}\left(s^7 + \frac{s^3}{3}\right) + \frac{64}{9}\left(\frac{4e_0}{3}\right)^{-\frac{1}{2}} \frac{s^6}{\tau^{4/3}} \end{aligned} \tag{5.137}$$

These two curvature invariants strongly suggest that our metric is an approximante solution to Einstein's equations with a constant negative curvature. After all, this is what the metric of Janik and Peschanski is in their Fefferman-Graham like coordinates. To take this idea further, we conjecture that our metric is the leading term in a series solution of the Einstein's equations of motion with a metric ansatz

$$ds^2 = \frac{1}{z^2}\left[-d\tau^2 + (dz - A(s,\tau)d\tau)^2 + B(s,\tau)\tau^2 d\eta^2 + C(s,\tau)dx_\perp^2\right]. \tag{5.138}$$

We leave the investigation of this idea for future work.

We note that there are two curvature singularities of our metric. One is at $\tau = 0$ and the other one is at $z = \infty$. The $\tau = 0$ singularity does not bother us that much, after all if our metric is to describe the evolution of a $\mathcal{N} = 2$ SYM quark-gluon plasma, that the instant of collision is singular is perfectly reasonable. The singularity at $z = \infty$ is more serious, and we have to show that it is hidden behind a genuine horizon. We leave this for future work.

Now, we have found a gravitational background, let us add D7-branes into the picture.

5.3.2 D7-brane Embeddings: the Dynamic Case

To describe the dynamical passage of a cooling quark-gluon plasma through the chiral phase transition point, we will embed a D7-brane into the geometry described by the metric (5.131). Simulating the evolution of D7-branes in this background is not an easy task. As will be seen below, the equations of motion are extremely nonlinear with very nontrivial dependence on coordinates. Simulations of realistic scenarios will require a serious research in numerical methods and will be attempted elsewhere. Here, we consider a simplified scenario and test to see if the model at hand gives sensible results, both theoretically and numerically. Specifically, we show that a (numerical) solution exists in which the D7-brane pulls out of the horizon, indicating the chiral phase transtion. We will discuss our numerical methods and simplifications in detail, hoping that it will benefit future attempts.

Like the AdS black hole case, the D7-brane is assumed to fill the five dimensional geometry and wrap an S_3 inside the S_5. The brane ends when S_3 shrinks to zero size. The three angular coordinates of S_3 and the five coordinates of the metric (5.131) are chosen to be the parameters that describe the D7-brane embedding. Throughout this section, we will call the time-like direction τ the time. Using the previously given form of the five-sphere metric (5.4), we assume $\phi = 0$ and $\theta = \theta(\tau, z)$. This does not take into account anisotropies formed in the dual plasma, in a more realistic simulation one would consider dependence on $\vec{x}_\perp$ and η. The asymptotic behavior of the $\theta(\tau, z)$ field as $z \to 0$ will be interpreted in the AdS/CFT sense. The quark mass M and chiral condensate C of the dual plasma will again be given by asymptotic behavior of the scalar field, but now they will be time dependent.

We set $e_0 = 4/3$. The induced metric on the D7-brane is

$$\begin{aligned} ds^2 =& \frac{1}{z^2}\left[-(1-\tau^{-\frac{4}{3}}z^4 - z^2\dot{\theta}^2)d\tau^2 + 2(z^2\dot{\theta}\theta' - \tau^{-\frac{2}{3}}z^2)d\tau dz + (1+z^2\theta'^2)dz^2 + \tau^2 d\eta^2 + d\vec{x}_\perp^2\right] \\ &+ \cos^2\theta dS_3^2. \end{aligned} \tag{5.139}$$

The D7-brane action, up to some normalization factor is,

$$S_{D7} = \int dz d\tau \, \frac{\tau}{z^5}\cos^3\theta \sqrt{1 + z^2\theta'^2\left(1-\tau^{-\frac{4}{3}}z^4\right) - z^2\dot{\theta}^2 - 2\tau^{-\frac{2}{3}}z^4\theta'\dot{\theta}}. \tag{5.140}$$

The equation of motion, after some simplifications, becomes

$$\begin{aligned} &3\tau^3 z^2\ddot{\theta} + 3\tau^3 z^4\ddot{\theta}\theta'^2 + \left(3\tau^{5/3}z^6 - 3\tau^3 z^2\right)\theta'' + 3\tau^3 z^4\dot{\theta}^2\theta'' + \left(3\tau^2 z^2 - 3\tau^{7/3}z^3\right)\dot{\theta} \\ &+ \left(3\tau^{5/3}z^5 + \tau^{4/3}z^4 + 9\tau^3 z\right)\theta' + \left(6\tau^{7/3}z^5 - 3\tau^2 z^4\right)\dot{\theta}^3 \\ &+ \left(6\tau^{1/3}z^{11} - 3z^{10} - 18\tau^{5/3}z^7 + \tau^{4/3}z^6 + 12\tau^3 z^3\right)\theta'^3 + \left(18\tau^{5/3}z^7 - 9\tau^{4/3}z^6 - 12\tau^3 z^3\right)\dot{\theta}^2\theta' \\ &+ \left(18\tau z^9 - 9\tau^{2/3}z^8 - 36\tau^{7/3}z^5 + 3\tau^2 z^4\right)\dot{\theta}\theta'^2 + 6\tau^{7/3}z^4\dot{\theta}' - 6\tau^3 z^4\dot{\theta}\theta'\dot{\theta}' \\ &- 9\tau^3\tan\theta + 9\tau^3 z^2\dot{\theta}^2\tan\theta + 18\tau^{7/3}z^4\dot{\theta}\theta'\tan\theta + \left(9\tau^{5/3}z^6 - 9\tau^3 z^2\right)\theta'^2\tan\theta = 0. \end{aligned} \tag{5.141}$$

This is a second order nonlinear partial differential equation. Polynomials of derivatives to third order appear, the tangent of θ contains polynomials of θ to all orders. The coefficients are both space and time dependent. We assume that the Cauchy problem is well-defined for this equation, in the sense that for some set of initial conditions defined on a space-like hypersurface, the equation will have a unique solution for the causal future. One should not expect this statement to hold for every initial condition, we propose consistency requirements on the initial condition below.

In the considered scenario, an embedding of the D7-brane is specified on an initial time slice. This embedding is chosen to be an infalling one, corresponding to the

high temperature, chiral symmetric phase. As the static D7-brane embedding in Lorentzian signature AdS black hole background, considered D7-brane embeddings will end at some point inside the horizon. Furthermore, boundary conditions are set at the boundary of the space at $z = 0$, the necessity of this will be apparent below. Then the embedding is iterated in time, during which the plasma is cooling. Geometrically, this corresponds to the horizon moving away from the boundary. We expect to see the D7-brane embedding to be "pulling out" of the horizon, through the mechanism discussed above, and at some point becoming non-infalling. This will be interpreted as the dynamical passage through the chiral phase transition.

We start by writing equation (5.141) in first order form. After many trials, we found the following form to be numerically more stable. First we define the variables,

$$u = \dot{\theta}, \qquad v = \theta', \tag{5.142}$$

and coefficient functions

$$\begin{aligned}
a &= 3\tau^3 z^2 + 3\tau^3 z^4 v^2, \\
b &= 6\tau^{7/3} z^4 - 6\tau^3 z^4 uv, \\
c &= 3\tau^{5/3} z^6 - 3\tau^3 z^2 + 3\tau^3 z^4 u^2, \\
d &= \left(3\tau^2 z^2 - 3\tau^{7/3} z^3\right) u + \left(3\tau^{5/3} z^5 + \tau^{4/3} z^4 + 9\tau^3 z\right) v \\
&\quad + \left(6\tau^{7/3} z^5 - 3\tau^2 z^4\right) u^3 + \left(6\tau^{1/3} z^{11} - 3z^{10} - 18\tau^{5/3} z^7 + \tau^{4/3} z^6 + 12\tau^3 z^3\right) v^3 \\
&\quad + \left(18\tau z^9 - 9\tau^{2/3} z^8 - 36\tau^{7/3} z^5 + 3\tau^2 z^4\right) uv^2 + \left(18\tau^{5/3} z^7 - 9\tau^{4/3} z^6 - 12\tau^3 z^3\right) u^2 v \\
&\quad - 9\tau^3 \tan\theta + 9\tau^3 z^2 u^2 \tan\theta + 18\tau^{7/3} z^4 uv \tan\theta + \left(9\tau^{5/3} z^6 - 9\tau^3 z^2\right) v^2 \tan\theta.
\end{aligned} \tag{5.143}$$

Then, equation of motion (5.141) can be written as

$$\begin{bmatrix} \dot{\theta} \\ \dot{u} \\ \dot{v} \end{bmatrix} + \begin{bmatrix} -u/v & 0 & 0 \\ d/(va) & b/a & c/a \\ 0 & -1 & 0 \end{bmatrix} \begin{bmatrix} \theta' \\ u' \\ v' \end{bmatrix} = \mathbf{0}. \tag{5.144}$$

Written in this form the equation is quasi-linear with no source term. The first component equation merely states a choice of integrating θ, it actually is a constraint equation. Through trial and error we found the above form to be numerically more stable. The second and the third component equations contain the real information of the equation of motion, they relate the second derivatives of θ. To classify this system as a hyperbolic, an elliptic or a parabolic system of equations, one has to solve for the eigenvalues and eigenvectors of the 3-by-3 matrix appearing on the left of equation 5.144, [26]. This matrix depends on the solution itself, as well as independent variables, therefore it is not possible to do a classification before obtaining a solution, which is crucial in posing the correct problem and choosing the numerical method. On the other hand, the physics of the problem asks for a hyperbolic equation, in which the information of the inital time embedding determines the embedding in later times (boundary conditions will also be needed as will be discussed below). Therefore, we assume that the equation is hyperbolic. This choice puts strict consistency conditions to the numerical solution. At every point in space and time, the 3-by-3 matrix appearing on the left of equation (5.144) should have real eigenvalues (characteristic velocities) with linearly independendent eigenvectors. The physics of the problem tightens this restriction. Within the horizon, we expect the information flow to be only in positive z direction pointing towards the singularity. Going back to the equation (5.144), we see that one of the eigenvalues of the 3-by-3 matrix appearing on the left will always be given by $-u/v$, corresponding to the constraint equation. The remaining two eigenvalues $(b/2a \pm \sqrt{b^2 - 4ac}/2a)$ come

form the second and the third equations, which relate the second derivatives of θ. These eigenvalues then must be real and inside the horizon they must be positive. In terms of the variables defined above, the reality condition for eigenvalues is (for real θ, u and v)

$$b^2 - 4ac > 0 \implies -z^6v^2 - 2\tau^{\frac{2}{3}}z^4uv + \tau^{\frac{4}{3}}(1 - u^2z^2 + v^2z^2) > 0. \tag{5.145}$$

For the positivity constraint, the additional condition is

$$ac > 0 \implies z^4 + \tau^{\frac{4}{3}}(-1 + z^2u^2) > 0. \tag{5.146}$$

In simplifying these equations, we made use of the positivity of τ and z. Recalling that the horizon is located at $z_h(\tau) = \tau^{1/3}$, the equation (5.146) is automatically satisfied inside the horizon for any embedding. This confirms our expectations. These restrictions should be taken into account when choosing an initial condition.

We use a simple first order upwind scheme to integrate the set of equations (5.144). Upwind scheme is a method for solving hyperbolic partial differential equations. In this scheme, the partial differential equation is discretized by using differencing biased in the direction determined by the sign of the characteristic speeds. The direction of propagation of information is taken into account through this mechanism. We refer the reader to literature for theoretical results on the upwind scheme. We found the discussions in [26, 48, 79, 83, 71, 4] to be very useful. Here we briefly describe the method, using the notation of [79].

Given a system of first order partial differential equations in two independent

variables,

$$\frac{\partial \mathbf{y}}{\partial t} + \mathbf{B}(t, x, \mathbf{y}) \frac{\partial \mathbf{y}}{\partial x} = \mathbf{f}(t, x, \mathbf{y}), \tag{5.147}$$

one first introduces a grid over the domain $[0, \infty) \times [0, \infty)$ with grid points (t^n, x_j) defined by

$$x_j := j\Delta x \qquad (j = 0, 1, 2, \ldots), \qquad t^n = \sum_{k=0}^{n-1} \Delta t^k \qquad (n = 0, 1, 2, \ldots). \tag{5.148}$$

with Δx the spatial grid size and Δt^k the time step. The time step is adaptive, it will be defined at each step by the Courant-Friedrichs-Lewy (CFL) condition as discussed below. The matrix $\mathbf{B}$ is assumed to have real eigenvalues and a complete set of eigenvectors at every point over the domain for the particular $\mathbf{y}$ in question; this it the condition of hyperbolicity. The upwind scheme is given by

$$\frac{1}{\Delta t^n}(\mathbf{y}_j^{n+1} - \mathbf{y}_j^n) + \frac{1}{\Delta x}\mathbf{B}_j^{n,+}(\mathbf{y}_j^n - \mathbf{y}_{j-1}^n) + \frac{1}{\Delta x}\mathbf{B}_j^{n,-}(\mathbf{y}_{j+1}^n - \mathbf{y}_j^n) = \mathbf{f}(x_j, t^n, \mathbf{y}_j^n). \tag{5.149}$$

The scheme is solved iteratively for $\mathbf{y}_j^{n+1}$. The matrices $\mathbf{B}_j^{n,+}$ and $\mathbf{B}_j^{n,-}$ are defined locally by

$$\mathbf{B}_j^{n,+} := \mathbf{S}_j^n \mathbf{\Lambda}_j^{n,+} (\mathbf{S}_j^n)^{-1}, \qquad \mathbf{B}_j^{n,-} := \mathbf{S}_j^n \mathbf{\Lambda}_j^{n,-} (\mathbf{S}_j^n)^{-1}. \tag{5.150}$$

$\mathbf{S}_j^n$ is the similarity transformation matrix that consists of the local eigenvectors of $\mathbf{B}_j^n$ as its columns, i.e. if $\mathbf{b}_{j,1}^n$, $\mathbf{b}_{j,2}^n$, and $\mathbf{b}_{j,3}^n$ are a complete set of (right) eigenvectors of $\mathbf{B}_j^n$ for the grid point (t^n, x_j) and the value of the function $\mathbf{y}$ at the grid point, $\mathbf{y}_j^n$, then $\mathbf{S}_j^n = (\mathbf{b}_{j,1}^n, \mathbf{b}_{j,2}^n, \mathbf{b}_{j,3}^n)$. $\mathbf{\Lambda}_j^{n,+}$ and $\mathbf{\Lambda}_j^{n,-}$ are diagonal matrices that contain the positive and negative eigenvalues of the matrix $\mathbf{B}_j^n$ as diagonal elements respectively, i.e. if $\lambda_{j,1}^n$, $\lambda_{j,2}^n$ and $\lambda_{j,3}^n$ are the eigenvectors corresponding to $\mathbf{b}_{j,1}^n$, $\mathbf{b}_{j,2}^n$, and $\mathbf{b}_{j,3}^n$, then

$(\mathbf{\Lambda}_j^{n,+})_{ii} = \max(\lambda_{j,i}^n, 0)$ and $(\mathbf{\Lambda}_j^{n,-})_{ii} = \min(\lambda_{j,i}^n, 0)$, $i = 1, 2, 3$. $\mathbf{B}_j^{n,+}$ and $\mathbf{B}_j^{n,-}$ give a decomposition of $\mathbf{B}_j^n$, $\mathbf{B}_j^n = \mathbf{B}_j^{n,+} + \mathbf{B}_j^{n,-}$. We note again that this decomposition has to be done at every grid point and will be different for different functions $\mathbf{y}$.

The eigenvalues $\lambda_{j,1}^n$, $\lambda_{j,2}^n$ and $\lambda_{j,3}^n$ are the local characteristic velocities of the system, they describe the direction and speed of information flow. The upwind scheme (5.149) uses a backward differencing to propagate information in the positive direction and a forward differencing to propagate information in the negative direction. The time stepping should be adaptively chosen by the CFL condition,

$$\max_{j,i}(\lambda_{j,i}^n)\frac{\Delta t^n}{\Delta x} < 1, \tag{5.151}$$

for stability [26, 48, 79, 83, 71, 4]. This condition prevents acausal information flow on the grid.

The upwind scheme is dissipative. There are many other schemes with better accuracy, but their implementation to the equation at hand is very difficult due to the nonlinearity and parameter dependent coefficients.

Having described the scheme, we now discuss the initial and boundary conditions required for solving the system of equations (5.144). Aside from specifying a D7-brane embedding at some initial time, the scheme (5.149) requires boundary conditions at the boundaries of the domain to propagate information. This is not just a numerical necessity, the boundary conditions carry information from the causal past of the solution that is not included in the initial condition. Recall that we consider the scenario in which the initial condition is an infalling D7-brane embedding. Initially the D7-brane extends from the boundary of the space given by the hypersurface $z = 0$ to its endpoint z_{end} which is inside the horizon. One needs to set

boundary conditions at the spatial boundary, $z = 0$, to accommodate for incoming information. The functions θ, u and v will be set at $z = 0$ and this will be fed to the backward differenced term in the upwind scheme (5.149) at the first grid point to be propagated in the positive direction. For our numerical simulation, the boundary condition at $z = 0$ is chosen to be

$$\theta(\tau, 0) = 0, \qquad u(\tau, 0) = 0, \qquad v(\tau, 0) = M, \tag{5.152}$$

where M is a constant quark mass up to some normalization. For realistic scenarios, one may need to consider a time dependent quark mass [98].

At the other hand of the brane, we do not expect a need for a boundary condition. In the expected evolution, the endpoint of the brane moves towards to boundary of space, "pulling out" of the horizon. The location of the endpoint changes over time, therefore the domain of the solution that we are looking for is dynamically being updated at every time step. We expect the endpoint of the brane to be determined only by the brane configuration in the previous time step. For infalling embeddings, due to our expectancy of characteristic speeds being positive inside the horizon there is no numerical necessity for a boundary condition at the endpoint. For a non-infalling embedding, we chose to ignore negative characteristic speeds at the endpoint and only propagate positive characteristic speeds. We suggest an alternative approach below, see footnote [10]. Even though one does not expect the necessity of a boundary condition at the endpoint, there is a natural consistency condition that comes from the equation of motion (5.141). The brane ends when S_3 shrinks to zero size. An inspection of the induced metric on the brane (5.139) shows that this happens when $\theta = \pi/2$. The point at which the brane ends evolves in time,

$z_{\rm end} = z_{\rm end}(\tau)$. However, $\theta(\tau, z_{end}(\tau)) = \pi/2$. Then

$$\left.\frac{d\theta}{d\tau}\right|_{z=z_{\rm end}(\tau)} = \theta'_{\rm end}\dot{z}_{\rm end} + \dot{\theta}_{\rm end} = 0, \tag{5.153}$$

where

$$\theta'_{\rm end} = \left.\frac{\partial\theta}{\partial z}\right|_{z=z_{\rm end}(\tau)}, \qquad \dot{\theta}_{\rm end} = \left.\frac{\partial\theta}{\partial\tau}\right|_{z=z_{\rm end}(\tau)}. \tag{5.154}$$

For an infalling embedding, we expect θ and its first and second derivatives to be nonsingular at the endpoint. The most singular terms of the equation of motion (5.141) are those that are proportional to $\tan\theta$. Requiring the coefficients of the most singular terms to cancel leads to

$$1 = z_{end}^2\dot{\theta}_{end}^2 + \tau^{-4/3}z_{end}^6{\theta'}_{end}^2 + 2\tau^{-2/3}z_{end}^4\dot{\theta}_{end}{\theta'}_{end} - z_{end}^2{\theta'}_{end}^2. \tag{5.155}$$

Combining these equations, one can solve for $z_{\rm end}(\tau)$,

$$\dot{z}_{end} = -\tau^{-2/3}z_{end}^2 \pm \sqrt{1 + \frac{1}{{\theta'}_{end}^2 z_{end}^2}}. \tag{5.156}$$

We use equations (5.155) and (5.156) to check the consistency of our numerical solution. For a non-infalling embedding θ is expected to be singular, so that the brane closes smoothly. To get a constraint on the endpoint one needs to know the exact asymptotic behavior of the embedding[10].

[10]Being inspired by the AdS black hole case, we propose the following form of the solution, for z near $z_{\rm end}$ for an non-infalling embedding

$$\theta(\tau, z) \sim \frac{\pi}{2} - (z_{\rm end}(\tau) - z)^{1/2}\sum_{n=0}\alpha_n(\tau)(z_{\rm end}(\tau) - z)^n \tag{5.157}$$

Although we have not used this proposal in our numerical simulations, in further studies this form could be used to propagate the endpoint by solving the equation of motion order by order for z near $z_{\rm end}$.

We choose an infalling embedding as an initial condition. This choice is subject to consistency conditions. First of all, it should be compatible with the boundary conditions. Moreover, it should obey the restrictions on characteristic velocities discussed above. The eigenvalues of the 3-by-3 matrix appearing on the left of equation (5.144) should have real eigenvalues with linearly independendent eigenvectors at every point on the grid, which requires the condition (5.145). The condition of two of the three eigenvalues corresponding to second and third equations of the system (5.144) being positive inside the horizon is automatically satisfied, as discussed below equation (5.146). The asymptotics of the embedding near the endpoint should satisy (5.155). It is not trivial to find an initial condition that satisfies all these properties. Our starting point was noticing that when $u = 0$, the constraint equation (5.155) on the brane endpoint is satisfied by an infalling D7-brane embedding in an AdS black hole background with static horizon at $z_h = \tau_i^{1/3}$. We chose such an embedding, which sets θ and v at the initial time slice, and $u = 0$ as initial conditions. For consistency, one should look for a D7-brane embedding with quark mass that is equal to the boundary condition for the whole evolution (which we chose to be static). This is numerically done by a shooting method. Moreover, we numerically verified that the reality of characteristic velocities condition (5.145) is also satisfied for this initial condition choice. Figures 5.6, 5.7 and 5.8 shows the results for a sample simulation. Some additional special techniques were used to stabilize the system, which are described below the figure. We were able to numerically integrate the D7-brane evolution into a non-infalling configuration. After some point numerical instabilites were not controllable, whose initial stages can be seen in the figure.

In the figures, the evolution starts from an infalling configuration at $\tau_i = 100$ and proceeds to a non-infalling configuration. The horizon crosses the endpoint at $\tau = 110.6280$. After some point numerical instabilities lead to uncontrollable

oscillations and the numerical integration fails. The initial stages of the formation of these oscillations can be seen in the top figure. The quark mass is set to $M = 0.1942$. Grid spacing in the z coordinate is $\Delta z = 0.05$. Numerical integration is done until the last point of the D7-brane that is on a grid point. Adaptive time steps are chosen to be 0.001 times the maximum time step allowed by the CFL condition (5.151). In the top and bottom figures we only present1 time step in every 1000 steps. The embedding lines become denser where the numerical integration proceeds by smaller step sizes. This was not sufficient to prevent the instability that discretization induced on the system. Unstable oscillations grew quickly in time and failed the numerical integration. To prevent this we introduced a sixth order sponge filter, see [4] for a discussion of sponge filters. Near $z = 0$, we used a polynomial fit to smooth out the unstable oscillations. To check the accuracy of the numerical solution, we checked the condition on the endpoint (5.155) at every time step at the last grid point for the infalling configuration. The absolute value of the difference between the left side and the right side was always much below the spatial grid size. The error increased when the grid point got away from the actual endpoint. For the infalling configuration, the absolute value of the error when averaged over all time steps was 0.0022, which we interpreted as a confirmation of the numerical result.

5.4 Discussion of Results

In this chapter, we discussed the high temperature first order phase transition of large N_c, $\mathcal{N} = \in$ SYM theory using the methods of AdS/CFT correspondence. We focused on contribution of subleading order in N_c expansion, whose AdS/CFT descripton involves inserting a probe D7-brane to specific gravitational backgrounds. We reviewed calculation of thermodynamic quantities using gravitational calcula-

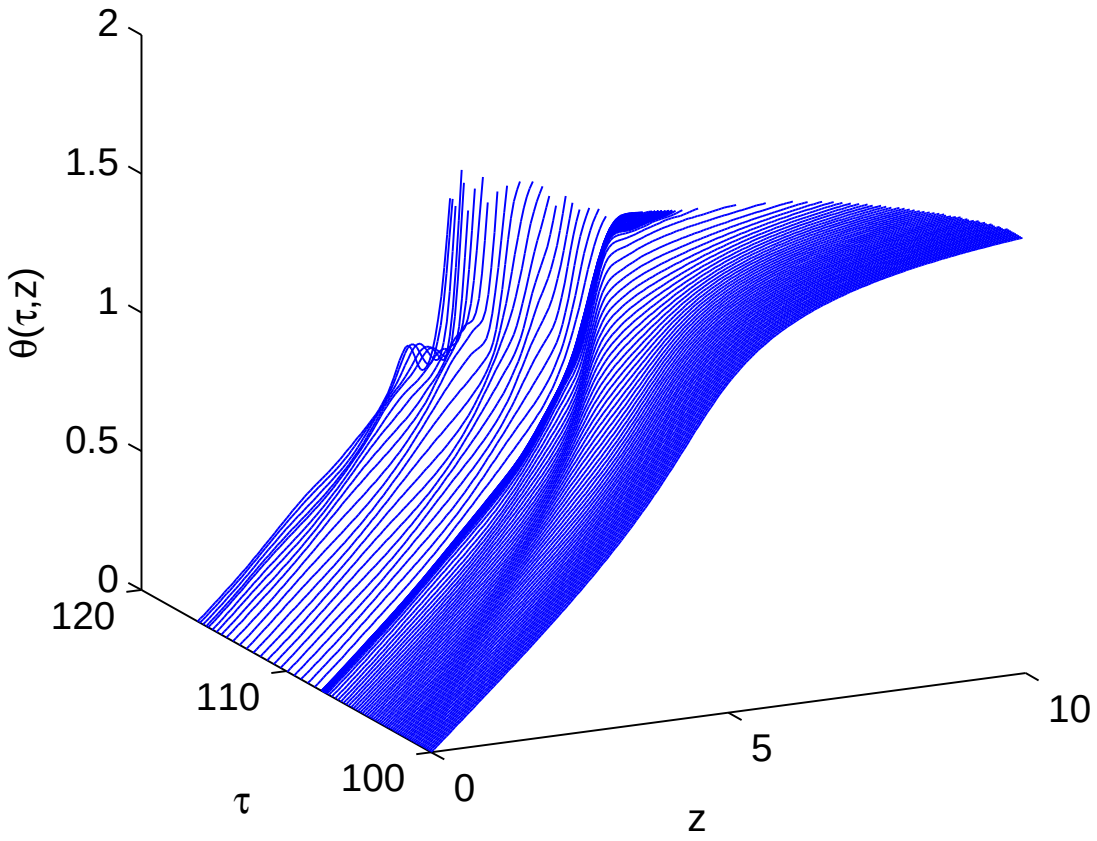

Figure 5.6: The evolution of a D7-brane with the inital condition discussed in the text.

tions. We first identified that the order N_f/N_c contribution to the thermodynamic internal energy of large N_c, $\mathcal{N} = \in$ SYM theory cannot be calculated only using the stress-energy tensor of the probe brane. The missing contribution is due to the back-reaction of the brane. We identified the latent heat of the first order phase transition to be purely of this sort. While doing this, we introduced methods to renormalize the stress-energy tensor of the D7-brane in a consistent way.

Then we looked at the dynamical evolution of a quark-gluon plasma. We first discussed the gravitational background, which corresponds to the leading order in

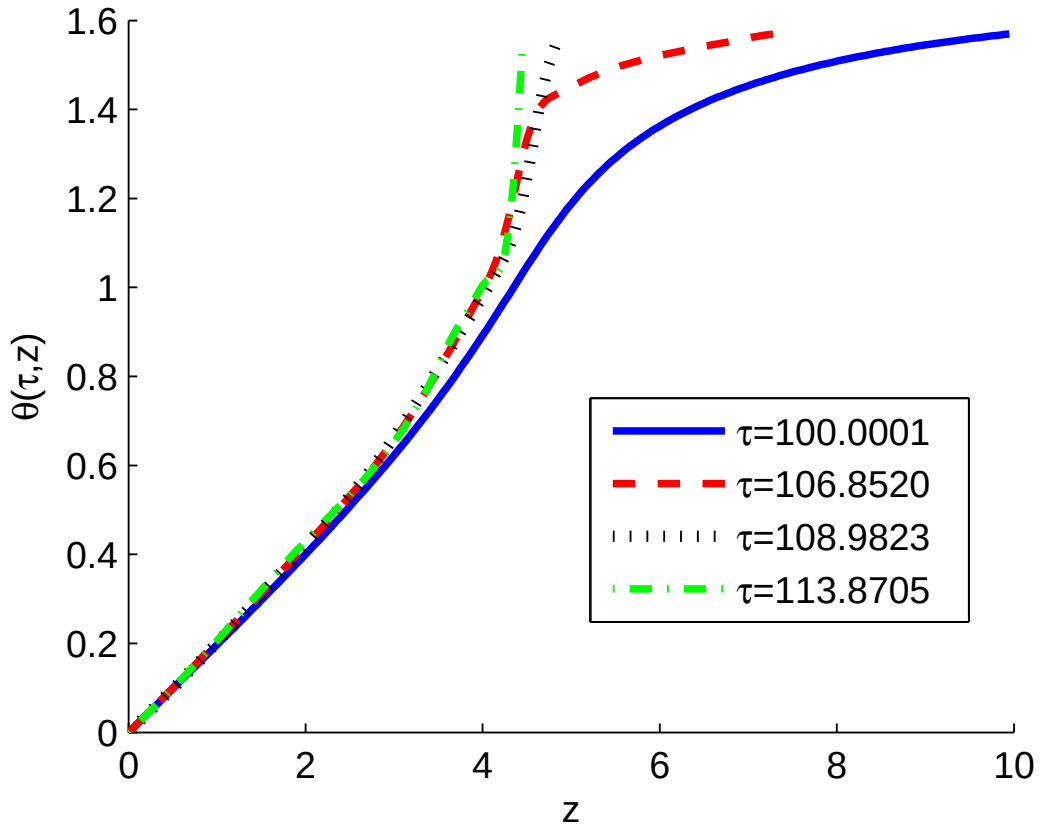

Figure 5.7: The embedding at different time slices.

the dual large N_c expansion. Even though we are working with a $\mathcal{N} = \in$ SYM theory, we chose our description to be as close to the experiment done in RHIC as possible. Using phenomenological observations from RHIC experiments, we proposed a gravitational background, which had several advantages over the previously proposed metric of Janik and Peschanski, [57]. Later on, we discovered that our metric is related to Janik and Peschanski metric by a coordinate transformation.

Using our background, we attacked the dynamical passage of a quark-gluon plasma through the chiral phase transition point. We showed numerically that our proposed time dependent background (5.131) leads to a topology changing D7-brane evolution. Simulation of realistic scenarios require much more work, with newer

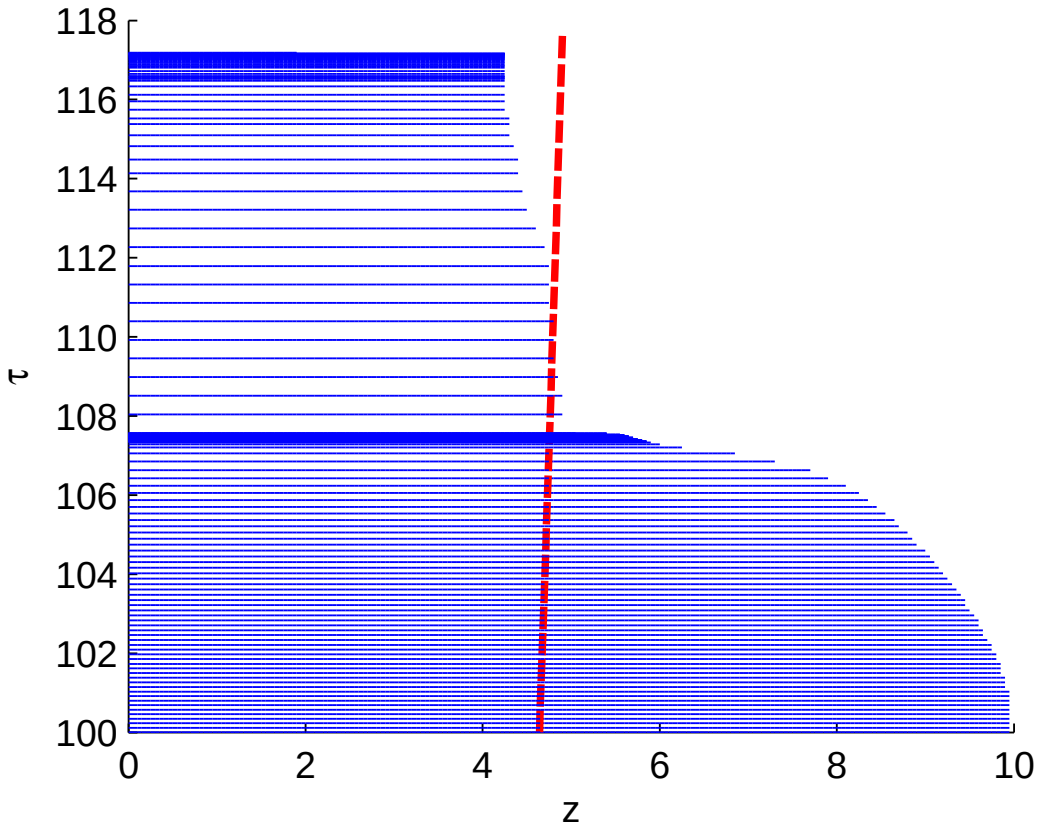

Figure 5.8: The same evolution with θ direction pointing outside the paper plane. In this figure, the red (dashed) line shows the evolution of the black hole horizon.

schemes, better instability controls, different initial[11] and boundary conditions that

[11] Another set of initial conditions could be given by setting $\dot{\theta}$, $\ddot{\theta}$ and $\dot{\theta}'$ to zero at some initial time τ_i, which we call the "static initial condition" (although the embedding appears static only momentarily and evolves in time), and solve for the embedding at this constant time slice. The equation of motion (5.141) gives

$$\theta'' = \frac{3\tan\theta}{z^2\left(\tau_i^{-4/3}z^4-1\right)} - \frac{\tau_i^{-4/3}z^4+3}{z\left(\tau_i^{-4/3}z^4-1\right)}\theta' - \frac{\tau_i^{-5/3}z^2}{3\left(\tau_i^{-4/3}z^4-1\right)}\theta' - 3\tan\theta\theta'^2 + 2z(2-\tau_i^{-4/3}z^4)\theta'^3 + \frac{3z^8-\tau_i^{4/3}z^4}{3\tau_i^{5/3}z^4-3\tau_i^3}\theta'^3. \tag{5.158}$$

This is to be contrasted with AdS black hole embedding (5.8). One sees that third and the sixth terms on the right hand side are new. Let's note that in the $z \to z_{\rm end}$ limit, the static initial condition does satisfy the consistency condition (5.155). This actually is a redundant statement since the static embedding is solved from the equation of motion anyway, as equation (5.155) also is. To find an infalling solution for this equation, we follow the same line of argument as in the AdS black hole case. The horizon is at $z_h(\tau) = \tau^{1/3}$. We choose a value for θ at the horizon that is less than $\pi/2$, $\theta_0 < \pi/2$. Then, from the equation above, one can solve for the condition on θ'_0

corresponds to physical situations and more independent variables in the embedding to accomodate for anisotropies.

Several things are needed to be done to complete the work presented in this section. One should first rigorously show that our proposed metric is the leading term of a controlled approximation to the Einstein's equations with a negative constant curvature. Next, one should show that there is a horizon analytically. For our time-dependent D7-brane action formed of our proposed action, renormalization should be discussed, which will lead into the precise definition of the quark condensate. Using this quark-condensate one can gain more insight into the nature of the dynamical passage of the dual plasma through the chiral phase transition point.

---

requiring the coeffiecients of the leading order singularity to cancel,

$$\frac{2}{3}\tau_i^{-1/3}\theta_0'^3 - \frac{1}{3}\tau_i^{-1}\theta_0' - 4\tau_i^{-1/3}\theta_0' + 3\tau_i^{-2/3}\tan\theta_0 = 0. \tag{5.159}$$

For an infalling embedding, we expect to have a positive slope at the horizon. The reality and positivity of roots depend on particular τ_i. As in the AdS black hole case, the equation (5.158) is numerically integrated both towards the singularity and the boundary starting from the horizon with boundary conditions θ_0 and θ_0'. We found that not all positive real roots of equation (5.159) led to boundary conditions that were numerically integrable. We tried this setting for a various θ_0 and τ_i and verified numerically the existence of initial condition that satisfies the reality condition of characteristic velocities (5.145). The time evolution of the corresponding initial conditions also led to topology changing D7-brane evolutions, satisfying the condition on the endpoint evolution (5.155) within numerical accuracy.

Appendix A

More on Complex Langevin Equations

Here we ask the following question: Which stochastic processes will have stationary distributions that satisfy the Schwinger-Dyson equations for the quantum field theory with action $S(\phi)$? If we can identify those processes, we can use them to study the solution set. We will first look at a general complex Langevin equation.

A.1 General Complex Langevin Equation

Consider a general complex Langevin equation:

$$d\phi(\tau) = -G(\phi)d\tau + \eta(\phi)dw(\tau), \tag{A.1}$$

where $dw(\tau)$ is a usual Brownian motion with the normalization

$$\langle dw(\tau)\rangle = 0, \qquad \langle dw(\tau)dw(\tau)\rangle = 2d\tau, \qquad \langle dw(\tau_1)dw(\tau_2)\rangle = 0 \quad (\tau_1 \neq \tau_2), \tag{A.2}$$

and $G(\phi)$ is a general complex function of the random variable $\phi(\tau)$. One can analyze this system by decomposing it to its real and imaginary parts:

$$\begin{aligned} d\phi_R(\tau) &= -G_R(\phi_R, \phi_I)d\tau + \eta_R(\phi_R, \phi_I)dw(\tau), \\ d\phi_I(\tau) &= -G_I(\phi_R, \phi_I)d\tau + \eta_I(\phi_R, \phi_I)dw(\tau), \end{aligned} \tag{A.3}$$

where $\phi(\tau) = \phi_R(\tau) + i\phi_I(\tau)$ and etc. This is a real stochastic system with two independent random variables but one Brownian motion.

In the following, we will use an identity for stochastic processes that is called

Ito's lemma, see e.g. [34]. Consider a general Langevin system

$$dq_i(t) = a_i(q,t)dt + \sum_j b_{ij}(q,t)dw_j(t). \tag{A.4}$$

Then the following identity holds:

$$dH[q(t)] = \sum_i \frac{\partial H}{\partial q_i(t)} \left\{ a_i(q,t)dt + \sum_j b_{ij}(q,t)dw_j(t) \right\} + \sum_{i,j,k} \frac{\partial^2 H}{\partial q_i(t)\partial q_j(t)} b_{ik}(q,t)b_{jk}(q,t)dt. \tag{A.5}$$

An informal proof of this can be given by noting that $dw \sim dt^{\frac{1}{2}}$. See wikipedia page for Ito's Lemma or [86].

This is useful in deriving the Fokker-Planck equation. Taking the expectation values of both sides, we obtain

$$d\left\langle H[q(t)]\right\rangle = \sum_i \left\langle \frac{\partial H}{\partial q_i(t)} a_i(t) \right\rangle dt + \sum_{i,j,k} \left\langle \frac{\partial^2 H}{\partial q_i(t)\partial q_j(t)} b_{ik}(t)b_{jk}(t) \right\rangle dt. \tag{A.6}$$

Dividing both sides by dt will give the time evolution, analogue of equation (2.21).

Now, using equation (A.6), we can write down the time evolution for the general Langevin process, i.e. equation (A.3)

$$\frac{d}{d\tau}\left\langle H[\phi_R(\tau),\phi_I(\tau)]\right\rangle = \left\langle -\sum_{\alpha=R,I} \frac{\partial H}{\partial \phi_\alpha(\tau)} G_\alpha + \sum_{\substack{\alpha=R,I \\ \beta=R,I}} \frac{\partial^2 H}{\partial \phi_\alpha(\tau)\partial \phi_\beta(\tau)} \eta_\alpha \eta_\beta \right\rangle \tag{A.7}$$

Now consider an analytic function $F(\phi)$

$$F(\phi = \phi_R + i\phi_I) = F_R(\phi_R,\phi_I) + iF_I(\phi_R,\phi_I). \tag{A.8}$$

F_R and F_I satisy equation (A.7) individually. Then:

$$\begin{aligned}\frac{d}{d\tau}\langle F[\phi(\tau)]\rangle &= \frac{d}{d\tau}\langle F_R[\phi_R(\tau),\phi_I(\tau)]\rangle + i\frac{d}{d\tau}\langle F_I[\phi_R(\tau),\phi_I(\tau)]\rangle \\ &= \left\langle -\sum_{\alpha=R,I}\frac{\partial F_R}{\partial\phi_\alpha(\tau)}G_\alpha + \sum_{\substack{\alpha=R,I\\ \beta=R,I}}\frac{\partial^2 F_R}{\partial\phi_\alpha(\tau)\partial\phi_\beta(\tau)}\eta_\alpha\eta_\beta\right\rangle \\ &\quad + i\left\langle -\sum_{\alpha=R,I}\frac{\partial F_I}{\partial\phi_\alpha(\tau)}G_\alpha + \sum_{\substack{\alpha=R,I\\ \beta=R,I}}\frac{\partial^2 F_I}{\partial\phi_\alpha(\tau)\partial\phi_\beta(\tau)}\eta_\alpha\eta_\beta\right\rangle \quad \text{(A.9)}\end{aligned}$$

Before simplifying this expression, we review Cauchy-Riemann equations of complex analysis.

Consider the analytic function of equation (A.8)

$$F(\phi) = F_R(\phi_R,\phi_I) + iF_I(\phi_R,\phi_I). \quad \text{(A.10)}$$

Cauchy-Riemann equations state that since F is analytic the following conditions hold:

$$\frac{\partial F_R}{\partial\phi_R} = \frac{\partial F_I}{\partial\phi_I}, \quad \text{(A.11)}$$

$$\frac{\partial F_I}{\partial\phi_R} = -\frac{\partial F_R}{\partial\phi_I}. \quad \text{(A.12)}$$

Also, $F'(\phi)$ can be written as

$$\begin{aligned}\frac{dF}{d\phi} &= \frac{\partial F_R}{\partial\phi_R} + i\frac{\partial F_I}{\partial\phi_R}, \\ &= \frac{\partial F_I}{\partial\phi_I} - i\frac{\partial F_R}{\partial\phi_I}, \quad \text{(A.13)}\end{aligned}$$

Another result that we will need is the expression for $F''(\phi)$:

$$\begin{aligned}\frac{d^2F}{d\phi^2} &= \frac{d}{d\phi}\left[\frac{\partial F_R}{\partial \phi_R} + i\frac{\partial F_I}{\partial \phi_R}\right] = \frac{\partial^2 F_R}{\partial \phi_R^2} + i\frac{\partial^2 F_I}{\partial \phi_R^2} \\ &= \frac{d}{d\phi}\left[\frac{\partial F_I}{\partial \phi_I} - i\frac{\partial F_R}{\partial \phi_I}\right] = -\frac{\partial^2 F_R}{\partial \phi_I^2} - i\frac{\partial^2 F_I}{\partial \phi_I^2} = -\left[\frac{\partial^2 F_R}{\partial \phi_I^2} + i\frac{\partial^2 F_I}{\partial \phi_I^2}\right] \\ &= \frac{d}{d\phi}\left[\frac{\partial F_I}{\partial \phi_I} - i\frac{\partial F_R}{\partial \phi_I}\right] = \frac{\partial^2 F_I}{\partial \phi_R \partial \phi_I} - i\frac{\partial^2 F_R}{\partial \phi_R \partial \phi_I} \end{aligned} \tag{A.14}$$

Now, time to simplify equation (A.9). Let's look at the first derivative terms:

$$\begin{aligned}-\sum_{\alpha=R,I}\frac{\partial F_R}{\partial \phi_\alpha(\tau)}G_\alpha - i\sum_{\alpha=R,I}\frac{\partial F_I}{\partial \phi_\alpha(\tau)}G_\alpha &= -\left[\frac{\partial F_R}{\partial \phi_R} + i\frac{\partial F_I}{\partial \phi_R}\right]G_R - \left[\frac{\partial F_R}{\partial \phi_I} + i\frac{\partial F_I}{\partial \phi_I}\right]G_I \\ &= -\frac{dF}{d\phi}G_R - i\frac{dF}{d\phi}G_I = -\frac{dF}{d\phi}G, \end{aligned} \tag{A.15}$$

where we used equation (A.13) in the second line. Now the second derivative terms:

$$\begin{aligned}&\sum_{\substack{\alpha=R,I\\ \beta=R,I}}\frac{\partial^2 F_R}{\partial \phi_\alpha(\tau)\partial \phi_\beta(\tau)}\eta_\alpha\eta_\beta + i\sum_{\substack{\alpha=R,I\\ \beta=R,I}}\frac{\partial^2 F_I}{\partial \phi_\alpha(\tau)\partial \phi_\beta(\tau)}\eta_\alpha\eta_\beta \\ &= \left[\frac{\partial^2 F_R}{\partial \phi_R^2} + i\frac{\partial^2 F_I}{\partial \phi_R^2}\right]\eta_R^2 + \left[\frac{\partial^2 F_R}{\partial \phi_I^2} + i\frac{\partial^2 F_I}{\partial \phi_I^2}\right]\eta_I^2 + 2\left[\frac{\partial^2 F_R}{\partial \phi_R \partial \phi_I} + i\frac{\partial^2 F_I}{\partial \phi_R \partial \phi_I}\right]\eta_R\eta_I \\ &= \frac{d^2F}{d\phi^2}\left[\eta_R^2 - \eta_I^2 + 2i\eta_R\eta_I\right]. \end{aligned} \tag{A.16}$$

Now, using equations (A.15) and (A.16)

$$\frac{d}{d\tau}\left\langle F[\phi(\tau)]\right\rangle = \left\langle \frac{d^2F}{d\phi^2}\left[\eta_R^2 - \eta_I^2 + 2i\eta_R\eta_I\right] - \frac{dF}{d\phi}G\right\rangle \tag{A.17}$$

This equation is equal to equation (2.21) only if

$$G = \frac{dS}{d\phi} \tag{A.18}$$

and

$$\eta_R^2 - \eta_I^2 + 2i\eta_R\eta_I = 1. \tag{A.19}$$

Remembering that η_R and η_I are real, the second equation is only satisfied if η_I is zero and $\eta_R = \pm 1$. But this is the original complex Langevin equation, i.e. equation (2.17). The minus sign in front of the Brownian motion does not change the process.

Conclusion: If we include one Brownian motion for a system with two independent random variables, only Langevin process that will converge to Schwinger-Dyson solutions is the one given by equation (2.17). However, this is not enough to recover the whole solution set. Therefore, we need to look at different systems.

A.2 Modified Complex Langevin Equation

Consider a new theory:

$$S_\alpha(\phi) = S(\phi/\alpha) \tag{A.20}$$

The Scwinger-Dyson equation for this new theory will be:

$$\left.\frac{\partial S_\alpha}{\partial \phi}\right|_{\phi=\frac{d}{dj}} Z_\alpha(j) = jZ_\alpha(j), \tag{A.21}$$

where $Z_\alpha(j)$ is the generating function(al) of this new theory.

DEFINITION: Say $Z(j)$ is a normalized generating function(al) for the theory $S(\phi)$, i.e. it satisfies the original Schwinger-Dyson equation

$$\left.\frac{\partial S}{\partial \phi}\right|_{\phi=\frac{d}{dj}} Z(j) = jZ(j), \tag{A.22}$$

and is normalized such that $Z(0) = 1$. We can expand it as follows:

$$Z_(j) = 1 + \sum_{n=1}^{\infty} \frac{\langle \phi^n \rangle}{n!} j^n, \tag{A.23}$$

where $\langle \phi^n \rangle$ are the Green's functions of the theory defined by $S(\phi)$. Now consider a new generating functional defined as follows:

$$Z_{new}(j) = 1 + \sum_{n=1}^{\infty} \frac{\langle \phi^n \rangle_\alpha}{n!} j^n = 1 + \sum_{n=1}^{\infty} \frac{\alpha^n \langle \phi^n \rangle}{n!} j^n, \tag{A.24}$$

where we define

$$\langle \phi^n \rangle_\alpha = \alpha^n \langle \phi^n \rangle . \tag{A.25}$$

CLAIM 1: Given the definition equations, if

$$Z(j) = \frac{\int_C d\phi \, e^{-S(\phi)+j\phi}}{\int_C d\phi \, e^{-S(\phi)}},$$

then

$$Z_{new}(j) = \frac{\int_C d\phi \, e^{-S(\phi)+\alpha j\phi}}{\int_C d\phi \, e^{-S(\phi)}}. \tag{A.26}$$

where C stands for an approapriate contour on the complex plane. Note that this construction, equation (A.26), is the unique construction that satisfies the definition conditions, since conditions set all the derivatives and the value of $Z_\alpha(j)$ at $j = 0$. Obviously the following transformation holds:

$$Z_{new}(j) = Z(\alpha j). \tag{A.27}$$

And also

$$Z_{new}(j) = \left\langle e^j \right\rangle_\alpha = \left\langle e^{\alpha j} \right\rangle . \tag{A.28}$$

CLAIM 2: $Z_{new}(j)$ defined as in equation (A.24) satisfies the new Schwinger-Dyson equation, i.e. equation (A.21).

PROOF: Note $'$ denotes differentiation with respect to argument.

$$\left.\frac{\partial S_\alpha}{\partial \phi}\right|_{\phi=\frac{d}{dj}} Z_\alpha(j) = jZ_\alpha(j), \tag{A.29}$$

$$\left.\frac{\partial S(\phi/\alpha)}{\partial \phi}\right|_{\phi=\frac{d}{dj}} Z_\alpha(j) = jZ_\alpha(j) \tag{A.30}$$

$$\left.\frac{S'(\phi/\alpha)}{\alpha}\right|_{\phi=\frac{d}{dj}} Z_\alpha(j) = jZ_\alpha(j) \tag{A.31}$$

$$S'(\phi/\alpha)|_{\phi=\frac{d}{dj}}\, Z_\alpha(j) = \alpha j Z_\alpha(j) \tag{A.32}$$

$$S'(\phi/\alpha)|_{\phi=\alpha\frac{d}{dj}}\, Z_\alpha(j/\alpha) = jZ_\alpha(j/\alpha) \tag{A.33}$$

$$S'(\phi)|_{\phi=\frac{d}{dj}}\, Z_\alpha(j/\alpha) = jZ_\alpha(j/\alpha). \tag{A.34}$$

Note that the last line is the original Schwinger-Dyson equation. Therefore $Z_\alpha(j/\alpha)$ is a generating function(al) for the theory defined by $S(\phi)$. Then equation (A.27) tells us that $Z_new(j)$ satisfies the new Schwinger-Dyson equation. Actually, the best proof is to do everything I did in reverse.

CLAIM 3: One can numerically study the generating function(al)s of $S_\alpha(\phi)$ by a new complex Langevin equation

$$d\phi = -\frac{\partial S_\alpha}{\partial \phi} d\tau + dW(\tau), \tag{A.35}$$

which can be rewritten in terms of $S(\phi)$ as

$$d\phi = -\frac{S'(\phi/\alpha)}{\alpha} d\tau + dW(\tau). \tag{A.36}$$

Then one can simulate this equation and by rescaling the resulting Green's functions,

one can obtain a solution to the original theory.

EXAMPLE: If $S(\phi) = \frac{1}{2}m^2\phi^2 + \frac{g}{4}\phi^4$, $S'(\phi) = \frac{1}{2\alpha^2}m^2\phi^2 + \frac{g}{4\alpha^4}\phi^4$ and the new Langevin equation is

$$d\phi = -\frac{m^2}{\alpha^2}\phi d\tau - \frac{g}{\alpha^4}\phi^3 d\tau + dW(\tau). \tag{A.37}$$

The point of all this is that introduced α factors will change the attractors of the system and will let the system to converge into new solutions.

A.3 General Two Dimensional Process

In this section, we want to get equation,

$$\frac{d}{d\tau}\langle F[\phi(\tau)]\rangle = \left\langle \frac{\partial^2 F}{\partial \phi^2} - \frac{\partial F}{\partial \phi}\left[\frac{\partial S}{\partial \phi}\right]\right\rangle. \tag{A.38}$$

from a general two dimensional system. The insight comes from equation (A.17). The first derivative term set $G = \frac{\partial S}{\partial \phi}$. This seems reasonable, the action has to enter the system somehow, and this is the most natural place. The problem is with the second derivative term. $i\eta_R\eta_I$ term forces one of ηs to be zero, since ηs are real and the coefficient of the second derivative has to be 1. The only way to do this consistently is to set $\eta_I = 0$. If we can get rid of $i\eta_R\eta_I$ term, then we don't have this restriction anymore. Note that $i\eta_R\eta_I$ term comes from the fact that in the general complex Langevin equation, equation (A.3), both equations are coupled to the same Brownian motion. Therefore it seems reasonable to decouple the equation by including a second Brownian motion for the second equation.

The system that we are going to analyze is:

$$\begin{aligned} d\phi_R(\tau) &= -G_R(\phi_R,\phi_I) + \eta_R(\phi_R,\phi_I)dw_1(\tau), \\ d\phi_I(\tau) &= -G_I(\phi_R,\phi_I) + \eta_I(\phi_R,\phi_I)dw_2(\tau), \end{aligned} \tag{A.39}$$

where $dw_1(\tau)$ and $dw_2(\tau)$ are independent Brownian motions with the normalization

$$\langle dw_i(\tau)\rangle = 0, \qquad \langle dw_i(\tau)dw_i(\tau)\rangle = 2\delta_{ij}d\tau, \qquad \langle dw_i(\tau_1)dw_j(\tau_2)\rangle = 0 \quad (\tau_1 \neq \tau_2). \tag{A.40}$$

Repeating the analysis done in the previous section for this system gives:

$$\begin{aligned} \frac{d}{d\tau}\langle F[\phi(\tau)]\rangle &= \frac{d}{d\tau}\langle F_R[\phi_R(\tau),\phi_I(\tau)]\rangle + i\frac{d}{d\tau}\langle F_I[\phi_R(\tau),\phi_I(\tau)]\rangle \\ &= \left\langle -\sum_{\alpha=R,I}\frac{\partial F_R}{\partial\phi_\alpha(\tau)}G_\alpha + \sum_{\substack{\alpha=R,I\\ \beta=R,I}}\frac{\partial^2 F_R}{\partial\phi_\alpha(\tau)\partial\phi_\beta(\tau)}\eta_\alpha\eta_\beta\delta_{\alpha\beta}\right\rangle \\ &\qquad + i\left\langle -\sum_{\alpha=R,I}\frac{\partial F_I}{\partial\phi_\alpha(\tau)}G_\alpha + \sum_{\substack{\alpha=R,I\\ \beta=R,I}}\frac{\partial^2 F_I}{\partial\phi_\alpha(\tau)\partial\phi_\beta(\tau)}\eta_\alpha\eta_\beta\delta_{\alpha\beta}\right\rangle \\ &= \left\langle \frac{d^2F}{d\phi^2}\left[\eta_R^2 - \eta_I^2\right] - \frac{dF}{d\phi}G\right\rangle, \end{aligned} \tag{A.41}$$

where the second line follows from equation (A.6) by noting that $b_{ij} = \eta_i\delta_{ij}$ for equation (A.39), and the third line follows from Cauchy-Riemann equations. This equation is equal to equation (2.21) only if

$$G = \frac{dS}{d\phi} \tag{A.42}$$

and

$$\eta_R^2 - \eta_I^2 = 1. \tag{A.43}$$

Now we have infinitely many different Langevin systems that converge to Schwinger-

Dyson equation solutions. Note that we want nonvanishing ηs: η_R cannot be zero and if η_I is zero we have the complex Langevin equation again. Choosing different ηs may result in different stationary solutions.

Appendix B

An Example of a Langevin Equation Simulation with Polynomial Chaos

In this section we explore the possibility of using Polynomial Chaos expansions to simulate Langevin type stochastic equations.

A theorem by Cameron and Martin [21], showed that every real or complex valued L_2 functional $F[x]$ has a Fourier expansion in terms of a complete orthonormal set of functionals, which converges in L_2 sense [21]. In terms of stochastic processes, this means that the homogeneous chaos expansion converges to any process with finite second-order moments. See [115] for a generalization to other type of stochastic processes. In this section we apply this method to a 0-dimensional free field.

The action is:

$$S = \frac{1}{2} m^2 \phi^2, \tag{B.1}$$

and the path integral solution for the Schwinger-Dyson equation is (with $Z(0) = 1$ normalization):

$$Z(j) = \sqrt{\frac{2m}{\pi}} \int_{-\infty}^{\infty} e^{-\frac{1}{2}m^2\phi^2 + j\phi} d\phi \tag{B.2}$$

The Langevin equation is:

$$\frac{d\phi(\tau)}{d\tau} = -\frac{1}{2} m^2 \phi + \eta(\tau). \tag{B.3}$$

For the generic initial condition $\langle \phi(0) \rangle = a_0$, the solution to equation (B.3) is:

$$\phi(\tau) = \int_0^{\tau} e^{-\frac{1}{2}m^2(\tau - \tau')} \eta(\tau') \, d\tau' + a_0 \, e^{-\frac{1}{2}m^2\tau}. \tag{B.4}$$

Then one can write the propagator:

$$\langle \phi(\tau_1) \phi(\tau_2) \rangle = \int_0^{\tau_1} \int_0^{\tau_2} e^{-\frac{1}{2}m^2(\tau_1 + \tau_2 - \tau' - \tau'')} \langle \eta(\tau') \eta(\tau'') \rangle \, d\tau' d\tau'' + a_0^2 \, e^{-\frac{1}{2}m^2(\tau_1 + \tau_2)}, \tag{B.5}$$

where we did not include the cross terms since $\langle \eta(\tau) \rangle = 0$. Now using $\langle \eta(\tau') \eta(\tau'') \rangle =$

$\delta(\tau' - \tau'')$:

$$\begin{aligned}\langle \phi(\tau_1)\,\phi(\tau_2)\rangle &= \int_0^{min(\tau_1,\tau_2)} e^{-\frac{1}{2}m^2(\tau_1+\tau_2-2\tau')}\,d\tau' + a_0^2\, e^{-\frac{1}{2}m^2(\tau_1+\tau_2)} \\ &= e^{-\frac{1}{2}m^2(\tau_1+\tau_2)}\left[a_0^2 - \frac{1}{m^2} + \frac{e^{m^2\min(\tau_1,\tau_2)}}{m^2}\right]. \end{aligned} \tag{B.6}$$

Now setting $\tau_1 = \tau_2 = \tau$ and taking the $\tau \longrightarrow \infty$ limit, we get:

$$G_2 = \lim_{\tau\longrightarrow\infty}\langle \phi(\tau)\,\phi(\tau)\rangle = \lim_{\tau\longrightarrow\infty}\left[a_0^2 + \frac{1}{m^2}\right]e^{-m^2\tau} + \frac{1}{m^2} = \frac{1}{m^2} \tag{B.7}$$

as expected.

To simulate this theory with Wiener-Hermite polynomials, we first expand the random variable ϕ in terms of Wick polynomials:

$$\phi(\tau) = \sum_{\alpha=0}^{\infty}\phi_\alpha(\tau)\,T_\alpha(\xi). \tag{B.8}$$

We also expand the gaussian noise in terms of gaussian random variables:

$$\eta(\tau) = \sum_{i=1}^{\infty} m_i(\tau)\,\xi_i, \tag{B.9}$$

where $m_i(\tau)$ are an orthonormal basis in $L^2([0,T])$. Note that $\xi_i = H_1(\xi_i)$. When we insert these expansions to the Langevin equation, we get a differential equation for each term:

$$\frac{d\phi_\alpha(\tau)}{d\tau} = -\frac{1}{2}m^2\phi + \delta_{\{\alpha_j=\delta_{ij}\}}m_i(\tau), \tag{B.10}$$

where $\delta_{\{\alpha_j=\delta_{ij}\}}$ equals 1 only if $\alpha_i = 1$ and $\alpha_j \neq 1$ for $j \neq 1$. For our simulations, we

will choose $m_i(\tau)$ to be:

$$m_1(\tau) = \frac{1}{\sqrt{T}}, \qquad m_k(\tau) = \sqrt{\frac{2}{T}} \cos\left(\frac{(k-1)\pi\tau}{T}\right), \qquad k = 2, 3, \ldots, \qquad 0 \leq \tau \leq T, \tag{B.11}$$

where T is the simulation time.

Another point to discuss is how to implement the initial conditions. Note that from equation (B.8), using $\langle T_\alpha \rangle = 0$ for $\alpha \neq 0$, and $\langle T_0 \rangle = 1$, we can conclude the following for a deterministic initial condition:

$$\langle \phi(0) \rangle = \phi_0(0). \tag{B.12}$$

Then, equation (B.10) shows that if we start the fictitious time evolution with a deterministic initial condition, only terms with $|\alpha| = 0$ and $|\alpha| = 1$ have nonzero evolutions. ϕ_0 decays exponentially starting with the initial condition value, $\phi_{|\alpha|=1}$ terms are driven by the orthonormal functions $m_i(\tau)$. Other terms do not start at all. This means that the free field is a gaussian random variable.

In Figure B.1 we plot this evolution and the Wiener-Hermite expansion for different truncations.

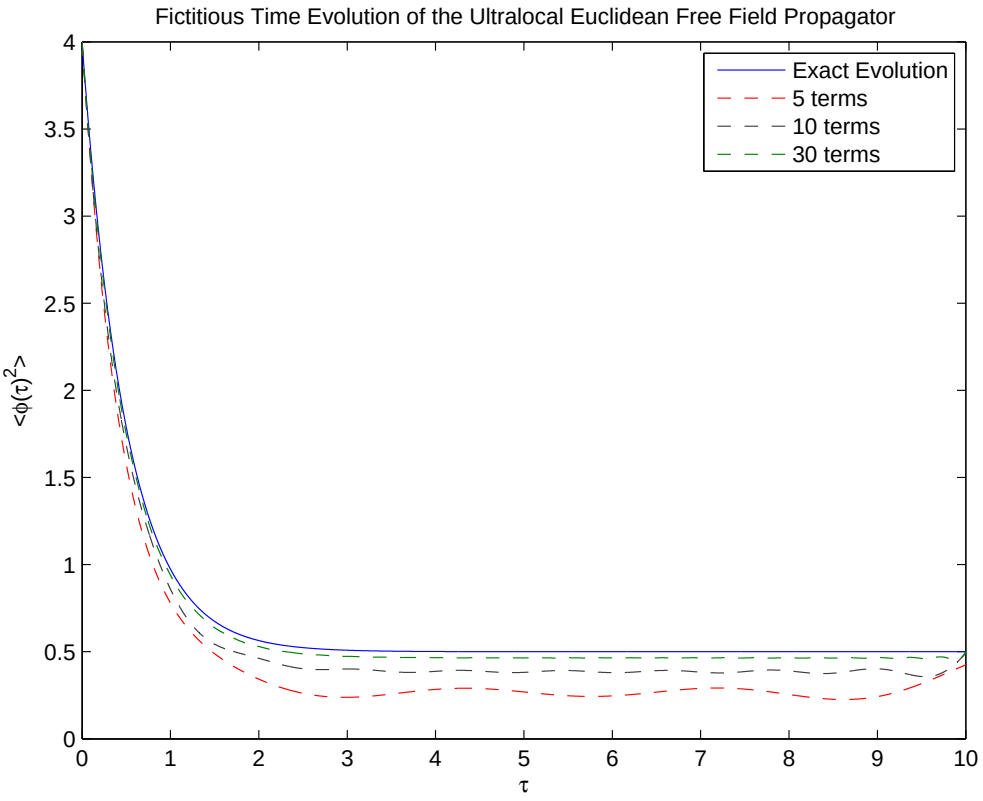

Figure B.1: The fictitious time evolution of the zero dimensional free field propagator. Simulation is done for 10 seconds. Initial condition is set at $\langle \phi(0) \rangle = 2$. $m^2 = 2$ and exact propagator is 0.5. The 30 terms evolution ends at 0.4997.

Appendix C

Series Expansion at the Tip of the Brane

We solved the static brane equation of motion (5.8) (in dimensionless form) in a power series around the tip of the brane, assuming that θ is regular there,

$$\theta(z) = \frac{\pi}{2} + \sum_{n=1}^{\infty} a_n (z'_{\rm end} - z')^n. \tag{C.1}$$

The first six coefficients are set by the equation of motion to be

$$\begin{aligned}
a_1 &= \frac{1}{z'_{\rm end}\sqrt{-1+z'^4_{\rm end}}},\\
a_2 &= \frac{-1+3z'^4_{\rm end}}{2z'^2_{\rm end}\left(-1+z'^4_{\rm end}\right)^{3/2}},\\
a_3 &= \frac{1-z'^4_{\rm end}+6z'^8_{\rm end}}{3z'^3_{\rm end}\left(-1+z'^4_{\rm end}\right)^{5/2}},\\
a_4 &= \frac{-1+4z'^4_{\rm end}+7z'^8_{\rm end}+10z'^{12}_{\rm end}}{4z'^4_{\rm end}\left(-1+z'^4_{\rm end}\right)^{7/2}},\\
a_5 &= \frac{2-9z'^4_{\rm end}+42z'^8_{\rm end}+75z'^{12}_{\rm end}+30z'^{16}_{\rm end}}{10z'^5_{\rm end}\left(-1+z'^4_{\rm end}\right)^{9/2}},\\
a_6 &= \frac{-2+11z'^4_{\rm end}-9z'^8_{\rm end}+231z'^{12}_{\rm end}+231z'^{16}_{\rm end}+42z'^{20}_{\rm end}}{12z'^6_{\rm end}\left(-1+z'^4_{\rm end}\right)^{11/2}}.
\end{aligned} \tag{C.2}$$

a_7 is not set, it is a free parameter. However, as much as we have investigated, higher order terms can be solved as a function of a_7.

The function $f(z'_{\rm end}, a_7)$ given in equation (5.119) is

$$\begin{aligned}
f(z'_{\rm end}, a_7) = -\frac{\left(z'^4_{\rm end}-1\right)^2}{z'^4_{\rm zend}} \Big[&56z'^{24}_{\rm end}+560z'^{20}_{\rm end}+1001z'^{16}_{\rm end}+201z'^{12}_{\rm end}+41z'^8_{\rm end}\\
&-13z'^4_{\rm end}+\sqrt{z^4_{\rm end}-1}\left(-14a_7z'^{31}_{\rm end}+84a_7z'^{27}_{\rm end}-210a_7z'^{23}_{\rm end}+280a_7z'^{19}_{\rm end}\right.\\
&\left.-210a_7z'^{15}_{\rm end}+84a_7z^{11}_{\rm end}-14a_7z'^7_{\rm end}\right)+2\Big]^{-1/2}.
\end{aligned} \tag{C.3}$$

Bibliography

[1] G. Aarts and I.-O. Stamatescu. Stochastic quantization at finite chemical potential. *JHEP*, 09:018, 2008.

[2] O. Aharony, J. Sonnenschein, and S. Yankielowicz. A holographic model of deconfinement and chiral symmetry restoration. *Annals Phys.*, 322:1420–1443, 2007.

[3] T. Albash, V. G. Filev, C. V. Johnson, and A. Kundu. A topology-changing phase transition and the dynamics of flavour. *Phys. Rev.*, D77:066004, 2008.

[4] M. Alcubierre. *Introduction to 3+1 Numerical Relativity*. Oxford University Press, USA, 2008.

[5] G Aldazabal, A Gonzalez-Arroyo, and N Parga. The stochastic quantisation of u(n) and su(n) lattice gauge theory and langevin equations for the wilson loops. *J. Phys. A: Math. Gen.*, 18(15):2975–2993, 1985.

[6] J. Ambjørn and S. K. Yang. Numerical problems in applying the langevin equation to complex effective actions. *Phys. Lett. B*, 165:140–146, December 1985.

[7] D. Anasov. Geodesic flows on a compact riemann manifold of negative geodesic curvature. *Proc. Steklov Inst. Math*, 90:1, 1967.

[8] R. Apreda, J. Erdmenger, N. Evans, and Zachary Guralnik. Strong coupling effective Higgs potential and a first order thermal phase transition from AdS/CFT duality. *Phys. Rev.*, D71:126002, 2005.

[9] J. Babington, J. Erdmenger, Nick J. Evans, Z. Guralnik, and I. Kirsch. Chiral symmetry breaking and pions in non-supersymmetric gauge / gravity duals. *Phys. Rev.*, D69:066007, 2004.

[10] V. Balasubramanian and P. Kraus. A stress tensor for anti-de Sitter gravity. *Commun. Math. Phys.*, 208:413–428, 1999.

[11] C. M. Bender, D. C. Brody, J. H. Chen, H. F. Jones, K. A. Milton, and M. C. Ogilvie. Equivalence of a complex PT-symmetric quartic Hamiltonian and a

Hermitian quartic Hamiltonian with an anomaly. *Phys. Rev. D*, 74(2):025016, July 2006.

[12] C. M. Bender, F. Cooper, and G. S. Guralnik. Path integral formulation of mean-field perturbation theory. *Annals of Physics*, 109(1):165 – 209, 1977.

[13] C. M. Bender and S. A. Orszag. *Advanced Mathematical Methods for Scientists and Engineers*. Spreinger-Verlag, Berlin Heidelberg, 1999.

[14] J. Berges, Sz. Borsanyi, D. Sexty, and I. O. Stamatescu. Lattice simulations of real-time quantum fields. *Phys. Rev. D*, 75(4):045007, 2007.

[15] J. Berges and D. Sexty. Real-time gauge theory simulations from stochastic quantization with optimized updating. *Nucl. Phys.*, B799:306–329, 2008.

[16] C. Bernard and V. M. Savage. Numerical simulations of pt-symmetric quantum field theories. *Phys. Rev. D*, 64(8):085010, Sep 2001.

[17] G. Beuf, M. P. Heller, R. A. Janik, and R. Peschanski. Boost-invariant early time dynamics from AdS/CFT. 2009.

[18] R. Bowen. Markov partitions for axiom a diffeomorphisms. *Amer. J. Math.*, 92:725, 1975.

[19] J. D. Brown and J. W. York, Jr. Quasilocal energy and conserved charges derived from the gravitational action. *Phys. Rev.*, D47:1407–1419, 1993.

[20] K. Landsteiner C. Hoyos and S. Montero. Holographic meson melting. *JHEP*, 2007(04):031, 2007.

[21] R. H. Cameron and W. T. Martin. The orthogonal development of non-linear functionals in series of fourier-hermite functionals. *Annals of Mathematics*, 48(2):385, 1947.

[22] P. M. Chesler and L. G. Yaffe. Boost invariant flow, black hole formation, and far-from- equilibrium dynamics in N = 4 supersymmetric Yang-Mills theory. 2009.

[23] S. Coleman. *Aspects of Symmetry*. Cambridge University Press, 1988.

[24] Bjorken J. D. Highly Relativistic Nucleus-Nucleus Collisions: The Central Rapidity Region. *Phys. Rev.*, D27:140, 1983.

[25] P. H. Damgaard and H. Huffel. Stochastic quantization. *Phys. Rep.*, 152(5&6):227, 1987.

[26] P. DuChateau and D. Zachmann. *Applied Partial Differential Equations*. Dover Publications, 2002.

[27] J. Erdmenger, N. Evans, I. Kirsch, and E. Threlfall. Mesons in Gauge/Gravity Duals - A Review. *Eur. Phys. J.*, A35:81–133, 2008.

[28] D. D. Ferrante and G. S. Guralnik. Mollifying quantum field theory or lattice qft in minkowski spacetime and symmetry breaking. *arXiv:hep-lat/0602013*, 2006.

[29] P. Figueras, V. E. Hubeny, M. Rangamani, and S. F. Ross. Dynamical black holes and expanding plasmas. 2009.

[30] J. Flower, S. W. Otto, and S. Callahan. Complex langevin equations and lattice gauge theory. *Phys. Rev. D*, 34(2):598–604, Jul 1986.

[31] U. Frisch. *Turbulence, The Legacy of A. N. Kolmogorov*. Cambridge: Cambridge University Press, 1995.

[32] U. Frisch and R. Morf. Intermittency in nonlinear dynamics and singularities at complex times. *Phys. Rev. A*, 23:2673–2705, 1981.

[33] S. Garcia, G. Guralnik, and Z. Guralnik. Theta Vacua and Boundary Conditions of the Schwinger Dyson Equations. *hep-th/9612079*, December 1996.

[34] C. W. Gardiner. *Handbook of Stochastic Methods, Third Edition*. Springer-Verlag, Berlin Heidelberg, 2004.

[35] H. Gausterer. On the correct convergence of complex Langevin simulations for polynomial actions . *J. Phys. A*, 27:1325–1330, February 1994.

[36] H. Gausterer. Complex Langevin: a numerical method? *Nuc. Phys. A*, 642:239–250, November 1998.

[37] H. Gausterer and S. Lee. The Mechanism of Complex Langevin Simulations. *J. Stat. Phys.*, 73:147–157, 1993.

[38] E. Gozzi. Functional-integral approach to parisi-wu stochastic quantization: Scalar theory. *Phys. Rev. D*, 28(8):1922–1930, Oct 1983.

[39] J. Greensite and M. B. Halpern. Stabilizing bottomless action theories. *Nuc. Phys. B*, 242:167–188, August 1984.

[40] J. Grosse, R. A. Janik, and P. Surowka. Flavors in an expanding plasma. *Phys. Rev.*, D77:066010, 2008.

[41] S. S. Gubser, Igor R. Klebanov, and A. M. Polyakov. Gauge theory correlators from non-critical string theory. *Phys. Lett.*, B428:105–114, 1998.

[42] A. Gullstrand. Allgemeine Lösung des statischen Einkörperproblems in der Einsteinschen Gravitationstheorie. *Arkiv. Mat. Astron. Fys.*, 16:1–15, 1922.

[43] G. Guralnik and Z. Guralnik. Complexified path integrals and the phases of quantum field theory. *Annals of Physics*, In Press, Corrected Proof:–, 2010.

[44] G. Guralnik, Z. Guralnik, and C. Pehlevan. Remarks on Power Spectra of Chaotic Dynamical Systems.

[45] G. Guralnik and C. Pehlevan. Complex Langevin Equations and Schwinger-Dyson Equations. *Nucl. Phys.*, B811:519–536, 2009.

[46] G. Guralnik and C. Pehlevan. Effective Potential for Complex Langevin Equations. *Nucl. Phys.*, B822:349–366, 2009.

[47] Z. Guralnik. Exact statistics of chaotic dynamical systems. *Chaos*, 18:033114, 2008.

[48] B. Gustafsson, H.-O. Kreiss, and J. Oliger. *Time Dependent Problems and Difference Methods*. Wiley-Interscience, 1996.

[49] H. W. Hamber and H. C. Ren. Complex probabilities and the Langevin equation. *Phys. Lett. B*, 159:330–334, September 1985.

[50] S. Hammel, C. Grebogi, and J.A. Yorke. Do numerical orbits of chaotic dynamical processes represent true orbits? *J. Complexity*, 3:136, 1987.

[51] M. P. Heller and R. A. Janik. Viscous hydrodynamics relaxation time from AdS/CFT. *Phys. Rev.*, D76:025027, 2007.

[52] M. P. Heller, P. Surowka, R. Loganayagam, M. Spalinski, and S. E. Vazquez. On a consistent AdS/CFT description of boost-invariant plasma. 2008.

[53] D. Hochberg, C. Molina-París, J. Pérez-Mercader, and M. Visser. Effective action for stochastic partial differential equations. *Phys. Rev. E*, 60(6):6343–6360, Dec 1999.

[54] E. Hopf. Statistical hydromechanics and functional calculus. *J. Ratl. Mech. Anal*, 1:87, 1952.

[55] M. Ito and K. Morita. Note on Stochastic Quantization of Field Theories with Bottomless Actions. *Prog. Theor. Phys.*, 90:187–200, July 1993.

[56] R. A. Janik. Viscous plasma evolution from gravity using AdS/CFT. *Phys. Rev. Lett.*, 98:022302, 2007.

[57] R. A. Janik and R. B. Peschanski. Asymptotic perfect fluid dynamics as a consequence of AdS/CFT. *Phys. Rev.*, D73:045013, 2006.

[58] A. Karch and E. Katz. Adding flavor to AdS/CFT. *JHEP*, 06:043, 2002.

[59] A. Karch and A. O'Bannon. Chiral transition of N = 4 super Yang-Mills with flavor on a 3-sphere. *Phys. Rev.*, D74:085033, 2006.

[60] A. Karch, A. O'Bannon, and K. Skenderis. Holographic renormalization of probe D-branes in AdS/CFT. *JHEP*, 04:015, 2006.

[61] A. Karch, A. O'Bannon, and E. Thompson. The Stress-Energy Tensor of Flavor Fields from AdS/CFT. *JHEP*, 04:021, 2009.

[62] H. Kawara, M. Namiki, H. Okamoto, and S. Tanaka. Derivation of a generalized stochastic path-integral formulation based on ito calculus. *Prog. Theor. Phys.*, 84:749–766, 1990.

[63] S. Kinoshita, S. Mukohyama, S. Nakamura, and K.-y. Oda. A Holographic Dual of Bjorken Flow. *Prog. Theor. Phys.*, 121:121–164, 2009.

[64] S. Kinoshita, S. Mukohyama, S. Nakamura, and K.-y. Oda. Consistent Anti-de Sitter-Space/Conformal-Field-Theory Dual for a Time-Dependent Finite Temperature System. *Phys. Rev. Lett.*, 102:031601, 2009.

[65] I. Kirsch. Generalizations of the AdS/CFT correspondence. *Fortsch. Phys.*, 52:727–826, 2004.

[66] J. R. Klauder. Stochastic quantization. In H. Mitter and C. B. Lang, editors, *Recent Developments in High-Energy Physics*, page 251, Wien, 1983. Springer-Verlag.

[67] J. R. Klauder and W. P. Petersen. Spectrum of certain non-self-adjoint operators and solutions of langevin equations with complex drift. *J. Stat. Phys*, 39:53–72, 1985.

[68] S. Kobayashi, D. Mateos, S. Matsuura, R. C. Myers, and R. M. Thomson. Holographic phase transitions at finite baryon density. *JHEP*, 02:016, 2007.

[69] M. Kruczenski, D. Mateos, R. C. Myers, and D. J. Winters. Meson spectroscopy in AdS/CFT with flavour. *JHEP*, 07:049, 2003.

[70] M. Kruczenski, D. Mateos, R. C. Myers, and D. J. Winters. Towards a holographic dual of large-N_c QCD. *JHEP*, 5:41–+, May 2004.

[71] H. P. Langtangen. *Computational Partial Differential Equations - Numerical Methods for Scientific Programming*. Springer-Verlag, 1999. 682 pages.

[72] S. Lee. The convergence of complex Langevin simulations. *Nuc. Phys. B*, 413:827–848, February 1994.

[73] H. Q. Lin and J. E. Hirsch. Monte carlo versus langevin methods for nonpositive definite weights. *Phys. Rev. B*, 34(3):1964–1967, Aug 1986.

[74] J. M. Maldacena. The large N limit of superconformal field theories and supergravity. *Adv. Theor. Math. Phys.*, 2:231–252, 1998.

[75] D. Marolf. States and boundary terms: Subtleties of lorentzian ads/cft. *JHEP*, 0505:042, 2005.

[76] J. B. Marston and O. Ma. Exact equal time statistics of orszag-mclaughlin dynamics investigated using the hopf characteristic functional approach. *J.Stat.Mech.*, page P10007, 2005.

[77] D. Mateos, R. C. Myers, and R. M. Thomson. Holographic phase transitions with fundamental matter. *Phys. Rev. Lett.*, 97:091601, 2006.

[78] D. Mateos, R. C. Myers, and R. M. Thomson. Thermodynamics of the brane. *JHEP*, 05:067, 2007.

[79] R. M. M. Mattheij, S. W. Rienstra, and J. H. M. ten Thije Boonkkamp. *Partial Differential Equations: Modeling, Analysis, Computation*. SIAM, 2005.

[80] G. Menezes and N. F. Svaiter. Stochastic Quantization for Complex Actions. *J. Math. Phys.*, 49:102301, 2008.

[81] P. D. Miller. *Applied Asymptotic Analysis*. AMS Bookstore, 2006.

[82] B. Mohanty and J. Serreau. Disoriented chiral condensate: Theory and experiment. *Phys. Rept.*, 414:263–358, 2005.

[83] K. W. Morton and D. F. Mayers. *Numerical Solution of Partial Differential Equations*. Cambridge University Press, 2 edition, 2005.

[84] H. Nakazato. Thermal equilibrium minkowski stochastic quantization. *Prog. Theor. Phys.*, 77(1):20–25, 1987.

[85] H. Nakazato and Y. Yamanaka. Minkowski stochastic quantization. *Phys. Rev. D*, 34(2):492–496, Jul 1986.

[86] M. Namiki. *Stochastic Quantization*. Springer-Verlag, Berlin Heidelberg, 1992.

[87] M. Namiki. Basic Ideas of Stochastic Quantization. *Prog. Theor. Phys. Suppl.*, 111:1–41, 1993.

[88] E. A. Novikov. Functionals and the random-force method in turbulence. *Sov. Phys. JETP*, 20:1290, 1964.

[89] Andy O'Bannon. Holographic Thermodynamics and Transport of Flavor Fields. 2008.

[90] H. Okamoto, K. Okano, L. Schülke, and S. Tanaka. The role of a kernel in complex langevin systems. *Nuc. Phys. B*, 324:684–714, 1989.

[91] P. Painlevé. La mécanique classique et la théorie de la relativité. *C. R. Acad. Sci. (Paris)*, 173:677–680, 1922.

[92] G. Parisi. On complex probabilities. *Phys. Lett. B*, 131:393–395, 1983.

[93] G. Parisi and Y. Wu. Perturbation theory without gauge fixing. *Sci. Sin.*, 24(4):483, 1981.

[94] A. Parnachev and D. A. Sahakyan. Chiral phase transition from string theory. *Phys. Rev. Lett.*, 97:111601, 2006.

[95] D. Petrov. *Novel Approaches to Numerical Solutions to Quantum Field Theories*. PhD thesis, Brown University, 2005.

[96] R. D. Pisarski and F. Wilczek. Remarks on the chiral phase transition in chromodynamics. *Phys. Rev. D*, 29(2):338–341, Jan 1984.

[97] G. Policastro, D. T. Son, and A. O. Starinets. The shear viscosity of strongly coupled N = 4 supersymmetric Yang-Mills plasma. *Phys. Rev. Lett.*, 87:081601, 2001.

[98] J. Randrup. Probing chiral dynamics by charged-pion correlations. *Phys. Rev. C*, 63(6):061901, May 2001.

[99] H. Risken. *The Fokker-Planck Equation: Methods of Solution and Applications 2nd edn*. Berlin: Springer, 1996.

[100] L. L. Salcedo. Spurious solutions of the complex langevin equation. *Phys. Lett. B*, 305:125–130, 1993.

[101] L. L. Salcedo. Representation of complex probabilities. *J. Math. Phys.*, 38:1710–1722, March 1997.

[102] L. L. Salcedo. The existence of positive representations for complex weights. *J. Phys. A: Math. Gen.*, 40:9399–9412, August 2007.

[103] E. Shuryak. Physics of Strongly coupled Quark-Gluon Plasma. *Prog. Part. Nucl. Phys.*, 62:48–101, 2009.

[104] E. V. Shuryak. What RHIC experiments and theory tell us about properties of quark-gluon plasma? *Nucl. Phys.*, A750:64–83, 2005.

[105] D. Sigeti. Exponential decay of power spectra at high frequency and positive lyapunov exponents. *Physica D*, 82:136–153, 1995.

[106] K. Skenderis. Lecture notes on holographic renormalization. *Class. Quant. Grav.*, 19:5849–5876, 2002.

[107] K. Skenderis and B. C. van Rees. Real-time gauge/gravity duality: Prescription, Renormalization and Examples. *JHEP*, 05:085, 2009.

[108] B. Söderberg. On the complex langevin equation. *Nuc. Phys. B*, 295:396–408, 1988.

[109] M. Srednicki. *Quantum Field Theory*. Cambridge University Press, 2007.

[110] M. A. Stephanov. QCD phase diagram: An overview. *PoS*, LAT2006:024, 2006.

[111] S. Tanaka, M. Namiki, I. Ohba, M. Mizutani, N. Komoike, and M. Kanenaga. Stochastic quantization of bottomless systems based on a kerneled Langevin equation. *Phys. Let. B*, 288:129–139, August 1992.

[112] S. Tanaka, I. Ohba, M. Namiki, M. Mizutani, N. Komoike, and M. Kanenaga. Stabilization of ϕ^3-Model Based on Stochastic Quantization Method with Kerneled Langevin Equation. *Prog. Theor. Phys.*, 89:187–196, January 1993.

[113] D. Weingarten. Complex Probabilities on R^N as Real Probabilities on C^N and an Application to Path Integrals. *Phys. Rev. Lett.*, 89(24):240201–+, November 2002.

[114] E. Witten. Anti-de Sitter space and holography. *Adv. Theor. Math. Phys.*, 2:253–291, 1998.

[115] D. Xiu and G. Karniadikis. The wiener-askey polynomial chaos for stochastic differential equations. *Society for Industrial and Applied Mathematics*, 24(2):619, 2002.

[116] S. S. Xue. The fokker-planck equations in lattice gauge theories. *Phys. Lett. B*, 180:275–280, 1986.

[117] J. Zinn-Justin. *Quantum Field Theory and Critical Phenomena, Fourth Edition*. Oxford University Press, 2002.